

**REVEALING ZEBRAFISH EMBRYONIC DEVELOPMENTAL
BIOELECTRICITY USING GENETICALLY ENCODED TOOLS**

by

Martin R. Silic

A Dissertation

Submitted to the Faculty of Purdue University

In Partial Fulfillment of the Requirements for the degree of

Doctor of Philosophy



Department of Comparative Pathobiology

West Lafayette, Indiana

December 2022

THE PURDUE UNIVERSITY GRADUATE SCHOOL
STATEMENT OF COMMITTEE APPROVAL

Dr. GuangJun Zhang, Chair

Department of Comparative Pathobiology, Purdue University

Dr. Donna Fekete

Department of Biological Sciences, Purdue University

Dr. Mark Hall

Department of Biochemistry, Purdue University

Dr. Timothy Ratliff

Department of Comparative Pathobiology, Purdue University

Approved by:

Dr. Sanjeev K. Narayanan

Dedicated to my mother; Marianne Silic, my father; Nino Silic; and all others who have supported me along the way

ACKNOWLEDGMENTS

Foremost, I want to thank my advisor Dr. GuangJun Zhang. When we first met about 6 years ago, I never could have imagined being here. Fate must have played some small role in our time working together, as it almost did not happen. However, I am very grateful that I was able to join the lab and experience your excellent tutelage. I am truly a different person than when I started from it, a better version of myself. The amount of knowledge, logic, and practical ability gained from the time you have spent training me is hard to measure. You always provided thoughtful advice and suggestions through the good times and the tough times. I deeply appreciate everything you have done for me, the wonderful research environment you provided, and all the opportunities I have been afforded.

I would also like to thank my committee members: Dr. Donna Fekete, Dr. Mark Hall, and Dr. Timothy Ratliff. I appreciate all of you taking time out of your busy schedules to help me along this journey and guide me down the right path. Thank you to all the other professors who have collaborated with us as well. Everyone's input has been very meaningful. Thank you to the national institute of health for providing funding to these projects I was able to be a part of during my time.

Thank you to all other graduate students, past and current in the lab, who have been collaborative and given back their time and effort. I will always value everybody's reassurance and friendships. Also, to all other graduate students that I have met and worked with from other labs over the years. The cooperative and friendly environment I experienced was very enjoyable. I would also thank the numerous undergraduate students who have assisted me and the lab during my time. Without your help, the overall productivity would not have been possible.

Additionally, I need to thank the many friends who have encouraged and supported me over the years. The understanding provided to me, and the quite different lifestyle of research was always appreciated. I would not have been able to make it without you.

Lastly, to all my family members that have always believed in me, I thank you. Your constant words of kindness meant more to me than you know. I especially would like to thank my mother and father for raising me to be the person I am. You provided me with every opportunity one could ask for. I am extraordinarily fortunate to have you as my parents.

TABLE OF CONTENTS

| | |
|--|----|
| LIST OF ABBREVIATIONS..... | 9 |
| LIST OF TABLES | 10 |
| LIST OF FIGURES | 11 |
| LIST OF SUPPLEMENTARY VIDEOS | 12 |
| ABSTRACT..... | 14 |
| CHAPTER 1. BIOELECTRICITY: ADVANCES IN BIOLOGICAL UNDERSTANDING AND NEW TOOLS..... | 15 |
| 1.1 Introduction: Bioelectricity..... | 15 |
| 1.1.1 Membrane potential and concentration gradients..... | 15 |
| 1.1.2 Ion channels, gap junctions, and solute carriers | 18 |
| 1.1.3 History and experimental evidence of bioelectric research..... | 21 |
| 1.2 Zebrafish as a superior model for bioelectric research | 22 |
| 1.2.1 Zebrafish embryonic development | 22 |
| 1.2.2 Zebrafish fin development..... | 24 |
| 1.2.3 Zebrafish pigmentation..... | 25 |
| 1.3 The difficulties of studying developmental bioelectricity | 26 |
| 1.3.1 GEVIs and GECIs..... | 27 |
| 1.3.2 Genetically encoded indicator application: visualizing electric fields across tissues and whole organisms throughout development..... | 28 |
| 1.3.3 Chemogenetic and Optogenetic application: perturbing electric fields in groups of cells and tissues to study bioelectricity | 31 |
| 1.4 Conclusions and future challenges for studying V_m | 35 |
| CHAPTER 2. VISUALIZATION OF CELLULAR ELECTRICAL ACTIVITY IN ZEBRAFISH EARLY EMBRYOS AND TUMORS..... | 37 |
| 2.1 Abstract..... | 37 |
| 2.2 Introduction..... | 37 |
| 2.3 Protocol..... | 39 |
| 2.3.1 Tol2 Transposon Plasmid Construct Preparation..... | 39 |
| 2.3.2 Prepare Tol2 Transposase mRNA and Injection Solution | 41 |

| | | |
|---|--|----|
| 2.3.3 | Microinjection..... | 42 |
| 2.3.4 | Establish Transgenic ASAP1 fish, Tg (<i>ubi</i> : ASAP1) | 44 |
| 2.3.5 | Imaging | 44 |
| 2.4 | Representative Results | 45 |
| 2.5 | Discussion | 50 |
| CHAPTER 3. ZEBRAFISH EMBRYOS DISPLAY CHARACTERISTIC BIOELECTRIC SIGNALS DURING EARLY DEVELOPMENT | | 53 |
| 3.1 | Abstract..... | 53 |
| 3.2 | Introduction..... | 53 |
| 3.3 | Results..... | 55 |
| 3.3.1 | Cleavage Furrow Hyperpolarization Precedes Cytokinesis and Becomes More Dynamic as Zebrafish Embryos Develop in the Cleavage Period..... | 56 |
| 3.3.2 | Whole-Cell Vm Transient Signals Are Located in the Superficial Blastomere during the Zebrafish Blastula Period..... | 60 |
| 3.3.3 | Whole-Cell Vm Transient Signals Occur More Frequently during the Zebrafish Gastrula Period but with Similar Signal Duration | 62 |
| 3.3.4 | During the Segmentation Period, There Are Tissue-Level Dynamic Cellular Bioelectric Signals | 64 |
| 3.4 | Discussion | 67 |
| CHAPTER 4. TISSUE-SPECIFIC MODIFICATION OF CELLULAR BIOELECTRICAL ACTIVITIES USING THE CHEMOGENETIC TOOL, DREADD, IN ZEBRAFISH..... | | 73 |
| 4.1 | Abstract..... | 73 |
| 4.2 | Introduction..... | 73 |
| 4.3 | Results..... | 75 |
| 4.3.1 | Developing transgenic zebrafish lines to express DREADD | 75 |
| 4.3.2 | DREADDs work in zebrafish embryos, evidenced by ASAP2s fluorescence intensity changes | 77 |
| 4.3.3 | DREADD activation causes dynamic bioelectric changes in zebrafish melanophores | 79 |
| 4.3.4 | DREADD functional validation by melanophore morphological changes | 81 |
| 4.3.5 | Discussion..... | 82 |

| | |
|---|-----|
| CHAPTER 5. OVERALL DISCUSSION | 85 |
| CHAPTER 6. MATERIALS AND METHODS | 88 |
| 6.1 Visualization of Cellular Electrical Activity in Zebrafish Early Embryos and Tumors... | 88 |
| 6.1.1 Materials | 88 |
| 6.2 Zebrafish embryos display characteristic bioelectric signals during early development . | 89 |
| 6.2.1 Zebrafish Strains and Transgenic Fish Line Husbandry..... | 89 |
| 6.2.2 Imaging Early Zebrafish Embryo Vm Fluorescence and Data Analysis..... | 90 |
| 6.3 Tissue-specific modification of cellular bioelectrical activities using the chemogenetic tool, DREADD, in zebrafish | 91 |
| 6.3.1 Zebrafish husbandry | 91 |
| 6.3.2 Tol2 constructs, microinjection, and zebrafish transgenic lines..... | 91 |
| 6.3.3 DREADD ligand addition and fluorescence imaging..... | 92 |
| 6.3.4 Tracking 1-week larvae for DREADD induced phenotype | 93 |
| REFERENCES | 95 |
| PUBLICATIONS..... | 113 |

LIST OF ABBREVIATIONS

| | |
|------------------|---|
| ASAP1-4 | Accelerated sensor of action potentials 1-4 |
| Ca ²⁺ | Calcium |
| Cl ⁻ | Chloride |
| DCZ | Deschloroclozapine |
| DREADD | Designer receptor exclusively activated by designer drugs |
| EVL | Enveloping layer |
| FPs | Fluorescence proteins |
| FRET | Forester resonance energy transfer |
| GECI | Genetically encoded calcium indicator |
| GEVI | Genetically encoded voltage indicator |
| IRES | Internal ribosomal entry site |
| K ⁺ | Potassium |
| KCa | Calcium-gated potassium channels |
| Kcnj/ Kir | Inwardly rectifying potassium channels |
| Kcnk/ K2p | Potassium leak channels/ two-pore domain |
| LSM | Light sheet microscopy |
| mV | Millivolt |
| Na ⁺ | Sodium |
| PSAM | Pharmacologically selective actuator module |
| PSEM | Pharmacologically Selective Effector Molecules |
| SLCs | Solute carrier proteins |
| Tg | Transgene |
| <i>Ubi</i> | <i>Ubiquitin</i> |
| V _m | Membrane potential |
| VSDs | Voltage-sensitive domains |
| YSL | Yolk syncytial layer |

LIST OF TABLES

| | |
|--|----|
| Table 1 Vm of common cell types | 17 |
| Table 2 List of GEVIs and GECIs | 30 |
| Table 3 Chemogenetic and optogenetic tools | 34 |
| Table 4 Materials | 88 |

LIST OF FIGURES

| | |
|---|----|
| Figure 1-1 Cell membrane diagram showing ionic regulators and ionic concentrations when the cell is in a non-excitabile state. | 16 |
| Figure 2-1 Illustration of the Tol2 transposon-based plasmid construction. | 46 |
| Figure 2-2 Typical results of injected embryos by epifluorescence and Tol2-excise assay. | 47 |
| Figure 2-3 Dynamic voltage changes during zebrafish embryo development. | 49 |
| Figure 2-4 Electrical voltage changes of the fish body during fish embryo movement. | 49 |
| Figure 2-5 Tumor cells tend to be more polarized..... | 50 |
| Figure 3-1 Overall experimental procedure..... | 56 |
| Figure 3-2 Zebrafish Cleavage period embryos display furrow-related dynamic hyperpolarization. | 58 |
| Figure 3-3 Unfertilized Egg Vm signaling, $\Delta F/F$, and diagonal pattern of 4-cell stage..... | 60 |
| Figure 3-4 Whole-cell Vm transients occurred in the zebrafish superficial blastomeres during the blastula period..... | 62 |
| Figure 3-5 Zebrafish gastrulation exhibited whole-cell transient hyperpolarization in both superficial and deep cells..... | 64 |
| Figure 3-6 During the segment period, more complex and dynamic cellular bioelectric signals occurred at the tissue level..... | 66 |
| Figure 3-7. Deep cell Vm transient during the 30% epiboly period..... | 67 |
| Figure 3-8 Summary of bioelectric signaling during zebrafish embryogenesis. | 69 |
| Figure 4-1 Illustration of DREADD transgenic fish lines and experimental workflow. | 76 |
| Figure 4-2 Cell membrane voltage manipulation by DREADD in zebrafish embryos. | 78 |
| Figure 4-3 Melanophores show dynamic fluorescence changes after DREADD modification. .. | 81 |
| Figure 4-4 Activation of the hM4DGi receptor causes hyperpigmentation in 1-week old fish larvae. | 82 |

LIST OF SUPPLEMENTARY VIDEOS

Supplementary Video 2-1. Epifluorescence imaging of electrical signaling during cleavage stages in Tg (*ubi*: ASAP1) fish embryo. This movie was recorded from the view of animal pole. The ASAP1 fluorescence is associated with the formation of the cell cleavage furrow, a temporary structure during cell division.

Supplementary Video 2-2. Epifluorescence imaging of electrical signaling during 2-day old Tg (*ubi*: ASAP1) fish embryo movement. The movie was recorded from the lateral view of the 2-day old fish embryo after anesthetization. The ASAP1 fluorescence alterations are evident in neuromuscular tissue during the moving process.

Supplementary Video 3-1. Light-sheet imaging of Vm signaling during 2-4 cell cleavage stage in Tg (*ubi*: ASAP1). This video shows max projections from the animal pole view of ASAP1 fluorescence localized at the cleavage furrows during positioning and propagation processes.

Supplementary Video 3-2. Light-sheet imaging of Vm signaling during 4-8 cell cleavage stage in Tg (*ubi*: ASAP1). This video shows ASAP1 fluorescence localized at the cleavage furrows from the animal pole view.

Supplementary Video 3-3. Light-sheet imaging of Vm signaling during 8-16 cell cleavage stage in Tg (*ubi*: ASAP1). This video shows ASAP1 fluorescence localized at the cleavage furrows from the animal pole view.

Supplementary Video 3-4. Light-sheet imaging of Vm signaling in unfertilized Tg (*ubi*: ASAP1). This video shows ASAP1 fluorescence signals occurring within an unfertilized embryo from the animal pole view.

Supplementary Video 3-5. Light-sheet imaging of Vm signaling during early blastula stage in Tg (*ubi*: ASAP1). This video shows ASAP1 transient fluorescent signals occurring over the surface of an embryo from the lateral view.

Supplementary Video 3-6. Light-sheet imaging of Vm signaling limited to superficial blastomere during early blastula stage in Tg (*ubi*: ASAP1). This video shows a single z-slice ASAP1 transient fluorescent signals limited to the superficial blastomere margins- an embryo from the lateral view.

Supplementary Video 3-7. Light-sheet imaging of Intercellular Vm signaling during early blastula stage in Tg (*ubi*: ASAP1). This video shows ASAP1 transient fluorescent signals occurring followed by adjacent signals signaling in seemingly an intercellular correlation.

Supplementary Video 3-8. Light-sheet imaging of Vm signaling during gastrula stage in Tg (*ubi*: ASAP1). This video shows Vm transients in the EVL and YSL from early to late gastrula stage in a dorsal to lateral view.

Supplementary Video 3-9. Light-sheet imaging of Vm signaling within deeper cell layers during gastrula stage in Tg (*ubi: ASAP1*). This video shows Vm transients occurring within deeper cell layers during mid-gastrulation.

Supplementary Video 3-10. Light-sheet imaging of Vm signaling during the early segmentation stage in Tg (*ubi: ASAP1*). This video starts at the end of gastrulation and shows Vm signals becoming stronger in certain tissue regions, such as the somites.

Supplementary Video 3-11. Light-sheet imaging of left lateral Vm signaling during somite stage in Tg (*ubi: ASAP1*). This video shows a continuation of Vm transients, highly dynamic somite hyperpolarizations, and increased signals in the developing heart from the left lateral view.

Supplementary Video 3-12. Light-sheet imaging of Dorsal Vm signaling during the somite stage in Tg (*ubi: ASAP1*) This video shows a continuation of Vm transients and highly dynamic unilateral or bilateral, whole and/or partial somite signals from the dorsal view.

Supplementary Video 4-1. Epifluorescence imaging of melanophore Vm signaling in 2 dpf Tg (*mitfa2.1: ASAP2s-IRES-hM4DGi*) fish larva after hM4DGi activation. This video shows dynamic ASAP2s fluorescence changes in the melanophores after the agonist DCZ is added on the dorsal side of the head (dorsal view).

ABSTRACT

Bioelectricity, or endogenous electrical signaling mediated by the dynamic distribution of charged molecules, is an ancient signaling mechanism conserved across living organisms. Increasing evidence has revealed that bioelectric signals play a critical role in many diverse aspects of biology such as embryonic development, cell migration, regeneration, cancer, and other diseases. However, direct visualization and manipulation of bioelectricity during development are lacking. Neuroscience has developed tools such as GEVIs (genetically encoded voltage indicators) and chemogenetics like DREADDs (designer receptors exclusively activated by designer drugs) which allow for real-time voltage monitoring and activation of mutated receptors by inert molecules for perturbing membrane potential (V_m). To uncover bioelectric activity during development, we generated a whole-zebrafish transgenic GEVI reporter line and characterized the electrical signaling during early embryogenesis using light sheet microscopy (LSM). Additionally, we generated tissue-specific transgenic lines that combined GEVIs and chemogenetic DREADD tools to manipulate V_m . We found zebrafish embryos display stage-specific characteristic bioelectric signals during the cleavage, blastula, gastrula, and segmentation periods. Furthermore, activation of DREADDs was able to alter cell-specific GEVI fluorescence intensity and could cause a melanophore hyperpigmentation phenotype. Ultimately, these results provide the first real-time systematic analysis of endogenous bioelectricity during vertebrate embryonic development. Additionally, we generated and tested zebrafish transgenic lines for simultaneous visualization and chemogenetic manipulation of V_m during development. These results provide a better understanding of developmental bioelectricity and new tools for future studies, which could eventually help uncover the cellular electric mechanisms behind tissue patterning and disease.

CHAPTER 1. BIOELECTRICITY: ADVANCES IN BIOLOGICAL UNDERSTANDING AND NEW TOOLS

1.1 Introduction: Bioelectricity

Cell-to-cell communication is perhaps one of the most important necessities of multicellular organisms. Without these interactions, life would not have evolved distinct tissues, organs, and complex species. While there are a variety of ways for cells to communicate, one of the most essential is electrical signaling. Bioelectricity can be defined as endogenous electrical signaling mediated by the dynamic distribution of charged molecules [1-6]. This is represented by a difference in the net charge of cations and anions inside versus outside a cell. Many components are required for differences in electrical potential to be formed [7]. In essence, the semipermeable lipid-based plasma membrane acts as an electrical insulator, but also a capacitor that can accumulate charge, while specialized passages (ion channels, pumps, connexins/ gap junctions, and solute carriers) regulate ionic flow from one side to the other altering the voltage of the cell (Fig. 1-1). All systems and all cell types form ionic gradients across their cell membranes because channels exist throughout all organisms in all domains of life including plants, fungi, and bacteria [8-15]. Thus, ionic regulation, and the resulting bioelectricity, is considered an essential property of living cells across evolution and the innate properties can be used for cellular communication [16]. Therefore, deeply understanding all aspects of bioelectricity in cells and organisms, including outside of a neuromuscular context, is fundamental.

1.1.1 Membrane potential and concentration gradients

Bioelectricity encompasses several different components. Membrane potential (V_m), the electric potential difference between the intracellular and extracellular space is an essential element (Fig. 1). V_m is involved with nutrient, salt, and water transport across the cell membrane as well as essential physiological processes like cell volume and excitability [4]. Additionally, it allows for cognitive and motor function through neuronal signaling resulting in organismal, tissue, or cellular sensory detection and movement [4, 16]. In typical neuronal signaling, the steady-state, baseline voltage is called resting V_m , whereas the excited “signaling” state is called an action potential.

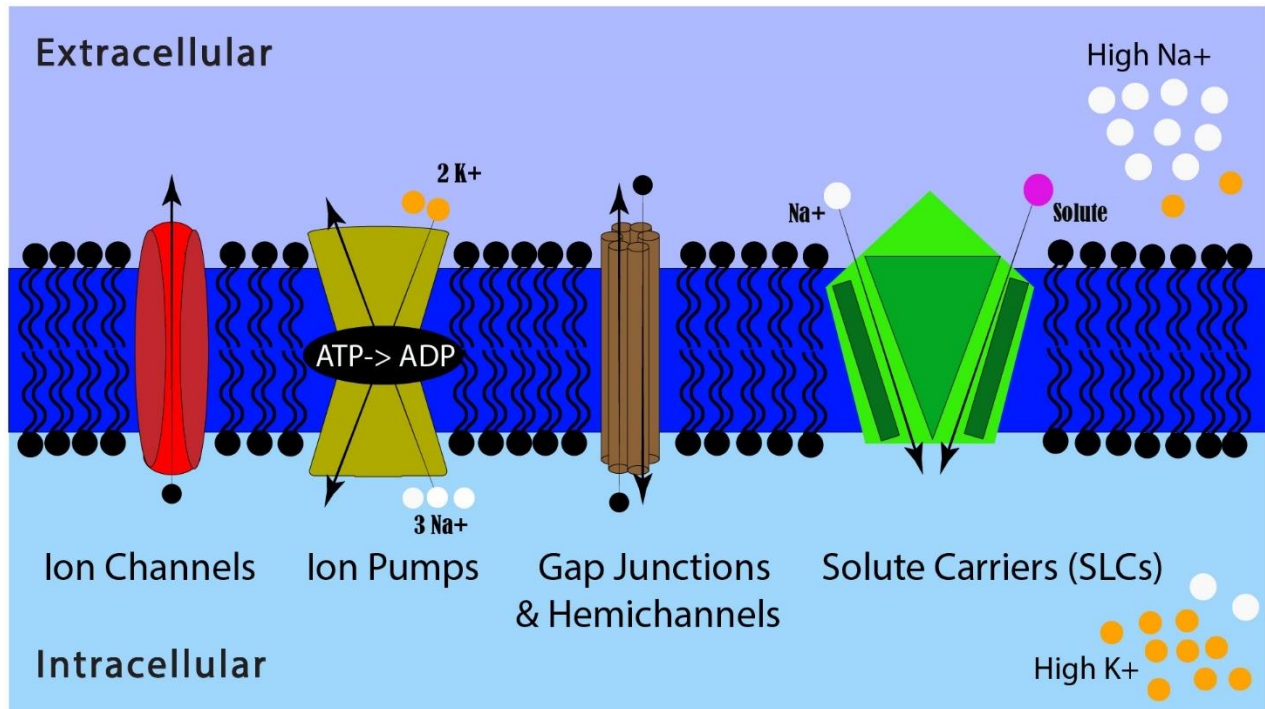


Figure 1-1 Cell membrane diagram showing ionic regulators and ionic concentrations when the cell is in a non-excitable state.

The resting potential is the overall combination of ions for a cell, but the equilibrium potential for each ion is different in different cell types, resulting in a range of resting membrane potentials [17]. Although this generally results in a range between -30 to -80 mV, resting V_m can even exceed a range of -5 mV to -150 mV depending on cell type (Table 1) [1]. These resting V_m values will fluctuate and can have small or large fluctuations. Large jumps from negative to more positive membrane potential (V_m) events are generally referred to as action potentials in neuronal and muscular signaling. These action potentials are triggered by ion channels that respond to changes in voltage reaching a certain threshold. More specifically, these events happen when action potential trains travel down an axon to a synapse repeatedly in waves, eventually passing the V_m threshold for voltage-gated ion channels [17]. These action potential waves can propagate from multiple locations and if two meet from opposing directions, they will annihilate each other [18]. While this quick (millisecond) and extreme (≥ 100 mV difference) swing in voltage caused by altering intracellular ion concentration is unique to excitatory cells, increasing evidence shows smaller and longer duration types of electrical signaling events in other, non-excitable cell types can have significant effects [19]. Changes in V_m of non-excitable somatic cells could come from

a variety of factors and would not be classified as a traditional action potential signal. Smaller and less extreme increases or decreases of V_m can occur within embryonic neural and non-neural tissues over various time periods, such as milliseconds, seconds, minutes, hours, or even days. Moreover, these could have important developmental functions [20-22]. These are the types of bioelectric signals that might be important during development, tissue patterning, regeneration, migration, and cancer [23-25].

Table 1 V_m of common cell types. [3, 17-27]

| Normal somatic cells | Millivolts (mV) |
|--------------------------------|------------------------|
| Skeletal muscle | From -90 to -70 |
| Heart Muscle | About -90 |
| Smooth muscle | From -60 to -50 |
| Glia | About -90 |
| Neuron | From -90 to -70 |
| Adrenal cortex | About -70 |
| Thyroid | From -55 to -45 |
| Kidney/ tubule | From -70 to -55 |
| Fibroblast | From -70 to -25 |
| Liver | From -55 to -35 |
| Pancreas | From -70 to -40 |
| Epithelial | From -70 to -25 |
| Melanocyte | From -50 to -40 |
| Fat | About -50 |
| Bone | About -60 |
| Proliferating cells | From -25 to -10 |
| Embryonic cells | From -25 to -10 |
| Stem cells | From -25 to -5 |
| Cancer cells and tumors | From -50 to -5 |

In addition to differences in electric potential across the cell membrane generated by the electromagnetic force of the ions, the concentration gradient of the molecules also influences V_m [16]. For example, cells contain elevated levels of intracellular potassium (K^+) and low levels of sodium (Na^+). High K^+ levels within cells are mostly established by the sodium/potassium ATPase pump (Fig. 1). This ion pump will bind three intracellular Na^+ ions, utilize ATP to change conformation via phosphorylation, and release the Na^+ into the extracellular space. Next, two extracellular K^+ will bind to this outward-facing conformation causing dephosphorylation and

reversal of conformation that allows the potassium into the cell against its concentration gradient [2, 28]. This form of active transport and the resulting electrochemical gradient is responsible for high intracellular potassium. These two ions are the main contributors to membrane potential, but Cl^- and Ca^{2+} can also influence changes, as well as other charged molecules such as H^+ . Maintenance of high intracellular potassium is critical for establishing resting V_m [29, 30]. An adult human has an estimated 45mEq/kg, (1mEq=1mmol=39mg) concentration of K^+ which ends up being about 1.76 g/kg of body weight and only about 2% is extracellular [28, 31]. This difference in concentration is hard to maintain, and potassium ions can exit the cell through a variety of leak channels (K2P) present in the plasma membrane [32]. Removal of positively charged K^+ from the cell will result in a more negative electrical charge, which would generate a force for more positive ions to be pulled back into the cell, against the chemical gradient. This constant cycling of potassium being pumped into cells and leaking out helps to establish the electric potential of resting V_m [5]. Eventually, these electric and gradient forces will reach equilibrium. This balance is mathematically described in the Nernst equation [29]. Thus, the combination of pumps and channels within the cell membrane is crucial to generate and maintaining cellular resting V_m .

1.1.2 Ion channels, gap junctions, and solute carriers

Ion channels are a group of transmembrane proteins that significantly contribute to the overall cellular bioelectricity. Channels are essentially small pores in the cell membrane that alter permeability for specific ions based on selectivity (molecular charge and size) and gating (what is required to open the channel) [33]. Since channels are simply open or closed holes in the membrane, they do not require energy to function and allow for a high rate of ion-selective transport when opened. However, they will only allow for ions to flow down their concentration gradient (moving from high to low concentration areas). The composition of these channels on the cell membrane has been compared to an electronic component called a field-effect transistor [34]. In the human genome, there are more than 400 family members of ion channels currently characterized, which accounts for around 1.5% of the genome [35]. A comprehensive list of human ion channel details can be found on the HUGO Gene Nomenclature Committee website, as well as the IUPHAR/BPS Guide to Pharmacology [36, 37].

Characterizations are based mainly on selectivity such as sodium (Na^+), calcium (Ca^{2+}), potassium (K^+), and chloride (Cl^-) though there are other channels for other charged and non-charged molecules, such as proton channels and aquaporins [38, 39]. The most direct contributors to V_m are K^+ and Na^+ , while the others play a smaller role or secondary messenger role like Ca^{2+} . Individual ion types can then be further categorized by method of gating. One group, Voltage-gated channels, will open or close when their voltage-sensitive domains detect a specific change in membrane potential, usually a large depolarization from action potentials in neurons. Another type, ligand-gated ion channels, rely on their receptor binding a specific ligand to cause or prevent ionic flow. A third category, leak channels, continually allow a small amount of potassium to leave the cell, regardless of V_m state [32]. This can have a profound impact on V_m because it can heavily impact the ion gradient. There are additional mechanisms to regulate or gate channels, such as those sensitive to temperature, mechanical force, and light [40-42]. Another interesting group of channels is inwardly rectifying potassium channels (Kir). These cause K^+ to move more easily into rather than out of a cell, which will impact concentration gradients and therefore resting membrane potential [43]. However, because the intracellular concentration of potassium is so high at rest, and this type of ion movement is against the concentration gradient, even when these are functioning it is difficult for K^+ to enter the cell and might leak out. Furthermore, different channels can show distinct levels of rectification (e.g., high, or low). This type of channel can be further regulated by the lipid PIP2 (phosphatidylinositol 4,5-bisphosphate), Mg^{2+} , polyamines, phosphorylation, or protein-protein interactions [43]. These channels are intriguing targets with multiple roles that vary through an individual organism depending on location, subtype, etc.

Although ion channels and pumps are usually the main contributors to V_m , there is a third contributor to bioelectric changes known as gap junctions [44]. Gap junctions are much larger than ion channels and will create a connection physically between adjacent cells, but they do not rely on ATP like ion pumps. They are formed by connecting proteins called connexins and pannexins in vertebrates and innexins in invertebrates (depending on the number of cys residues in their extracellular loop and glycosylation) [45]. These connexins each have their own unique properties for permeability and gating. They are composed of six individual connexin subunits on one cell that oligomerize with another six connexins of a different cell. When these connexins are not coupled to form a gap junction they are known as hemichannels [46]. The connection of the same

connexin isoform is called homogenous/homomeric but these properties can change and become more complex by the formation of heterogenous/heteromeric gap junctions [47]. The large pores generally connect cells near one another and usually do not have high selectivity for specific ions. These junctions have been found to play significant roles in cell-to-cell communication through the exchange of vesicles, ions, and even organelles [48]. Electrical synapses between neurons are considered a specialized gap junction. They have also been found needed for direct cell communication in tunneling nanotubules (TNTs) [49, 50]. The gap junction connexin 43 has been implicated in multiple organisms and diseases to contribute to electrical signaling [51]. Its misregulation has also been shown to cause birth defects and disease in both mice and humans [52, 53].

In addition to channels, pumps, and gap junctions, there is another group of ionic regulators called solute carrier proteins (SLCs). These proteins utilize secondary active transport, where thermodynamically favorable reactions (i.e., ions moving down their concentration gradient) are paired with one or more other molecules to be transported in an unfavorable reaction [54]. The free energy provided by the movement in the favorable direction makes movement in the less favorable direction possible and allows transport without the need for cellular energy. These reactions utilizing the electrochemical gradient can occur with both substrates moving in the same direction, known as symporters, or substrates moving in the opposite direction known as antiporters. This superfamily of over 450 transporter proteins is found in the plasma membrane of cells and cellular organelles. They have a large range of substrate specificity, including ions, organic ions, sugars, vitamins, amino acids, nucleotides, oligopeptides, drugs, and metals. Some SLCs can transport multiple different biomolecules, others can only transport a single biomolecule, and there remains up to 30% “orphan” proteins whose substrates remain unknown. Similarly, to other ionic regulators, SLCs have been linked to more than 190 diseases resulting in thyroid, hearing, neurological, metabolic, and congenital defects [54, 55]. Mutations in SLCs have also been found to cause alterations to pigmentation and fin size in zebrafish [56, 57]. Furthermore, there are striking changes to SLC protein expression in a variety of cancers making them enticing targets for drug treatment [58].

1.1.3 History and experimental evidence of bioelectric research

The field of neuromuscular bioelectricity has a long and diverse history [59]. Luigi Galvani is credited with demonstrating the first relationship between electricity and animals in 1780 by electrically stimulating frog limbs to cause movement. However, it was almost another hundred years before the first measurements of action potentials in 1865 by Julius Bernstein using a differential rheotome. The first intracellular electrical measurements of resting membrane in the protozoon, *Paramecium*, were performed in 1934 [60]. However, some of the most iconic research done on bioelectricity was that of Hodgkin and Katz in the giant squid axon [61]. Their intracellular recording studies paved the way for neurology and the fundamental understanding of action potentials [62]. What we know today, when an action potential train has traveled down a neuron to its synaptic terminals, it depends on the frequency and the duration of this electrical signal to cause changes to voltage-gated Ca^{2+} ion channels. When the membrane potential becomes more positive past a threshold, the voltage gate is triggered and unlocked, allowing for Ca^{2+} ions to flow into the synapse. This increased concentration of calcium in the synapse of a nerve causes changes to proteins, and intracellular vesicles, and alters the conformation of the voltage-gated channels on the membrane. The resulting calcium signal causes neurotransmitter-filled intracellular vesicles to fuse to the nerve cells' synapse membrane, resulting in diffusion into the extracellular space. These neurotransmitter molecules then bind to ligand-gated channels on the other side of the synaptic cleft to resume the electrical signal [63].

The connection between electrical signaling and Ca^{2+} is important, as Ca^{2+} is one of the most important secondary messengers in many cellular signaling processes including during development [64]. Expanding on these concepts; it is not inconceivable that other electrical signals could travel across the membranes of non-nerve cells and trigger responses, resulting in the opening or closing of ion channels. This could cause other ions to enter the cell (or be released from internal stores) and change transcriptional regulation of the machinery, protein modifications such as conformation or phosphorylation to affect function, as well as modifying anything on the plasma membrane such as receptors, kinases, and lipids [65-68]. Understanding biological electrical signaling from multiple fields and cell types could help elucidate what unknown mechanisms utilized by organisms remain. This general idea could be used to explain how

electrical signaling in non-excitatory contexts could be causing downstream changes to gene expression, cell behaviors, and/or eventual tissue organizational modifications.

1.2 Zebrafish as a superior model for bioelectric research

The zebrafish has become one of the main model organisms used in research since its debut in the 1970s [69]. These advantages can translate into a variety of fields, but it is also particularly suited to bioelectric research. Zebrafish are a powerful example of how alterations to normal endogenous bioelectricity can result in large-scale changes in adult organisms. The combination of excellent and well-established genetic tools with its transparent external embryonic development can allow for manageable mutant generation and cutting-edge microscopy to explore previously unattainable information. Additionally, their vertebrate biology with around 70% orthologous genes with humans makes them popular for studying human disease as well as in drug screens [70-74]. This can also be useful in bioelectric research as there are current efforts underway to determine which already FDA-approved ion channel drugs or drug combinations could be used to improve outcomes of amputations, regeneration of limbs, organ development, and channelopathies [75]. Furthermore, there is a large source of mutant lines available through the repository ZFIN and the greater zebrafish research community is highly collaborative. Therefore, studying bioelectricity with zebrafish could explain a variety of questions that remain. Below, I highlight bioelectric-related zebrafish studies that demonstrate the importance of the model as an optimal way to characterize, investigate, and uncover the yet-to-be-determined characteristics and mechanistic roles bioelectricity plays during development.

1.2.1 Zebrafish embryonic development

There is increasing evidence demonstrating bioelectricity is an important regulator during embryonic development. There has been some evidence for the importance of membrane potential during embryonic development [76], such as ion currents measured in a dividing *Xenopus* embryo at the cleavage furrow [77]. Using electric probes to measure electrical changes, researchers were able to detect an increase in current as the cleavage furrow formed. Electrochemical dyes have also been used with some success to demonstrate a variety of calcium and voltage changes occurring during *Xenopus* and zebrafish embryonic development [78-80]. Even though these dyes have

improved, they lack the same reliability as genetically encoded indicators for either voltage or calcium. GEVIs and GECIs have already provided improved results via sensitivity and dynamics. GCaMP6s was used in zebrafish to further validate the furrow, blastula, and gastrula-associated calcium dynamics seen with dyes [81]. GCaMP6s was able to reveal additional signals previously missed and show new calcium dynamics not seen with dyes. The importance of calcium for cleavage furrow formation has been studied, however not been directly visualized in real-time [82]. Traditionally Ca^{2+} does not play as great of a role in its contribution to membrane potential, but serves mainly as a secondary messenger [64].

In our lab, utilizing the GEVI ASAP1 (Accelerated Sensor of Action Potentials 1) we were able to show detailed cleavage furrow hyperpolarizations [83, 84]. Moreover, Vm signals were observed within unfertilized embryos meaning these could be essential even at the earliest stages of development. Membrane potential changes have been shown to influence the organization of phospholipids and these are known as critical components of the cleavage furrow and cytokinesis [68, 85, 86]. Additionally, Vm transients were seen within the superficial cells of the blastula and yolk syncytial layer (YSL). During gastrulation, Vm transients continued in the EVL, YSL, and started to occur in the deeper cells. Dynamic and complex bioelectric Vm signals were observed during the segmentation period as well. The information in this study provided for the first time a detailed understanding of real-time endogenous bioelectric signaling of tissues and structures during early zebrafish embryogenesis [84]. When compared to calcium studies, there is a partial overlap in the patterns, but it is hard to assess because of the properties of each reporter differing, as well as the imaging methods use. Furthermore, we characterized the evolution and early developmental expression of KCa (Calcium gated potassium channels) and Kir (inwardly rectifying) channels in zebrafish [87, 88]. Spatiotemporal regulation of channel expression was extensive and could vary considerably, depending on the stage of development. The presence of channels in non-neuronal cell types could also expose these channels as important regulators of embryonic development. Taken together, these studies demonstrate that diverse characteristic bioelectric activities are occurring during zebrafish embryogenesis and that this model organism is particularly well suited to illuminate these unknowns.

1.2.2 Zebrafish fin development

One prime example of the power of bioelectric signaling comes from zebrafish fin mutants [89]. The wild-type zebrafish has a bi-lobed morphology, where the dorsal and ventral lobes are slightly longer than the cleft middle region. This even, lightly forked shape, is relatively small compared to the overall body length of the fish. However, multiple mutants display either elongated or shortened fins. All these fin mutants share a common defect- modifications to normal ionic regulation via a channel, solute carrier, or connexin flaws. The lack of channel specificity resulting in similar phenotypic outcomes is an indication that it is not the channels themselves, but their functional purpose that causes changes to body patterning.

The classic long-fin zebrafish (*lof- longfin*^{l2}) is caused by the cis-ectopic expression of *kcnh2a*, a voltage-gated potassium channel [90]. The elongated fin mutant another longfin (*alf*) is caused by gain-of-function mutations in *kcnk5b*, a potassium leak channel [91]. The *schleier* fin mutant is caused by the inactivation of a K⁺ Cl⁻ co-transporter, *slc12a7a/ kcc4a* [57]. Furthermore, ectopic expression of the inward rectifying potassium channel, *kcnj13*, within somites and dermomyotome resulted in elongated fins due to a viral insertion in the non-protein-coding exon 5 (likely a cis-regulatory element) [92]. Conversely, the shortfin (*sof*) mutant is caused by a hypomorphic mutation in the gap junction, Cx43 [93]. There is also a mutant with short fins and pigmentation defects caused by a dominant missense mutation in Aqp3a (Aquaporin 3a) [39]. Another interesting case is that of the gain-of-function *rapunzel* mutant [94]. The *rpz* gene, which has an unknown function, has a long-finned phenotype in heterozygous adults. Furthermore, homozygous mutants are lethal but first develop a variety of channelopathy-like phenotypic defects such as jaw abnormalities, midface hypoplasia, abnormal hematopoiesis, and pericardial edema. These homozygous effects could be rescued with morpholino knockdown. In the context of these phenotypes, future studies might reveal the function of this protein to be related to ion regulation.

Multiple key points can be obtained from comparing these fin mutants. First, the expressed location of the ionic regulatory protein is critical. Ectopically adding functional channels where they are not normally supposed to be can impact fin size. Conversely, removing one of these proteins from its normal domain can cause the same result. Second, increasing activity like in the GOF mutants, or decreasing normal levels also leads to changes in fin size. There is a dosage effect

on expression level that can also be observed in *pax3a: kcnj13-IRES-EGFP* transgenic fish. Third, both the location and activity of these proteins are dependent on the type of ionic regulator. Since each has its own intrinsic properties and conductance, it becomes difficult to explain the bioelectric regulation as a one-size-fits-all theory as not all channels show the same degree of conductance (e.g., strong, intermediate, weak). Rather, it appears that the electric signaling mechanism is modular, where combinations of different independent parts with different properties can be used to construct and modify the bioelectric state of cell groups and tissues. Phenotypic changes resulting from a specific channel, its conductance strength, its activity level, and its expression level, might all be relevant to the situation. All these attributes might still be condensed down to the two most important questions of “when and where” or spatiotemporal regulation for fine-tuning tissues and structures. Then, the subsequent intensity of phenotypes is dependent on the previously mentioned attributes. Future studies mixing and matching ectopic/ *in situ* ionic regulators with varying degrees of function will give a better understanding of these concepts.

1.2.3 Zebrafish pigmentation

Another strong phenotypic example of bioelectricity in zebrafish development comes from pigmentation mutants. Zebrafish form distinct stripe patterns along their bodies with alternating rows of melanophores (dark pigments) and xanthophores (red-orange pigments) mixed with iridophores (iridescent pigments) [95-97]. Interactions and communication among these different pigment cells are essential to forming the stereotypical stripe patterns. Furthermore, considerable evidence has been accumulated implicating cell-cell and tissue-level communication using bioelectricity in many different cell types. The development of these normal stripe patterns can be found to be altered in many different mutant fish lines, including mutants that affect ion channels and bioelectricity. This electrical cellular communication has been partially demonstrated in Zebrafish pigments as well. When normal zebrafish pigment cells are cultured *in vitro* with voltage-sensitive dyes, contact-dependent depolarizations can be observed that result in a repulsive migration [98]. Interestingly, when the same experiment is performed with the pigment cells of the *obelix/jaguar* mutant, this repulsion is not observed and the melanophores appear consistently more depolarized. The *jaguar* mutant line has a non-functional version of the channel Kir7.1 (*kcnj13*) resulting in abnormal stripe patterning [99]. CRISPR mutations of *kcnj13* also result in

abnormal pigmentation patterning in zebrafish [92]. Another mutant, *leopard Danio*, causes a spot pattern due to a mutation in the *connexin 41.8* gene [100]. This mutation was shown to impact the ability of the protein to conduct ions, which might be responsible for the incorrect patterning. Similarly, mutations of Cx39.4 (*luchs*) cause a spotted pattern but with less effect on the caudal fins [100]. Interestingly, it was shown that these two connexins can form heteromeric in addition to homomeric gap junctions which are essential for melanophore and xanthophore cellular communication. Gap junctions and potassium channels in pigment cells are also important in the regulation of cytonemes used for transporting small molecules and ions over longer distances [49, 50]. In addition to zebrafish, when the modulatory wild-type B-subunit of the KCNQ1 channel was misexpressed in *Xenopus*, it caused neural crest pigment lineage melanocytes to hyperpigment the animal [101]. This could be another channel important for growth rates, cell patterning, and membrane potential control.

1.3 The difficulties of studying developmental bioelectricity

The phenotypic evidence for bioelectricity in development and other areas is robust, but the underlying changes to V_m and how these changes work mechanistically are unknown. The functional study of bioelectric dynamics of not just a single cell, but groups of cells, tissue regions, and even whole organisms has so far been limited. This is mostly because it has been difficult to measure endogenous electrical activity on an organismal level in a real-time and non-invasive manner. Luckily, recent advances in neuroscience have generated a variety of tools for these exact purposes. Biosensors/ genetically encoded indicators can provide us with the means to measure V_m fluctuations and even metabolic changes via fluorescence signals [102, 103]. Additionally, chemogenetic and optogenetic tools provide the means of cell-specific manipulation of bioelectricity to answer gap questions combined with fluorescent reporters [42, 104-109]. While initially developed for studying the neurons and the brain, these tools can be repurposed in other research contexts such as for studying developmental bioelectricity.

Using these new tools with this high level of control is required to study specific phenotypic changes after perturbing the system. This will allow for a deeper understanding of this type of signaling. Here, we will further discuss which of these neuroscience tools are available for

developmental-related studies and how some have already been successfully implemented resulting in novel discoveries not previously possible.

1.3.1 GEVIs and GECIs

One of the great advancements made to directly measure changes in the electrical activity of cells was the development of a variety of biosensors that can report changes in electrical activity. Genetically encoded voltage indicators (GEVIs) and genetically encoded calcium indicators (GECIs) are powerful dynamic fluorescent reporters that allow users to directly measure fluorescence intensity as an output of cellular membrane potential voltage or ionic concentrations (Table 2). Numerous advancements and variations of indicators have been developed. These GEVIs can fall into one of three categories. The first would be those that utilize voltage-sensitive domains (VSDs) within the cell membrane. They can be linked with either a single fluorescent protein (FP), dual FPs for FRET (Förster resonance energy transfer) signaling, or even bioluminescence. There are also opsin-based sensors with and without additionally combined FPs to improve brightness. Lastly, there is a group of hybrid GEVIs that utilize a combination of these different components with the addition of brighter and more photostable synthetic dyes [102].

The ability to perform optical measurements to visualize neural activity can be more advantageous than previously used methods. Traditional electrode measurements, such as patch clamp, are highly accurate but they are limited to single-cell recordings [110]. These non-invasive, endogenous fluorescent biosensors can function over multiple cells and tissues to get a collective understanding of real-time bioelectric activities versus single cells. These are also more advantageous over previously developed electrochemical dyes due to increased speed, genetic specificity, higher sensitivity, and no toxic effects [111]. The fastest GEVIs have reported speeds up to 1 ms [102]. Another advantage is the ability to provide results over longer periods of time. While these sensors offer several advantages, they do have some drawbacks. They have weaker fluorescence intensity which can make the cell-specific expression more difficult. Additionally, they have a variety of dynamic ranges and signal-to-noise ratios [102]. Together, these benefits help neuroscience study electrical signaling in neurons and brains, but they are also advantageous when studying other biological processes such as those in development. Understanding

bioelectricity during development requires real-time and non-invasive measurements over extended periods of time. Therefore, these types of biosensors are well suited to study embryonic bioelectricity.

1.3.2 Genetically encoded indicator application: visualizing electric fields across tissues and whole organisms throughout development

There has already been some successful implementation of GEVIs and GECIs into animal models to study endogenous electrical activity. In zebrafish research, these tools show promise within and outside of neuronal studies. GCaMP has previously been implemented into the zebrafish model for brain studies [112-114]. GCaMP has also been used within the brain of free-swimming larval zebrafish to show calcium dynamic signaling of transgenic animals when larvae saw paramecium swimming by their eyes [115]. GCaMP use followed in a variety of other neuronal studies. The first developmental study utilizing GCaMP6 was able to show in detail the characteristic calcium signals that occurred at different development stages in the zebrafish [81]. The cleavage furrow had increased levels of calcium signaling during the initial divisions. There were extensive transient Ca^{2+} signals that occurred during the blastula and gastrula stages as well. This study reported quantifiably more and previously unobserved Ca^{2+} activity than older studies employing calcium dyes. Thus, this study demonstrated genetically encoded indicators as a superior tool for developmental studies.

GEVIs have also been employed in the zebrafish model [116]. Our lab successfully generated a ubiquitous transgenic reporter line of ASAP1 (accelerated sensor of action potentials 1) [83, 84]. This was able to show Vm dynamics within the cleavage furrow, as well as certain tissue regions with more Vm signal such as the somites and notochord. Furthermore, we were able to observe fluorescent changes correlated with body movement and increased overall signal within a fish tumor. When we further performed a detailed characterization during development, we observed additional details not previously reported. For example, there was even more dynamic furrow signaling, an increased number of signaling events during the blastula and gastrula stages, signaling within the deep cells not previously seen, and complex Vm dynamic within the developing somites with this GEVI tool. While these are not directly comparable studies, our ASAP1 transgenic did show some similar signaling patterns to the GCaMP6s work. Additionally,

ASAP1 has been utilized in zebrafish neuronal imaging studies revealing signals within the cerebellum optic tectum and spinal cord [117, 118].

There have also been advancements for GEVIs *in vivo* in other organisms. Multiple studies have shown the utility of genetically encoded indicators in *drosophila* but have so far only been focused on neuronal-related studies [119-123]. In mice, fewer research studies have utilized GEVIs *in vivo* and have also been focused on neurological research [124-126]. In addition, *Xenopus* oocytes were used to further characterize Arclight and Arclight' but did not involve any developmental studies [127]. Their results showed that these sensors could potentially be employed to successfully characterize *Xenopus* bioelectricity during development. Even the yeast model *Saccharomyces cerevisiae* has utilized Arclight and ASAP sensors for monitoring voltage [128].

There is great promise in utilizing these tools to study bioelectricity outside of neuromuscular signaling. Though it is essential to visualize and measure these changes in electrical activity to characterize and understand how bioelectricity is utilized, the next steps will be to then change the normal signals to understand their purpose.

Table 2 List of GEVIs and GECIs

| GEVIs | Fluorescence Relationship | Fluorophore | Source |
|------------------------------|---|----------------------------|-----------------|
| VSD based | | | |
| ASAP1-3 | Hyperpolarize- brighter | GFP | [121, 129, 130] |
| ASAP4 | Depolarize- brighter | GFP | [131] |
| Marina | Depolarize- brighter | GFP | [132] |
| FlicR1 | Depolarize- brighter | RFP | [133] |
| Arclight | Hyperpolarize- brighter | GFP | [134] |
| Bongwoori | Hyperpolarize- brighter | GFP | [135] |
| Aahn | Hyperpolarize- brighter (external) | GFP | [136] |
| VSFP (x) | Depolarize- FRET increase | multiple | [137-142] |
| Mermaid | Depolarize- FRET increase | multiple | [143] |
| Nabi | Depolarize- FRET increase | UGK/ mKO | [144] |
| JEDI | Hyperpolarize- brighter | GFP | [145] |
| Opsin based | | | |
| Arch | Depolarize- brighter | GFP | [146] |
| QuasAr x | Hyperpolarize- brighter | multiple | [147-149] |
| Archon | Depolarize- brighter | GFP/RFP | [150] |
| Ace-x | Hyperpolarize- brighter | green/ RFP | [151, 152] |
| VARNAM | Hyperpolarize- brighter | RFP | [153] |
| Dye or bioluminescence based | | | |
| Voltron | Hyperpolarize- brighter | multiple- dye | [154] |
| positron | Depolarize- brighter | multiple- dye | [155] |
| hVOS | Depolarize- brighter | Green- dye | [156] |
| Voltage spy | Depolarize- brighter | Green- dye | [157] |
| LOTUS | Depolarize- FRET increase | blue/green bioluminescence | [158] |
| AMBER | Depolarize- voltage-gated luciferase increase | blue/green bioluminescence | [159] |
| GECIs | Fluorescence Relationship | Fluorophore | Source |
| GCaMPx | More Calcium- brighter | GFP | [160] |
| RGECOx / RCaMPx | More Calcium- brighter | RFP | [161] |

1.3.3 Chemogenetic and Optogenetic application: perturbing electric fields in groups of cells and tissues to study bioelectricity

Another requirement to elucidate the bioelectric signaling mystery is the direct and specific perturbation of the normal electrical state of cells and tissues. Chemogenetic and optogenetic tools are one experimental approach (Table 3) [104-106, 162-165]. These tools have so far demonstrated the capability to alter cell-specific electrical states in a variety of organisms in both more positive and more negative V_m directions allowing a high level of control. Chemogenetics function by utilizing either mutated GPCRs or ligand-gated ion channels that no longer function normally, but only in the presence of inert molecules. Optogenetics utilize light-sensitive ion channels which can only be activated by specific wavelengths of light. These tools can allow for downstream effects to be measured directly resulting from manipulations that can be linked to phenotypic changes. Moreover, the techniques described here will be essential to solidify bioelectric mechanisms when combined with additional validations.

Zebrafish models have applied a variety of tools to manipulate endogenous bioelectricity. One of the first studies to do this generated transgenic zebrafish expressing transient receptor potential (TRP) channels within Rohon–Beard and trigeminal sensory neurons under the *islet-1* enhancer [166]. TRPV1 was turned on by capsaicin, TRPM8 was activated by the addition of menthol, while TRPA1 activity required temperatures above 28°C. Activation was able to induce dose-dependent locomotion, and ablation, and alter wake-sleep behaviors. Other examples of chemogenetic tools applied to zebrafish neuron studies include PSAMs (pharmacologically selective actuator modules) expressed in horizontal cells (HCs) which connect rod and cone photoreceptors via synapses [167, 168]. These are mutated ligand-gated ion channels that can only be activated by Pharmacologically Selective Effector Molecules or PSMs. These were able to disrupt V_m in HCs resulting in altered light response and lateral inhibition in retinal ganglion cells. There is also evidence that DREADDs (Designer receptors exclusively activated by designer drugs) can be repurposed for use in the zebrafish model [169]. DREADDs are mutated GPCRs such as hM4DGi, hM3DGq, hM3DGs, and KORD that alter cellular V_m through downstream signaling changes such as intracellular Ca^{2+} release or activation of GIRK channels. Agonist treatment was able to induce dynamic ASAP2s fluorescence changes in multiple cell types using hM4DGi and hM3DGs. Furthermore, hM4DGi receptor activation in larval fish induced a hyperpigmented phenotype.

The use of optogenetics in zebrafish has been primarily targeted in neuroscience studies as well. Optogenetic tools work by exploiting light-gated ion channels. When exposed to specific wavelengths of light on expressing cells, channels open to allow specific ions in such as Na^+ , Ca^{2+} , or Cl^- into cells resulting in increased or decreased V_m . These have been used to modify swimming behavior [170], perturb hair cell sensory receptors [171], and alter olfactory responses [172]. One study demonstrated its practicality outside of the brain and within a developmental setting; inside zebrafish melanophores. ChR2 was expressed in the melanophores of zebrafish that were then placed in tanks exposed to blue light to stimulate depolarization [173]. These transgenic fish began to lose the boundaries of the normal stripe patterns. Interestingly, this was able to be partially reversed after allowing the depolarized cells to return to their normal membrane potential.

To validate the chemogenetic and optogenetic results, genetic manipulation of spatiotemporal channel expression and chemical inhibitors would be a logical next step. Deleting or expressing specific ion channels can also have the same effects when added or removed from expressing tissues or groups of cells. This has already been demonstrated, such as in the transgenic *pax3a:kcng13-IRES-EGFP* where transient ectopic expression of *kcng13* in zebrafish dermomyotome causes a long fin phenotype in adults [92]. Moreover, transient ectopic expression of multiple potassium channel genes with an *actinb* promoter could also induce elongated fins in adults. Further studies comparing the impact of different channels under multiple different tissue-specific promoters will help to better understand these phenomena. In addition to genetic manipulations, chemical treatments that can block or enhance channel function can also be useful as supporting evidence to show similar outcomes. For example, the calcineurin inhibitor FK506 was able to increase the growth rate and size of fins in both WT and *shortfin* mutants when treated after amputation but not within *kcng5b* deficient fish [174]. This same inhibitor was used on fish with fin excavations (a hole within the caudal fin) and was able to induce atypical growth within the posterior cutting edge rather than only the anterior cutting edge of untreated fish [175]. There is also evidence for other chemical treatments in *Xenopus* that could promote nerve regeneration [176], abnormal organ development [177], and craniofacial defects [178]. While chemical treatments are not ideal on their own, they can further support evidence generated through other methods.

The combination of genetically encoded indicators, chemogenetic and optogenetic tools, with the use of genetic manipulations to add or remove specific channels combined with chemical inhibition will lead to the explanation of bioelectricity outside the brain. These are necessary to solidify a deeper mechanistic understanding of bioelectricity as a bona fide developmental regulator.

Table 3 Chemogenetic and optogenetic tools

| Chemogenetic tools | Activation method | Activation result | Ref. | Optogenetic tools | Activation method | Activation result | Ref. |
|--------------------|------------------------|-------------------|-------|-------------------|-----------------------|-------------------|-------|
| hM4DGi | DREADD agonist | hyperpolarization | [179] | ChR2 | Blue light (470 nm) | depolarization | [180] |
| hM3DGq | DREADD agonist | depolarization | [179] | eNpHR3.0 | Yellow light (590 nm) | hyperpolarization | [181] |
| hM3DGs | DREADD agonist | depolarization | [179] | CoChR | Blue light (470 nm) | depolarization | [182] |
| KORD | DREADD agonist | hyperpolarization | [179] | GtACR1 | Green light (515 nm) | hyperpolarization | [183] |
| PSAM-5HT3-HC | PSEM ligand | depolarization | [184] | GtACR2 | Blue light (470 nm) | hyperpolarization | [185] |
| PSAM-5HT3-LC | PSEM ligand | depolarization | [184] | BLINK2 | Blue light (455 nm) | hyperpolarization | [186] |
| PSAM-GlyR | PSEM ligand | hyperpolarization | [184] | CheRiff | UV light (460 nm) | depolarization | [147] |
| TRPV1 | Capsaicin | depolarization | [166] | Chronos | Yellow light (500 nm) | depolarization | [187] |
| TRPM8 | Menthol | depolarization | [166] | eArchT3.0 | Yellow (570 nm) | hyperpolarization | [188] |
| TRPA1 | > 28° C | depolarization | [166] | ChrimsonR | Red light (590 nm) | depolarization | [189] |
| GluCl* | Ivermectin | hyperpolarization | [190] | | | | |
| NanoV1 | Electro-magnetic waves | bidirectional | [191] | | | | |

1.4 Conclusions and future challenges for studying V_m

Ultimately, the consequence of membrane potential and bioelectric signaling in non-excitatory cells has become evident. The ideology of electrical signaling only being vital in neuronal tissues has started to erode but is still largely present. While there is evidence that membrane potential is an important factor contributing to biosynthesis, energy storage, metabolite transportation, embryonic pattern formation, and disease, a critical mechanistic function of bioelectricity in many cellular processes has proven elusive [1, 192-195]. Discovering unknown downstream effects of V_m on different cellular mechanisms and machinery could help explain all the diverse unanswered questions. By incorporating these electromagnetic properties of charged atoms into biological roles, a much more profound relationship with living organisms and the universe around us is established.

The fact that ion channels are one of the most represented protein-coding genes can also give perspective; evolution held onto such a large amount of genetic information because of its vital functions. Something that is present in every system and cell type should be deeply considered for all possible contributions to an organism. A variety of channelopathies and cancers that up and down-regulate a huge diversity of ion channels demonstrate that ion channels and subsequent bioelectric dysregulation can significantly contribute to disease. The large amount of ion channel drugs could hopefully be repurposed in a way to mitigate these incorrect bioelectric signatures until better strategies are developed. Additionally, new therapeutic channel activation will continue to be discovered [196, 197]. Even folk medicine seems to have inadvertently discovered ion channel modulation helpful for medicinal purposes which are being re-examined [198, 199]. Furthermore, it has been shown that a pore-forming peptide from spider venom selectively targets K^+ channels by hyperpolarized cancer cells [200]. Such a treatment could help establish ion channel drugs a new class of cancer therapy treatment [201, 202]. Furthermore, cell-penetrating peptide uptake might also be reliant on membrane potential [203], warranting deeper investigation. Continually developed technology, such as wearable bioreactor devices for channel drug cocktails [75, 204], will also establish new applications for potential treatments to alter V_m .

The exact process that defines bioelectric regulation is still not well understood. One major contributor could come from maintaining high intracellular potassium, as it is crucial for regulating resting membrane potential. This is probably why potassium ion channels are frequently appearing in new studies as markers for disease [205]. Most likely the reason that the detailed mechanisms

involved have not been discovered stems from the difficulty of studying ion movement and electrical changes. While it has been known for many years that membrane potential changes are important for neuronal signaling, the depth of study on the importance of bioelectric signaling in non-neuronal tissues is still lacking. This can mostly be attributed to the difficulty of studying bioelectric interactions *in vivo*. Current modeling approaches will provide useful insight [206-209], but meticulous functional studies are still needed. Eventually, simultaneous analysis of multiple channels will be required for the clearest mechanistic understanding because of the complexity of channel cross-talk [210, 211]. Hopefully, new tools such as chemogenetic manipulators will provide functional data [167, 169], as this will complement already successful optogenetic manipulations as a complementary approach [108, 173, 212]. Additionally, genetically encoded voltage indicators (GEVIs), calcium indicators (GECIs), and related tools such as potassium reporters (GINKO1) will assist in visualizing these important changes [81, 83, 117, 118, 213]. Studying V_m , the composition of all channel and ionic regulator activity, should increase our understanding of bioelectric mechanisms and narrow down what channels are the most important contributors. Future works looking at how bioelectricity plays a role in well-known biological events such as embryonic development, cell cycle progression, and cancer growth are sure to cause unprecedented developments in our understanding of living organisms.

CHAPTER 2. VISUALIZATION OF CELLULAR ELECTRICAL ACTIVITY IN ZEBRAFISH EARLY EMBRYOS AND TUMORS

2.1 Abstract

Bioelectricity, endogenous electrical signaling mediated by ion channels and pumps located on the cell membrane, plays important roles in the signaling processes of excitable neuronal and muscular cells and many other biological processes, such as embryonic developmental patterning. However, there is a need for *in vivo* electrical activity monitoring in vertebrate embryogenesis. The advances in genetically encoded fluorescent voltage indicators (GEVIs) have made it possible to provide a solution to this challenge. Here, we describe how to create a transgenic voltage indicator zebrafish using the established voltage indicator, ASAP1 (Accelerated Sensor of Action Potentials 1), as an example. The Tol2 kit and a ubiquitous zebrafish promoter, *ubi*, were chosen in this study. We also explain the processes of Gateway site-specific cloning, Tol2 transposon-based zebrafish transgenesis, and the imaging process for early-stage fish embryos and fish tumors using regular epifluorescence microscopes. Using this fish line, we found that there are cellular electric voltage changes during zebrafish embryogenesis, and fish larval movement. Furthermore, it was observed that in a few zebrafish malignant peripheral nerve sheath tumors, the tumor cells were generally polarized compared to the surrounding normal tissues.

2.2 Introduction

Bioelectricity refers to endogenous electrical signaling mediated by ion channels and pumps located on the cell membrane [2]. Ionic exchanges across the cellular membrane, and the coupled electrical potential and current changes, are essential for the signaling processes of excitable neuronal and muscular cells. In addition, bioelectricity and ion gradients have a variety of other important biological functions including energy storage, biosynthesis, and metabolite transportation. Bioelectrical signaling was also discovered as a regulator of embryonic pattern formation, such as body axes, the cell cycle, and cell differentiation [2]. Thus, it is critical for understanding many human congenital diseases that result from the misregulation of this type of

signaling. Although patch clamp has been widely used for recording single cells, it is still far from ideal for the simultaneous monitoring of multiple cells during embryonic development *in vivo*. Furthermore, voltage-sensitive small molecules are also not ideal for *in vivo* applications due to their specificities, sensitivities, and toxicities.

The creation of a variety of genetically encoded fluorescent voltage indicators (GEVIs) offers a new mechanism to overcome this issue, and allows for easy application to study embryonic development, even though they were originally intended for monitoring neural cells [214, 215]. One of the currently available GEVIs is the Accelerated Sensor of Action Potentials 1 (ASAP1) [129]. It is composed of an extracellular loop of a voltage-sensing domain of voltage-sensitive phosphatase and a circularly permuted green fluorescent protein. Therefore, ASAP1 allows visualization of cellular electric potential changes (polarization: bright green; depolarization: dark green). ASAP1 has 2 ms on-and-off kinetics and can track subthreshold potential change [129]. Thus, this genetic tool allows for a new level of efficacy in real-time bioelectric monitoring in live cells. Further understanding of the roles of bioelectricity in embryonic development and many human diseases, such as cancer, will shed new light on the underlying mechanisms, which are critical for disease treatment and prevention.

Zebrafish have been proven a powerful animal model to study developmental biology and human diseases including cancer [72, 216]. They share 70% orthologous genes with humans, and they have similar vertebrate biology [70]. Zebrafish provide relatively easy care, a large clutch size of eggs, tractable genetics, easy transgenesis, and transparent external embryonic development, which make them a superior system for *in vivo* imaging [72, 216]. With a large source of mutant fish lines already present and a fully sequenced genome, zebrafish will provide a relatively unlimited range of scientific discoveries.

To investigate the *in vivo* real-time electrical activity of cells, we take advantage of the zebrafish model system and ASAP1. In this paper, we describe how to incorporate the fluorescent voltage biosensor ASAP1 into the zebrafish genome using Tol2 transposon transgenesis, and visualize cellular electrical activity during embryonic development, fish larval movement, and in tumors.

2.3 Protocol

The zebrafish are housed in an AAALAC-approved animal facility, and all experiments were carried out according to the protocols approved by the Purdue Animal Care and Use Committee (PACUC).

2.3.1 Tol2 Transposon Plasmid Construct Preparation

NOTE: Tol2, a transposon that was discovered in medaka fish, has widely been used in the zebrafish research community [217, 218]. It has been successfully adopted to the Gateway site-specific recombination-based cloning system and is known as the Tol2 kit [219]. The Tol2 kit allows for a more convenient way of creating customized expression constructs, while also increasing the efficiency of transgenesis. Thus, it was an easy decision to take advantage of this system and create a ubiquitous ASAP1 expression zebrafish line using a validated *ubiquitin* promoter to drive ASAP1[220].

1. Creating a middle entry ASAP1 construct: pDONR221-ASAP1

1. Acquire the genetically encoded voltage sensor ASAP1 construct, pcDNA3.1/Puro-CAG-ASAP1 (Plasmid#52519), from Addgene. To amplify the ASAP1 coding region, set up a PCR using the customized primers (attB1-ASAP1F and attB2-ASAP1R) flanked with attB sequences at the 5' end of the primers (Figure 2-1). Phusion DNA polymerase was chosen for its high efficiency, and PCR conditions were optimized based on the previously published protocol [221].
2. Load the 50 μ L PCR products into a 1% TAE gel using a regular pipette with 200 μ L tips, and perform electrophoresis at 160 V in a horizontal gel tank for about 30 min.
3. Check the gel under a UV transilluminator (353 nm), excise out the desired band using a blade/scalpel under a UV transilluminator as previously published [222, 223], and put the DNA-containing gel sample into a clean 1.5 mL microcentrifuge tube.
4. Perform gel purification for the ASAP1 PCR products. Recover the DNA in the excised gel using a commercial DNA gel purification kit following the manufacturer's instruction, and elute the DNA into 20 μ L of water. Take 1 μ L as a sample, and measure the DNA

concentration using a spectrophotometer. Follow the software instructions using water as a blank control [224].

5. Take 100 ng of purified PCR product and mix it with 150 ng of pDONR221 plasmid in 10 μ L of TE buffer (10 mM Tris, 1 mM EDTA pH 8.0) [225]. Add 2 μ L of BP Clonase II into the reaction and incubate the reaction at room temperature overnight.
6. On the second day, add 1 μ L of proteinase K into the reaction and incubate the reaction at 37 °C for 30 min.
7. Perform transformation. Transfer the reaction and mix it with 50 μ L of Top10 competent *E. coli* cells and incubate the cells on ice for 30 min. Then, transfer the reaction tube into a 42 °C water bath for 1 min. Immediately remove the tube and incubate on ice for 2 min. Next, put the tube into a 37 °C shaker and incubate it for 1 h.
8. Take the tube out and plate the cells onto a kanamycin LB plate. Next, incubate the plate overnight (16-18 h) at 37 °C.
9. Pick single and well-separated colonies and inoculate them into 14 mL cell culture tubes with 3 mL of LB medium. Culture them overnight at 37 °C in a shaker with a rotation speed of 250 rpm (rotation per minute).
10. Perform miniprep using a commercial miniprep kit following its instruction manual [226].
11. Sequence 3-4 plasmids with Sanger sequencing to identify positive pDONR221-ASAP1 clones using M13F and M13R sequencing primers.

2. Creating the Tol2 construct for microinjection: pDestTol2-ubi-ASAP1

1. Choose the sequencing verified pDONR221-ASAP1 clone and measure its DNA concentration using a spectrophotometer following the software instruction using water as a blank control [224].
2. Take 100 μ g of pDONR221-ASAP1 and mix it with 100 μ g of Tol2 kit 5-end plasmid (pENTR5'_ubi, Addgene #27320), 100 μ g of p3E- polyA (Tol2 kit #302) and 150 μ g of pDestTol2pA2 (Tol2 kit #394). Adjust total volume to 8 μ L using TE buffer (10 mM Tris, 1 mM EDTA, pH 8.0) in a 1.5 mL microcentrifuge tube and mix well by a 2-5 s brief vortex. Then, add 2 μ L of LR Clonase II plus, and incubate the reaction at room temperature overnight.
3. On the second day, add 1 μ L of proteinase K into the reaction using a 10 μ L pipette and

incubate the reaction at 37 °C for 30 min.

4. Perform transformation and identify positive clones as described above (steps 1.1.7-11).
5. Measure the DNA concentration of sequencing verified pDestTol2-ubi-ASAP1 clone (Figure 2-1B) using a spectrophotometer [224]. Usually, the concentration is around 200ng/μL.

2.3.2 Prepare Tol2 Transposase mRNA and Injection Solution

1. Streak *E. coli* glycerol stock of pCS2FA-transposase plasmid (Tol2 kit #396) onto an LB plate (with 100 μg/mL ampicillin) using a sterilized inoculation loop. Incubate the plate at 37 °C in an incubator overnight. The next day, pick a single colony and inoculate it into 3 mL of LB (100 μg/mL ampicillin) using a sterilized 10 μL pipette tip. Culture it overnight at 37 °C in a shaker with a rotation speed of 250 rpm.
2. Perform miniprep on the *E. coli* culture using a commercial miniprep kit following its instruction manual. Elute plasmid DNA into 30-50 μL of TE buffer in a 1-minute centrifuge at 14,000 rpm, and measure its DNA concentration with a spectrophotometer.
3. Linearize 1-2 μg of plasmid with Not I endonuclease and purify the DNA with a DNA cleaning kit following its instruction manual after Not I digestion. Elute the DNA into 5 μL of water by centrifuging at 14,000 rpm for 1 minute. The expected concentration is about 200-300 ng/μL.
4. Perform *in vitro* transcription with Not I linearized pCS2FA-transposase as a DNA template using a commercial SP6 transcription kit.
5. Once the reaction is finished, purify Tol2 transposase mRNA using a commercial RNA cleaning kit following the manufacturer's instructions. Finally, elute mRNA into 20 μL RNase-free water and measure the RNA concentration in a spectrophotometer. The expected concentration is about 1-3 μg/μL. Samples can be stored in a -80 °C freezer if needed.
6. Prepare the microinjection solution by mixing 20 ng/μL pDestTol2-ubi-ASAP1 and Tol2 transposase mRNA (100 ng/μL) in a microcentrifuge tube by pipetting. To prevent nucleic acid degradation caused by repeated thawing and refreezing, aliquot 6 μL per tube and store it in a -80 °C freezer for future use.

2.3.3 Microinjection

1. Set up 4-6 breeding tanks with at least 2 males and 2 females in the afternoon before injection. These fish must not be fed in the afternoon. This step will reduce the amount of fish waste and save time to clean them out the next morning, while also helping to induce a breeding response.
2. The following morning, remove the prepared injection solution (pDestTol2-*ubi*-ASAP1 construct and Tol2 mRNA) from the -80 °C freezer, and place it on ice.
3. Pull the dividers in the fish breeding tanks and allow the fish to mate. In general, fish lay eggs within 20-30 minutes after pulling out the divider. If not, wait 1-2 hours longer. Some fish may not lay eggs at all. In this case, repeat this experiment for fish embryo collection.
4. While waiting, make sure there are needles prepared with the tip broken at an angle creating a beveled edge with forceps, or by breaking on a delicate task wiper.
 1. Pull needles from the capillary glass on a micropipette puller using the following parameters: heat 545; pull 60; velocity 80; time 250; pressure 500. Break the needle with forceps underneath a dissection scope (with an eye-piece ruler for diameter estimation) by holding the forceps at an angle of approximately 45°. Desired needle diameters can be variable depending on the microinjector settings, but a smaller diameter is preferred for decreasing embryo mortality.
5. Once the fish have laid eggs, collect them in a 10-cm diameter Petri dish and bring them to the dissection scope. Remove all abnormal embryos and fish waste.
6. Pipet the fertilized embryos into the prepared 3% agarose injection mold. Remove excess water to help keep the embryos in place.
7. Once all of the rows are filled with viable embryos, arrange them so that the single cells all face the same direction toward the needle, which is about a 45° angle horizontally. This will make injection much easier later.
8. While wearing gloves, use a 20 µL loading pipet tip and remove 5 µL of the prepared construct from the tube on ice.
9. Carefully insert the tip into the back end of the broken capillary tube all the way to where it begins to taper, to get the reagent as close to the tip. If there are still air bubbles, shake the needle, making sure to not break the tip.

10. Insert the needle straight into the microinjection needle holder and carefully tighten it until the needle stays in place. Adjust the angle to about 45°.
11. Once the needle is prepared and attached, turn on the microscope and gas pressure tank. Commercial CO₂ tanks are generally good for this purpose. The injection volume is adjusted by the holding and ejection pressure: approximately 0.5 psi for holding and 30 psi for ejection. Be sure to check that the solution comes out when pressing the pedal.
12. Using a stage micrometer with a drop of mineral oil, adjust the volume and flow of the solution to ~150 µm in diameter (about 2 nL). Ensure that the back pressure will let a small amount drip out of the needle. If there is not enough back pressure, capillary action will cause liquid to enter the needle and destroy the mRNA.
13. Once the needle is calibrated, begin injecting the construct into the single cell of the fertilized embryos.

NOTE: This takes a large amount of practice, patience, and finesse, due to the cell membrane being hard to pierce. It is important to inject the solution into the cell, not the yolk, for generating transgenic zebrafish. This is different from morpholino injection. It does not matter which side the needle enters the cell as long as the construct goes into the cell. Transgenesis will have a very low rate of success if injected into the yolk instead of the cell. Single-cell stage injection is also important, or somatic chimera fish will be created. This will reduce the chance of the transgene going into the germ cells.
14. Use the edge of the gel notch to provide a backing that keeps the embryo in place and allows the needle to apply pressure without moving the embryo. Once the tip of the needle is in the single cell, press the pedal to release the desired amount of solution. Repeat this process for all of the embryos.
15. When completed, transfer the injected embryos into a labeled dish by rinsing them out of the agarose notch with fish system water and a disposable 3.4 mL transfer pipette. Store the embryos in a 28.5 °C incubator to let them develop. Check back throughout the day removing dead fish embryos and replace water with 0.1% methylene blue in fish water.
16. Around 6-8 hours after injection, take 10 individual injected fish embryos and prepare genomic DNA from them using the Hotshot method [227].

17. The following morning, use a dissection microscope with a fluorescence light source to sort out the embryos showing GFP in the non-yolk tissues. These fish embryos should contain the injected construct.
18. Perform Tol2 excise assay to check the transposon activity as described previously [228]. If excised plasmid can be detected, keep the injected fish embryos, and raise them. If no excised plasmid can be detected, repeat the Tol2 mRNA synthesis and microinjection process until achieving the positive results of the Tol2 excise assay.

2.3.4 Establish Transgenic ASAP1 fish, Tg (*ubi*: ASAP1)

1. Raise the injected fish (F₀ generation) to adulthood as described previously in the zebrafish book [229]. This usually takes about 4 months.
2. Take a single adult F₀ fish and cross it with a single opposite-gender wild-type fish. Collect fish embryos after breeding later in the day. Keep the collected fish embryos in the 28.5 °C incubator in fish water with 0.1% methylene blue.
3. On the third day, check the fish embryos underneath a fluorescent dissection microscope with a GFP filter. Sort out green fish embryos, if there are any, and raise them to adulthood as F₁ generation transgenic fish, Tg (*ubi*: ASAP1).

NOTE: Mendelian ratio is not expected since most of the parental F₀ fish are germ-line genetic chimeras.

4. Cross single F₁ adult fish with wild-type fish and collect fish embryos. Sort out green fish embryos and raise them to adulthood as F₂ generation fish.

NOTE: Green and non-green fish embryos should be close to 1:1 if there is a single transgene.

5. To view electric potential changes in tumor-like malignant peripheral nerve sheath tumors (MPNST), cross the F₂ generation Tg (*ubi*: ASAP1) fish with *rpl35^{hi258/wt}* fish. It is known that visible tumors start to be found in 6-8 month old adults [230, 231].

2.3.5 Imaging

1. To image zebrafish embryos, take multiple F₂ generation founder fish and cross them with wild-type fish in individual pairs. Collect fish embryos at different desired developmental

- stages according to the zebrafish staging guide [232].
2. For the early stages of fish embryos, peel and remove chorions of the embryos carefully using a pair of forceps under a dissection scope in a 10-cm diameter Petri dish with fish system water.
 3. Transfer a few fish embryos onto a concaved glass slide with 3% methylcellulose using a 3.4 mL disposable transfer pipette. Adjust the embryos to the desired positions to view the cellular GFP activity using a needle underneath a fluorescent dissection scope.
 4. For the moving stages of fish embryos (older than 12 somite stage), use 0.05% tricaine mesylate to anesthetize the fish embryos before transferring them to slides. Briefly, fish embryos were emerged into 0.05% tricaine mesylate in fish water until they stopped swimming and lost body balance. Also, add a drop of 0.05% tricaine mesylate with the methylcellulose on the slide.
 5. For less than 12 somite-stage fish embryos, use an epi-fluorescence compound microscope with a compatible camera and software for imaging. For older than 12 somite stage fish embryos, use a fluorescence dissection microscope.
 6. To image tumor cell voltage, first identify the fish with MPNST tumors. Then, anesthetize the fish with 0.05% tricaine mesylate. For whole-mount imaging, put the fish into a 10-cm diameter Petri dish. To view the tumor cell electrical activity, fish tumors may be dissected out after whole-mount imaging.

2.4 Representative Results

In a successful injection, more than 50% of injected fish embryos will display some degree of green fluorescence in the somatic cells, and most of them will be positive by Tol2 transposon excise assay (Figure 2-2). After 2-4 generations of out-cross with wildtype fish (until the fluorescent fish reach 50%, the expected Mendelian ratio), the transgenic fish were used for the imaging experiment to track cell membrane potentials during embryonic development. First, membrane potential changes were examined throughout the cell cycle during zebrafish's early embryonic developmental stages. It was observed that the cells hyperpolarized before the cleavage furrow formation (Figure 2-3A-3C, and Supplementary Video 2-1). Moreover, different tissues showed a variety of membrane potentials in 1-3 day old fish embryos. (Figure

2-3D-3G). For example, the somites and notochord are generally hyperpolarized, compared to the adjacent tissues/organs. Once the zebrafish embryos were able to move, we were also able to detect the neuromuscular electrical activities (Figure 2-4, Supplementary Video 2-2). As bioelectric properties of cancer cells could be altered, we took advantage of this ASAP1 reporter fish and crossed it with an *rpL35* gene mutant, which is prone to spontaneous malignant peripheral nerve sheath tumors [230, 233, 234]. Although only a few fish tumors were examined, due to the long potential growth period for the fish tumor mutant, it was noticeable that there were voltage differences between tumors and surrounding tissues in live tumor-bearing zebrafish (Figure 2-5). Thus, these representative results demonstrated the successful generation of a cellular electric reporter fish line, and its potential application to developmental and cellular biology.

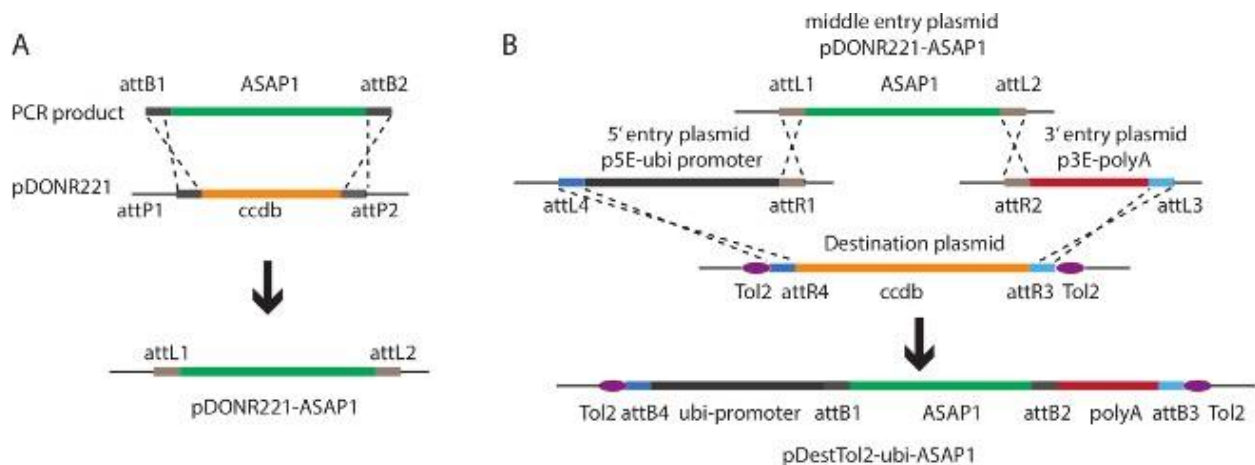


Figure 2-1 Illustration of the Tol2 transposon-based plasmid construction.

(A) BP recombination was used for ASAP1 sub-cloning into the pDONR221 middle entry vector. attB sequences were added to the 5-end of the primers for ASAP1. (B) Diagram for Tol2 transposon-based construct assembling based on LR recombination. Purple oval shape shows Tol2 inverted repeats. The dashed lines indicate homologous recombination.

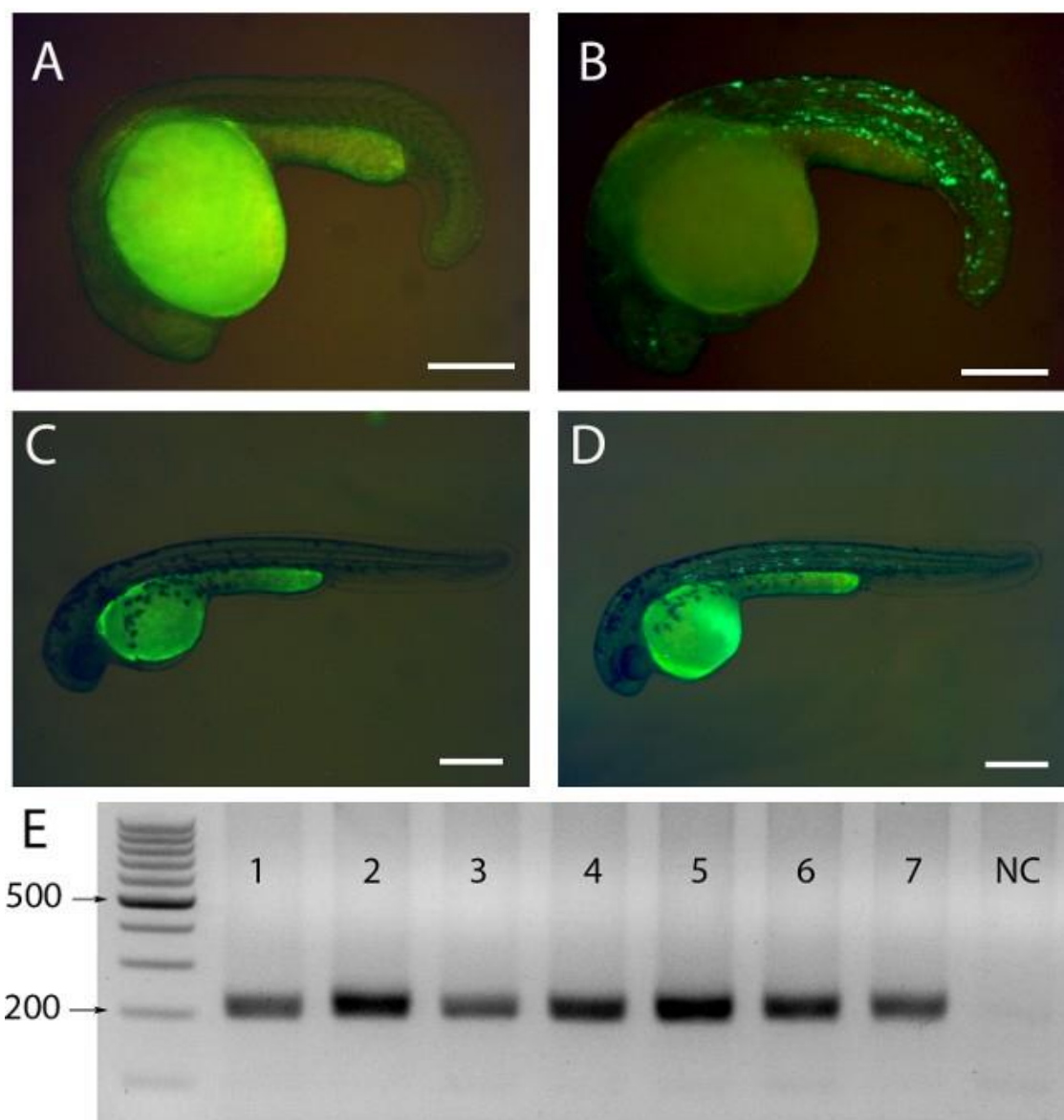


Figure 2-2 Typical results of injected embryos by epifluorescence and Tol2-excision assay.

(A) Non-positive 1dpf fish embryo. (B) Successfully injected 1dpf fish embryo. GFP spots are evident in the trunk. (C) Non-positive 2dpf fish embryo. (D) Successfully injected 2dpf fish embryo. GFP spots are evident in the trunk. (E) A representative result of Tol2 excision assay. Lane 1-7 PCRs were amplified from 7 randomly selected fish embryos 8 hours after injection. The last one is a negative control (NC) without any genomic DNA. Scale bar = 250 μ m.

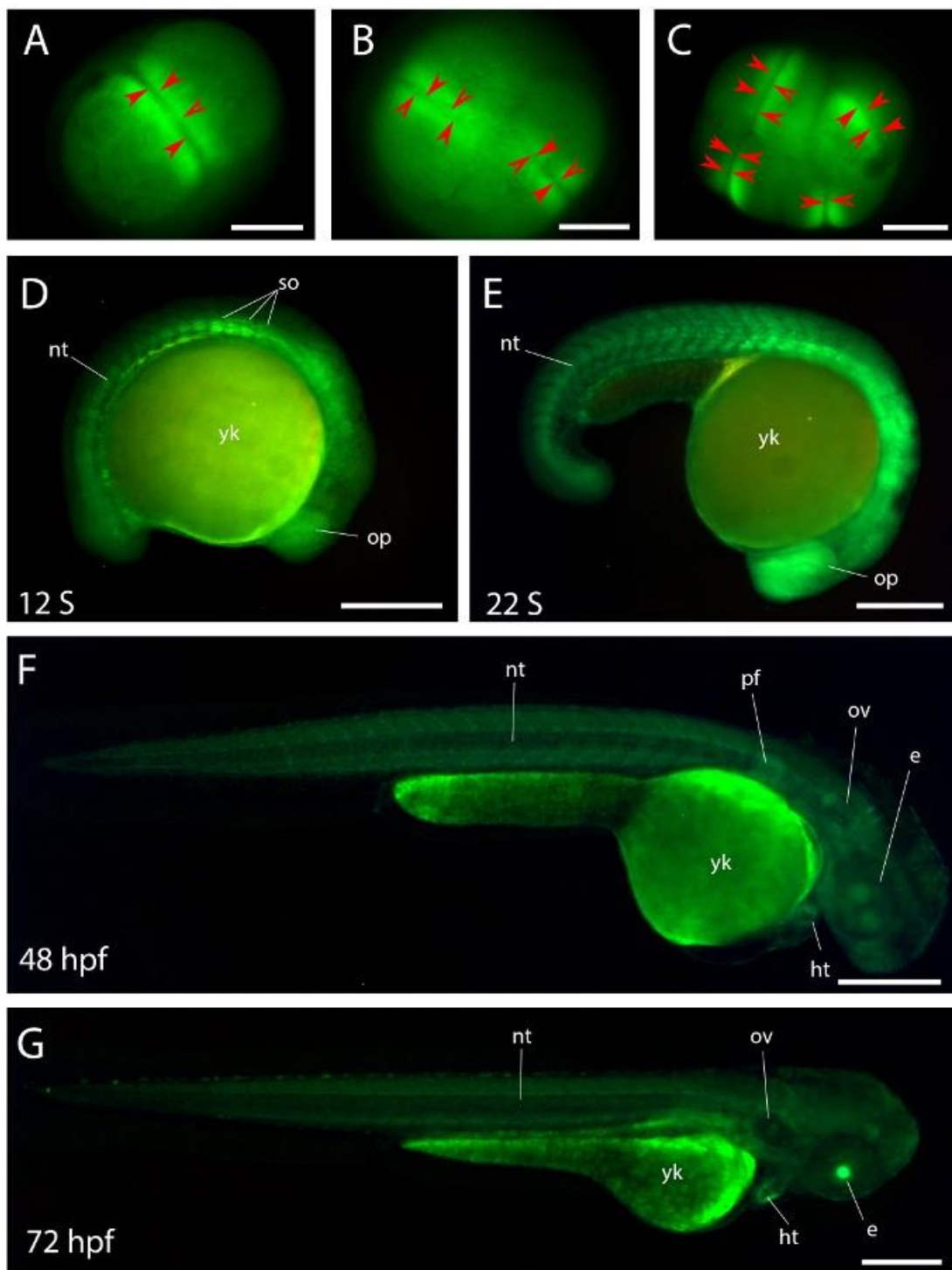


Figure 2-3 Dynamic voltage changes during zebrafish embryo development.

(A-C) Differential cellular voltage polarity during mitosis in the fish embryos. (A) 2-cell stage zebrafish embryo. (B) 4-cell stage embryo. (C) 8-cell stage embryo. The red arrowheads indicate the positions of the cleavage furrows in the panels (A-C). The changes are also evident in the corresponding movie (Supplementary Video 2-1). The region around the cleavage furrow is more polarized compared to the rest of the cell. (D-G) Dynamic electric voltage changes in the different early stages of zebrafish embryos. (D) 12-somite stage. (E) 22-somite stage. (F) 48 hours post fertilization. (G) 72 hours post fertilization. *e*, eye; *ht*, heart; *nt*, notochord; *op*, optic vesicle; *ov*, otic vesicle; *pf*, pectoral fin; *so*, somite; *yk*, yolk. Scale bar = 250 μ m.

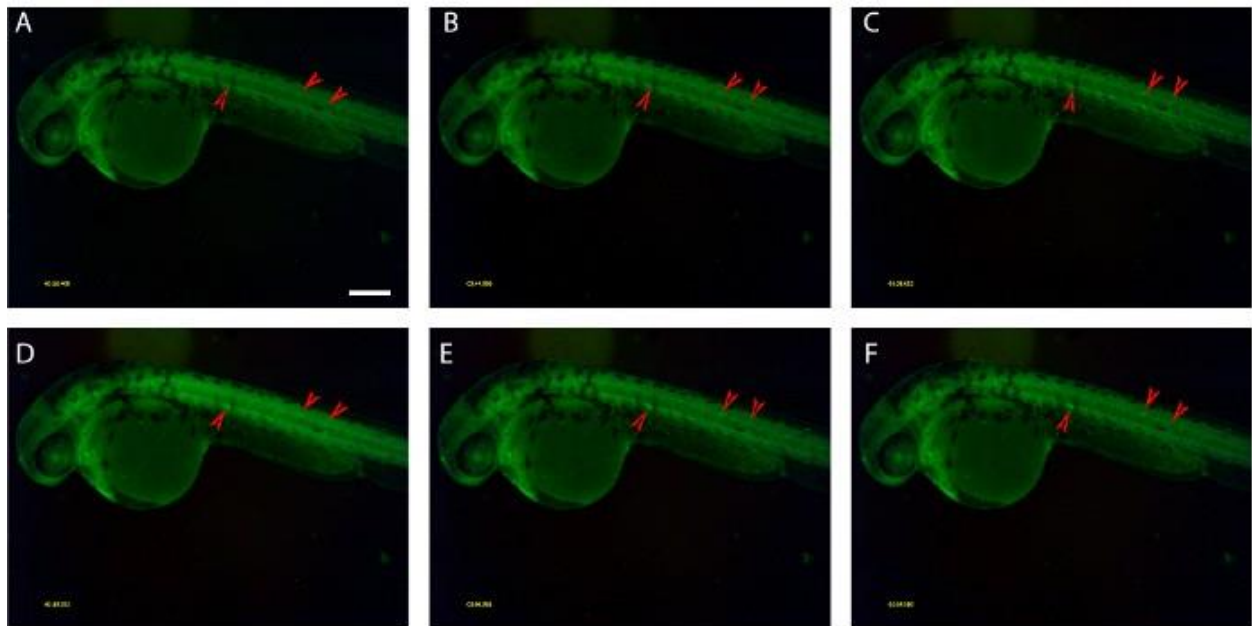


Figure 2-4 Electrical voltage changes of the fish body during fish embryo movement.

2-day old fish embryos show neuro-muscular electric activities during movement. (A) - (F) Sequential imaging of the same fish embryo. Color density changes are corresponding to the electric signaling transduction. The interval time between two consecutive images is about 12.4 milliseconds. The red arrows indicate the positions where voltage changed during the imaging period. The changes are also evident in the corresponding movie (Supplementary Video 2-2). All the panels are on the same scale. Scale bar = 250 μ m.

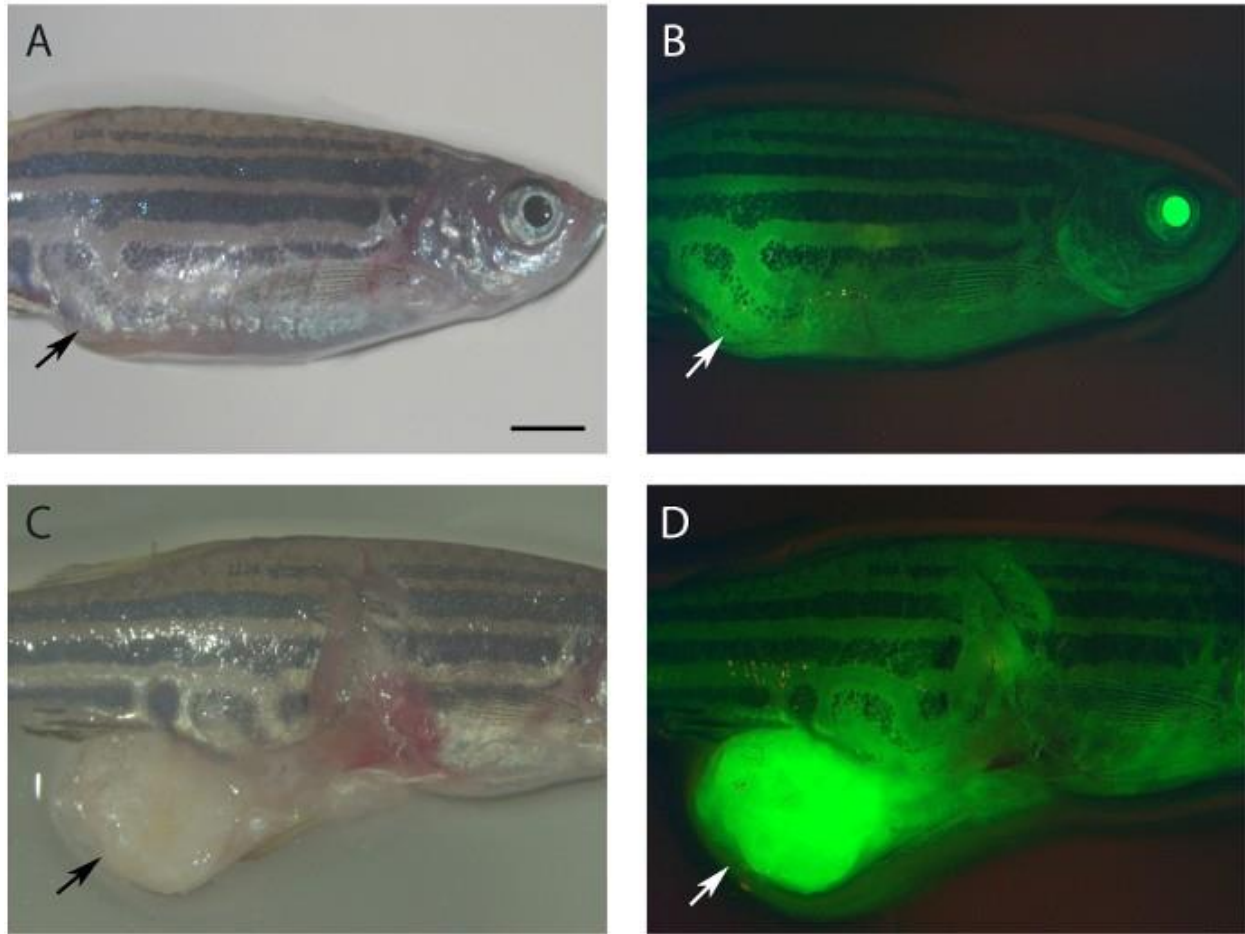


Figure 2-5 Tumor cells tend to be more polarized.

A 10-month old fish (*rpL35^{hi258/wt}*; Tg(*ubi*: ASAP1) developed a malignant peripheral nerve sheath tumor in the abdomen. (A) & (C) Bright field image. (B) & (D) Image with GFP channel. (A) & (B) Intact fish. (C) & (D) Abdomen tumor was dissected out. Tumor cells are more polarized (brighter green) compared to surrounding tissues (dark green). Arrow heads show the tumors. All the panels are in the same scale. Scale bar = 25 mm.

2.5 Discussion

Although the cellular and tissue level electrical activities during embryonic development and human disease were discovered a long time ago, the *in vivo* dynamic electrical changes and their biological roles still remain largely unknown. One of the major challenges is to visualize and quantify the electrical changes. Patch clamp technology is a breakthrough for tracking single cells, but its application to vertebrate embryos is limited because they are composed of

many cells. The current chemical voltage dyes are also not ideal due to their sensitivities, specificities, and toxicities. The recent efforts on the invention of GEVIs provide us with a new path to visualize cellular electric activities *in vivo* in real-time time. Here, we showed the process of creating a zebrafish electric reporter line, Tg (*ubi*: ASAP1).

Using this reporter fish line, we show cellular electrical activities that can be monitored in zebrafish embryos. The electric voltage change is highly related to the cell cycle during early embryonic development. We have observed that hyperpolarization happens before the formation of the cleavage furrow/cell division (Figure 2-3). This is in contrast to the current knowledge that depolarization happens before cell division [235]. Thus, more details of cell membrane voltage changes during the cell cycle of other animal and human cells, and whether this is related to tissue context, require further studies. Related studies are currently underway in our laboratory. Moreover, we have verified that ASAP1 is able to track physiological voltage changes in the neural-muscular system (Figure 2-4), in which the alteration is relatively fast compared to the changes during cell cycles.

It was also demonstrated that this reporter can also be used to visualize zebrafish tumors (Figure 2-5). It was interesting to find tumor cells were generally more polarized compared to the surrounding normal tissues. However, whether this is a general phenomenon for all malignant tissues requires further investigation, due to the limitation of tumor samples and fish tumor types in this study. Future investigations on cell membrane polarization and voltage quantification on other types of tumors and human cancer cells will be informative for better understanding its roles during tumorigenesis.

In this protocol, we chose a ubiquitous promoter to drive ASAP1 expression to track all the cells in fish embryos. Tissue or organ-specific promoters could be another option if only a certain cell/tissue type is preferred. The ASAP1 voltage sensor is a relatively well-characterized biosensor, and it is composed of a voltage-sensitive domain of sea squirt voltage-sensitive phosphatase (S3-S4 loop) and a circular permutation of GFP (default is low

fluorescence). It was reported to be expressed on the outside cellular membrane in human neuron cells and mouse brain slices^{4,27,28}. The brightness of the sensor is dominantly determined by the conformational positions of the S3-S4 loop and GFP. The rapid green fluorescence change was unlikely caused by protein concentration, due to the speed of the brightness changes and protein synthesis. However, the transgene, ASAP1, may have altered expression in tumor cells, due to the nature of genomic instability. In addition to ASAP1, other GEVIs, such as archaerhodopsin-based voltage indicators (QuasAr1 and QuasAr2), may also be a good complementary option, since they use a completely different mechanism and they also have a high sensitivity and speed [147]. In addition, their emission is in the red color range. This makes them particularly complimentary to the green ASAP1, if there is already another fluorescent protein in the same cell. For example, ASAP1 and QuasAr can be combined with Fucci zebrafish [236] for studying the relationship between cell cycle and electric potential changes.

CHAPTER 3. ZEBRAFISH EMBRYOS DISPLAY CHARACTERISTIC BIOELECTRIC SIGNALS DURING EARLY DEVELOPMENT

3.1 Abstract

Bioelectricity is defined as endogenous electrical signaling mediated by the dynamic distribution of charged molecules. Recently, increasing evidence has revealed that cellular bioelectric signaling is critical for regulating embryonic development, regeneration, and congenital diseases. However, systematic real-time *in vivo* dynamic electrical activity monitoring of whole organisms has been limited, mainly due to the lack of a suitable model system and voltage measurement tools for *in vivo* biology. Here, we addressed this gap by utilizing a genetically stable zebrafish line, Tg (*ubiquitin: ASAP1*), and ASAP1 (Accelerated sensor of action potentials 1), a genetically encoded voltage indicator (GEVI). With light-sheet microscopy, we systematically investigated cell membrane potential (V_m) signals during different embryonic stages. We found cells of zebrafish embryos showed local membrane hyperpolarization at the cleavage furrows during the cleavage period of embryogenesis. This signal appeared before cytokinesis and fluctuated as it progressed. In contrast, whole-cell transient hyperpolarization was observed during the blastula and gastrula stages. These signals were generally limited to the superficial blastomere, but they could be detected within the deeper cells during the gastrulation period. Moreover, the zebrafish embryos exhibit tissue-level cell V_m signals during the segmentation period. Middle-aged somites had strong and dynamic V_m fluctuations starting at about the 12-somite stage. These embryonic stage-specific characteristic cellular bioelectric signals suggest that they might play a diverse role in zebrafish embryogenesis that could underlie human congenital diseases.

3.2 Introduction

All living cells have a membrane potential (V_m), making bioelectricity an essential property of life. Bioelectricity is endogenous electrical signaling mediated by the dynamic distribution of charged molecules [1-4]. The importance of bioelectric regulation has been shown in various fields such as neuromuscular, embryogenesis, cancer, wound healing, regeneration, tissue patterning,

and cell migration [192, 193, 205, 237]. The critical functions of electrical signaling during early embryonic development have been proposed for years, mainly based on indirect results. Mutations in a variety of ion channels and other regulators of charged molecules have been shown to cause a vast range of phenotypes, such as alterations to normal limb formation, craniofacial malformations, as well as heart and neurological disorders in multiple distinct species [238-241]. For example, the injection of *KCNA5* mRNA into *Xenopus* embryos induced the growth of ectopic eyes [242]. In addition, we recently found that transient ectopic expression of *kcnj13* in the somites can cause a long-finned phenotype in adult zebrafish [92]. Furthermore, changes to channels and gap junctions can alter normal pigment patterning [57, 90, 91, 243, 244]. All these results point to bioelectric signals playing an essential role in normal embryonic development. However, systematic real-time direct evidence of bioelectricity during vertebrate embryonic development has been lacking. Although, electrochemical dyes and electric probes in *Xenopus* embryos give some indications of the role bioelectricity plays in embryonic development [77, 79]. The main reasons for this lack of data are the limitations of the model system and voltage measurement tools for *in vivo* biology.

Zebrafish embryos are a superior system for studying developmental biology due to many advantages such as rapid external development, transparency of early embryos, and tractable genetics [216, 232]. The stages of zebrafish embryogenesis have been well characterized. Females and males release their gametes into the water, where oocytes are fertilized and begin a synchronous meroblastic cleavage process. They are classified as discoidal, where the group of dividing cells sit atop a large yolk and eventually form the blastula. This ball of cells continues to multiply and eventually migrates down the yolk to form the three germ layers during gastrulation. The early embryo transparency and ease of genetic manipulation make zebrafish an ideal model for vertebrate imaging studies, and much progress has already been made in many research fields such as neuroscience and organogenesis [245-249].

With advances in modern neuroscience, genetically encoded biosensors have been developed to overcome the limitations of chemical dyes [111]. Genetically encoded biosensors generally allow sensitive and real-time dynamic assays for monitoring cells under natural physiological conditions. While chemical dyes/probes usually have limited lifetimes, relatively slow response, and delivery challenges due to tissue specificity and penetration. Thus, the use of GECIs (genetically encoded

calcium indicators) and GEVIs (genetically encoded voltage indicators) has increased in recent years. These tools have already been applied successfully in many model systems for monitoring real-time dynamic bioelectric signals *in vivo* [250]. Moreover, both types of genetically encoded indicators have also been validated in zebrafish embryos [81, 83, 112, 117]. For example, GCaMP6s provided an excellent temporal and spatial resolution of calcium signaling during zebrafish embryogenesis, and revealed previously missed signal information not visible with dyes [81]. One of the commonly used GEVIs, ASAP1 (Accelerated Sensor of Action Potentials 1), has also been effective at reporting zebrafish neuronal activities within developing embryos [83, 117]. Thus, these newly developed GEVIs and improved fluorescent imaging tools such as light sheet microscopy (LSM) provide an unprecedented opportunity to measure endogenous bioelectricity with enhanced sensitivity, signal-to-noise, acquisition speed, kinetics, and reduced toxicity and tissue damage [251, 252].

In this work, we took advantage of our Tg (*ubi*: ASAP1) transgenic zebrafish and systematically analyzed endogenous bioelectric signals in early zebrafish embryos using LSM. To our knowledge, this is the first real-time systematic analysis of endogenous bioelectric signals during vertebrate embryonic development. We found zebrafish embryos show characteristic bioelectric signals at corresponding embryonic developmental stages, suggesting their versatile functions.

3.3 Results

We have generated a Tg (*ubi*: ASAP1) transgenic fish line that can report endogenous bioelectric signals. The *ubi/ubiquitin* promoter lines allow for expression in all cells during embryogenesis, and the fluorescent signal can be visualized using an epifluorescence microscope [83]. However, we have not systematically investigated the electric signal due to the relatively low fluorescence intensity, high signal speed, and phototoxicity. To record these changes with sufficient speed and reduced tissue damage, we turned to LSM (Fig. 3-1A-C), which overcomes the challenges presented by this type of imaging with epi-fluorescent microscopy.

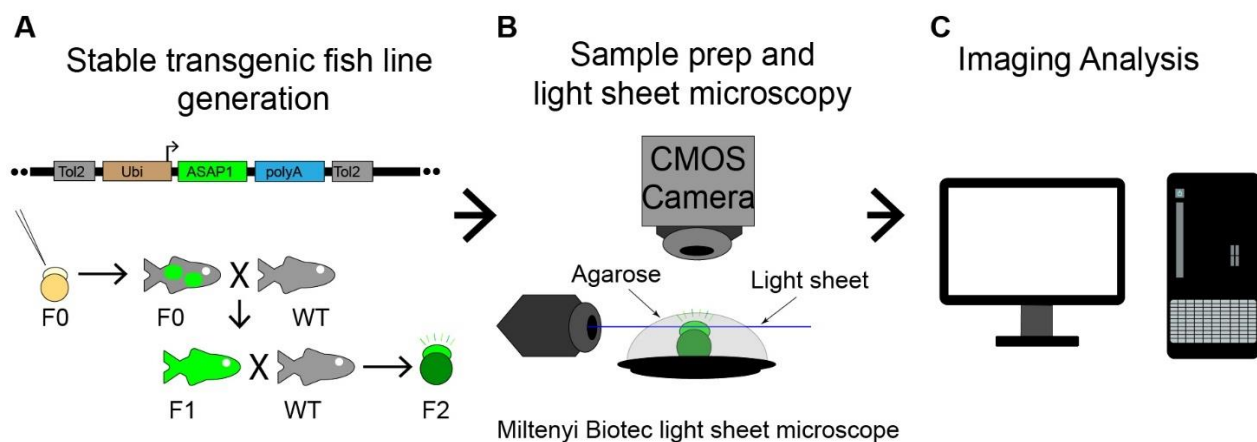


Figure 3-1 Overall experimental procedure.

(A) Illustration of a Tol2 construct, the method to produce stable ASAP1 zebrafish line, Tg (*ubi*: ASAP1), and zebrafish crosses. X indicates fish cross. Black arrows show fish raising or producing. The green color labels the ASAP1 transgene. (B) Experimental setup to image zebrafish Tg (*ubi*: ASAP1) embryos with Miltenyi Biotec light sheet ultramicroscope II. ASAP1-positive embryos were mounted in agarose on a platform to keep them stable during imaging. (C) Image analysis was performed using ImageJ (v1.53e) and Imaris programs (9.7.2, Bitplane AG).

3.3.1 Cleavage Furrow Hyperpolarization Precedes Cytokinesis and Becomes More Dynamic as Zebrafish Embryos Develop in the Cleavage Period.

An intriguing phenomenon we have noticed in Tg (*ubi*: ASAP1) fish embryos, is the local cell membrane hyperpolarization during the cleavage stage (Fig. 3-2, Supplementary Videos 3-1 to 3-3). To better understand and quantify this hyperpolarization, we examined the Vm signal of cleavage-stage embryos using a high-speed LSM. Cell membrane voltage can be detected even in unfertilized embryos, which showed randomly positioned signals and variable shapes of Vm fluctuations (Fig. 3-3A-H, Supplementary Video 3-4). In fertilized 1-cell stage fish embryos, we first observed ASAP1 signals (brighter fluorescence) localized to the initial cleavage plane before the cell was cleaved in half (Fig. 3-2A-G). The initial “center furrow” from the first cleavage of the 1-cell stage remained hyperpolarized (Fig. 3-2H), and this dynamic signal persisted into the subsequent cell division. Meanwhile, the 2-cell stage embryo began to show a hyperpolarization signal at the center of each cell (parental cells, P1 and P2) (Fig. 3-2H-N, Supplementary Video 3-

1). One of the parental cells, P1, showed stronger signaling throughout the division. This signal started in the middle of each cell perpendicular to the first division plane and moved bidirectionally outward. The cell membrane of the P2 cell showed a similar bioelectric signal to P1, which could potentially be linked with cleavage furrow positioning and propagation. To better understand these signals, we defined regions of interest (ROIs) to calculate changes in fluorescence intensity at the locations of the furrows over time. Indeed, the furrows of the 2–4 cell stage transition showed that the fluorescent change (ΔF) in P1 was the strongest overall, with P2 following a weaker change (Fig. 3-2CC). The center furrow also displayed V_m changes while the two new furrows formed. Noticeably, all furrow-related hyperpolarized signals did not remain stable, as fluctuations were clearly noticed as cytokinesis processed. (Fig. 3-2I-N, CC, Fig. 3-3I).

The 4-cell stage embryos had signals remaining at P2 furrows (Fig. 3-2O, white arrow) before new signals appeared at the center of the newly dividing cells. All four cells showed different initial fluorescence intensities (Fig. 3-2O-U). By our ROI quantifications, the furrows of the 4–8 cell stage transition showed a similar pattern to the 2–4 cell stage divisions (Fig. 3-2CC, DD, Fig. 3-3I-J). The remaining signals from the previous furrows were stronger before the new divisions (P1, P2, Fig. 3-2DD, Fig. 3-3J), but gradually decreased before the new furrows formed. The initial four peaks of DC1-4 matched up well but became less synchronized as cytokinesis progressed (Fig. 3-2P-U). In most embryos we imaged ($n = 8$ out of 9), the left daughter cells (DC1 or 2) showed signals first (Fig. 3-2P), then the right daughter cells, (DC3 or 4) (Fig. 3-2Q, Supplementary Video 3-2). However, this observation is not always consistent. One fish embryo showed a diagonal pattern (DC1 to DC3) (Fig. 3-3K-N). The cleavage furrow hyperpolarization signals continued in a comparable way for the 8–16 and 16–32 cell stages. However, the initial signal timing and intensity difference were more variable than in the 4-cell stage. Starting at 8–16 cells, less synchronized and more dynamic oscillations occurred at the furrows of newly dividing cells (Fig. 2V-BB, Supplementary Video 3-3).

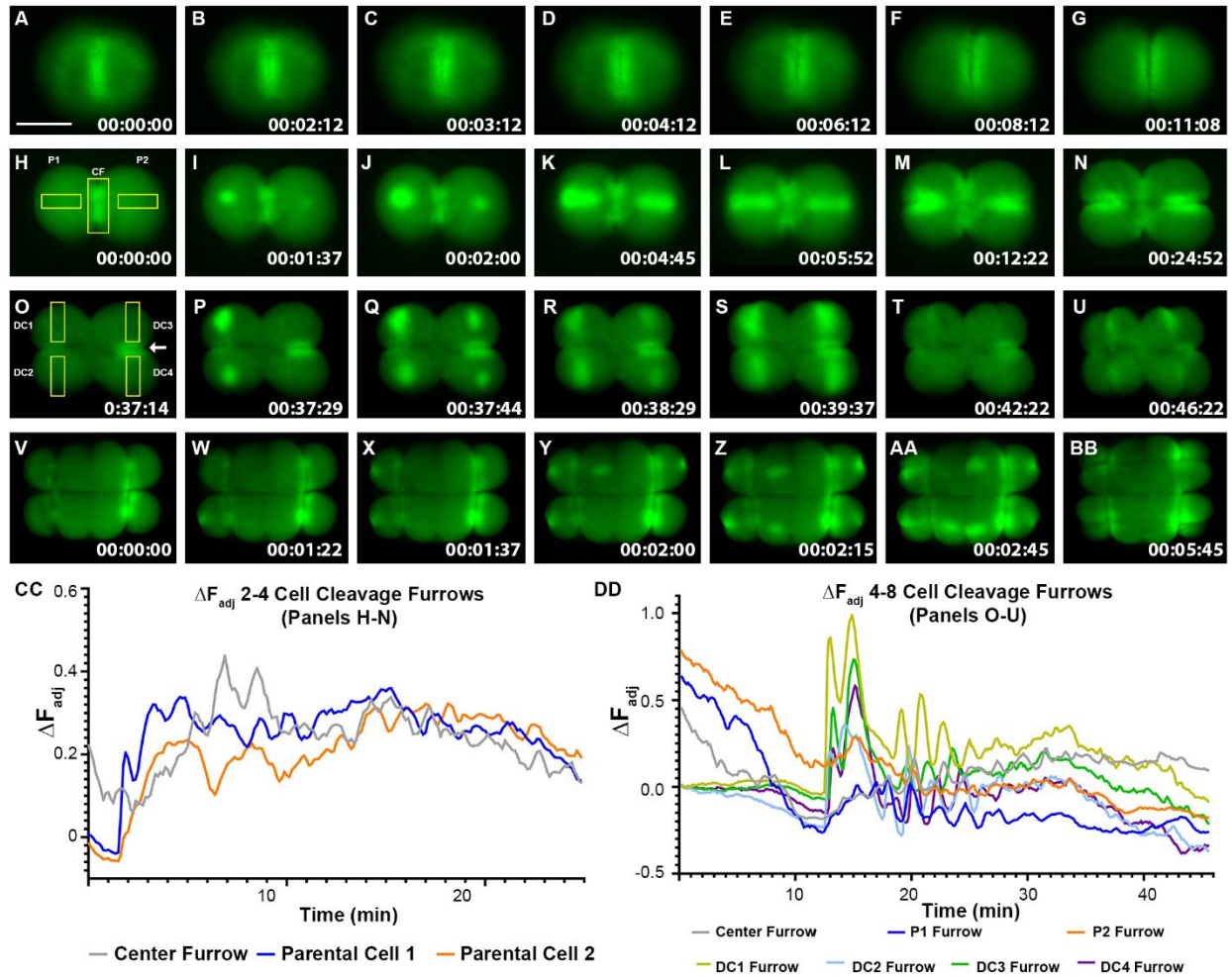


Figure 3-2 Zebrafish Cleavage period embryos display furrow-related dynamic hyperpolarization.

(A–BB) Still-frame representative max-projection images from time-lapse videos (Supplementary Video S1–S3). 1–16 cell stages of Tg (*ubi: ASAP1*) zebrafish embryos were imaged from the animal pole position. (A–G) Representative Vm images from 1–2 cell stage fish embryo. (H–U) Representative Vm images from 2–8 cell stage fish embryo. (V–BB) Representative Vm images from an 8–16 cell stage fish embryo. Areas of bright green indicate hyperpolarization. Yellow boxes show regions of interest (ROIs) for measuring fluorescence intensity over time. The white arrow in (O) points to the P2 furrow signal. Signals appeared before cleavage furrows formed and then fluctuated as cytokinesis progressed. (CC) Adjusted fluorescence intensity, ΔF_{adj} , of ROIs in panels (H–N). (DD) Adjusted fluorescence intensity, ΔF_{adj} , of ROIs in panels (O–U). All lines in panels (CC,DD) represent the change in adjusted fluorescence intensity of ROIs for the designated cleavage furrows over time. CF (center furrow), a fertilized embryo's initial division plane. P1, parental cell one. P2, parental cell two. DC1, daughter cell one. DC2, daughter cell two. DC3, daughter cell three. DC4, daughter cell four. Time (lower right corner), hours: minutes: seconds. Scale Bar = 250 μ m.

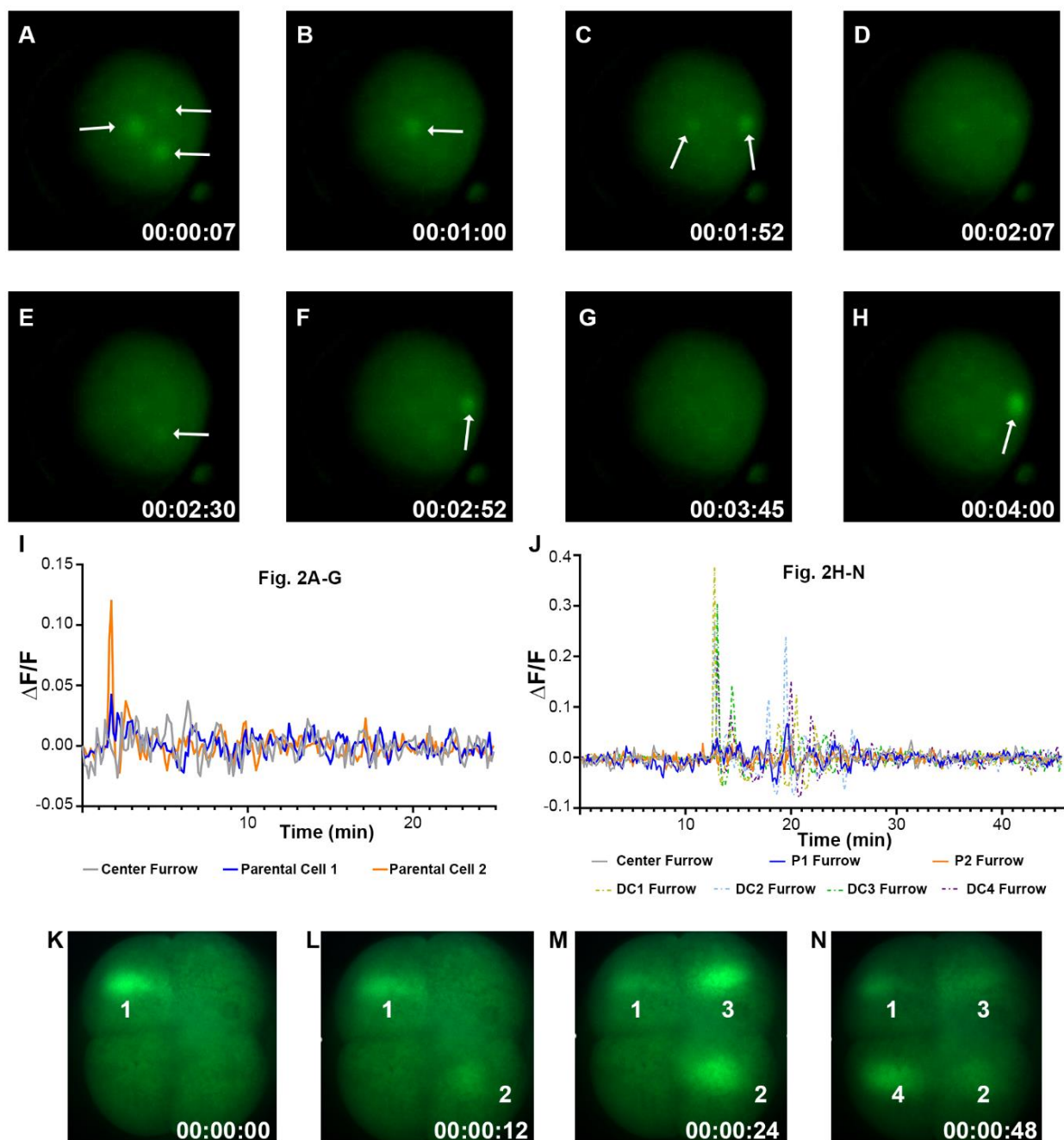


Figure 3-3 Unfertilized Egg Vm signaling, $\Delta F/F$, and diagonal pattern of 4-cell stage fish embryo.

A–H. Still-frame representative max-projection images from a time-lapse video (Supplementary Video 3-4) of an unfertilized Tg (*ubi: ASAP1*) zebrafish embryo imaged from the animal pole position. The white arrowheads point to random Vm transient spots. **I.** $\Delta F/F$ quantifications of ROIs in panels **H–N** of Figure 2. **J.** $\Delta F/F$ quantifications of ROIs in panels **O–U** of Figure 2. All lines in panels **I** and **J** represent the standard change in fluorescence intensity of ROIs for the designated cleavage furrows over time. **K–N.** Representative Vm images from a 4–8 cell stage fish embryo showing a different pattern of furrow signaling (the second signal was diagonal from the initial). Scale Bar= 250 μ m.

3.3.2 Whole-Cell Vm Transient Signals Are Located in the Superficial Blastomere during the Zebrafish Blastula Period

As zebrafish embryos develop into the blastula stage, cell number increases, but cell volumes decrease due to discoidal cleavage. With max intensity projections of Z-stack timelapse videos, we found that the electric signal mainly exhibits whole-cell Vm transients instead of cleavage-furrows membrane local signal (Fig. 3-4A-L, Supplementary Video 3-5.). Interestingly, most whole cell Vm transients (Fig. 3-4A-B) were distributed over the embryo surface of the enveloping layer (EVL) as well as the yolk syncytial layer (YSL). Individual cells (in multiple frames) showed a dynamic nature of electric signals during this embryonic period (Fig. 3-4A-C, H-L). To further detect and track these signals, we turned to Oxford Instruments Imaris software (9.7.2 Bitplane AG) for signaling analysis. With time-lapse videos (Total time 30 min, 5-s intervals between Z-stacks), we were able to count the number of Vm transients over time and calculate the duration of transients. Embryos ($n \geq 5$) were either classified as “early” (2.5–3.5 h. or 512 cells to high stage) or “late” (3.5–4.5 h. or oblong to dome) blastula stage. Imaging analysis of the early blastula stage revealed that transient numbers fluctuated over time, with periods of a higher and lower number of signals in each frame (Fig. 3-4M). We then turned to the tracking feature in the Imaris program, which allowed one transient event to be counted once, even if the same cell displayed bright fluorescence in multiple frames. We found that more Vm transients were occurring in the early blastula (~727) compared to the later blastula period (~284) (Fig. 3-4N). The average transient duration (about 10 s) did not differ much between the two blastula stages (Fig. 3-4O). To examine whether these signals were within the deeper cells, we examined a single plane Z-slice and found that the signals were limited to the outer edge of the blastomere with a lateral slice from

both the lateral position (Fig. 3-4P, Supplementary Video 3-6) and from the view of animal pole (Fig. 3-4Q). The superficial blastomere signaling was observed in both the early and late blastula stages. Intriguingly, we observed sequential Vm signaling occurrences between adjacent cells (Fig. 3-4R-AA, Supplementary Video 3-7), suggesting that Vm could function as an intercellular signal.

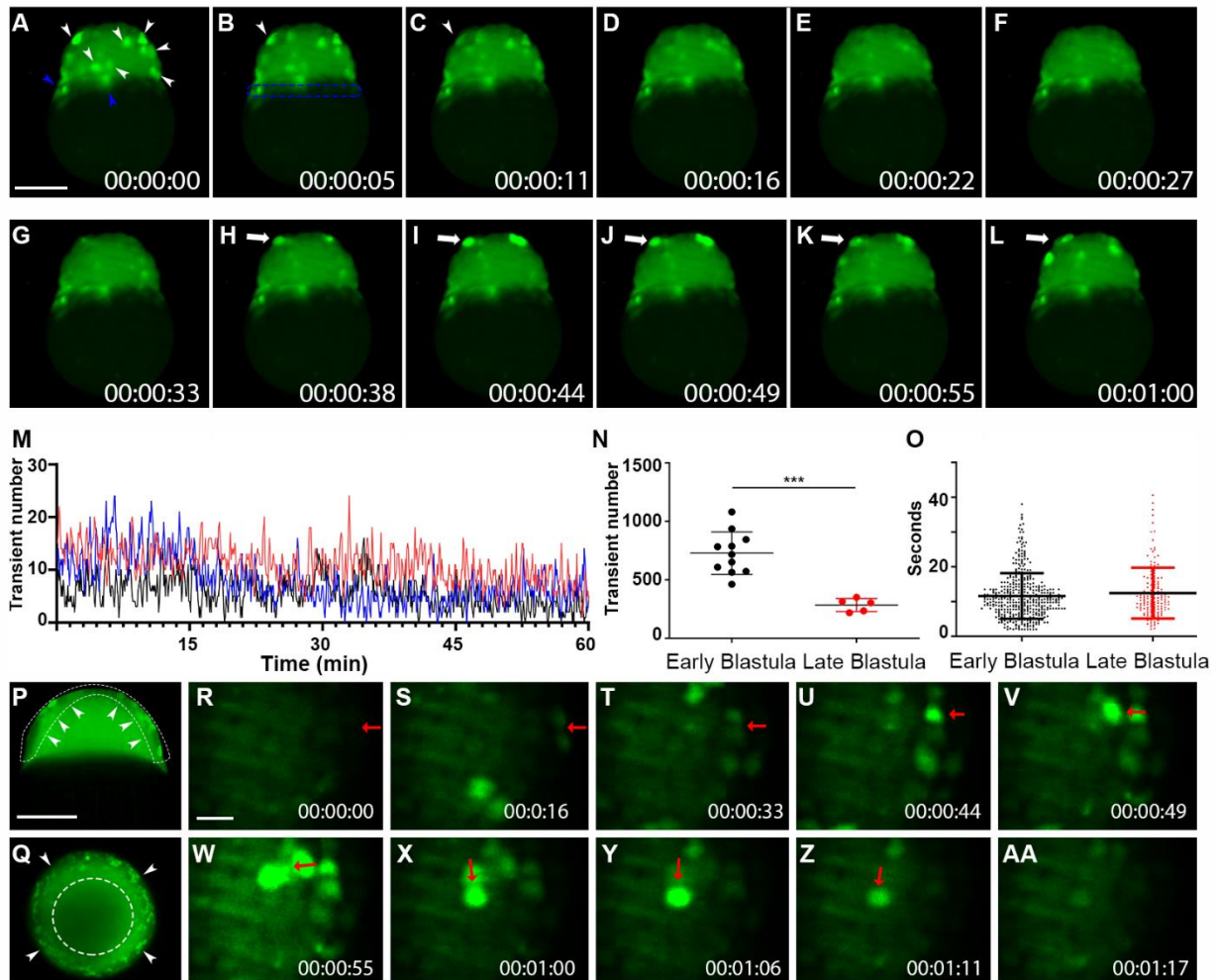


Figure 3-4 Whole-cell Vm transients occurred in the zebrafish superficial blastomeres during the blastula period.

(A–L) Still-frame representative max-projection images from a time-lapse video (18 min total time, 5.5-s intervals, Supplementary Video S5). Early-stage blastula of the Tg (*ubi: ASAP1*) zebrafish embryo was imaged from a lateral position. (A) White arrowheads indicate whole cells that were hyperpolarized. Blue arrowheads point to Vm signals in YSL. (B) The blue dashed line indicates the YSL region of cells. Arrowheads in panels (B,C) show the same cell with signal fading over time. (H–L) White arrows show a cell that became hyperpolarized and eventually faded after about 20 s. (M) Average number of transients occurred at a given time point from a 60 min acquisition. The total number of hyperpolarized cells fluctuated over time. Each colored line indicates different fish embryos. (N) The total number of Vm transients occurred within the early (2.5–3.5 h) and the late (3.5–4.5 h) blastula ($n \geq 5$ embryos for each group). Asterisks indicate a statistical significance of $p < 0.001$. (O) Vm transient duration of the early (2.5–3.5 h $n = 4$) and the late (3.5–4.5 h $n = 3$) blastula. (P) Max time projection ($t = 2$ min) of a 3.5 h blastula embryo imaged with a single Z-plane through the center (lateral position). Arrowheads point to the hyperpolarized cells only appearing within the superficial blastomere (Supplementary Video S6). A white dashed line indicated the EVL region of the embryo. (Q) Max time projection ($t = 3$ min) of a 3.5 h blastula embryo imaged with a single Z-plane through the center (animal pole position). Arrowheads point to the hyperpolarized cells only appearing within the superficial blastomere. The white segmented circle in the center of the blastula contains no hyperpolarized cells. Scale Bar = 250 μm . (R–AA) Early-stage blastula embryo (3 hpf) zoomed still-frame images from a time-lapse video (1 min 17-s total time, Supplementary Video S7). Red arrows indicate whole cells that were hyperpolarized. (U) The red arrow points to a strongly hyperpolarized cell. (V) The red arrow points to an adjacent cell that signaled 5 s later. (W) The red arrow points to a new adjacent cell signaled after another 5.5 s. This pattern continued, with the arrow in panel (X) pointing to another new adjacent cell from panel (W). This pattern finally dissipated with the earlier signaling cells fading. Eventually, the last signaling cell in panel (X) faded in (AA). Time (lower right corner), hours: minutes: seconds. Scale Bar = 50 μm

3.3.3 Whole-Cell Vm Transient Signals Occur More Frequently during the Zebrafish Gastrula Period but with Similar Signal Duration

When the fish embryos develop to the gastrula period, we chose imaging with longer total times and intervals to capture an overall picture of Vm dynamics during this stage. Time-lapse imaging revealed a continuation of Vm transients within the early stages of gastrulation (4.5–6 hrs or 30% epiboly to shield) and within the later stages (6–8 hrs or shield to 75% epiboly) (Fig. 3-5 A-AA, Supplementary Video 3-8). Early gastrulation period Vm transients frequently fluctuated as in the blastula period. However, the number of Vm transients increased without the Vm transient duration being significantly affected (Fig. 3-5G-I vs. Fig. 3-4M-O). Since Vm transients were only observed within the EVL (enveloping layer) and YSL (yolk syncytial layer) during the blastula

stage, we decided to check if this held true during the gastrula period, in which the three germ layers are formed by dynamic cell movements and internalizations. Indeed, we found signaling within the deep cells during the gastrula period, starting at around 30% epiboly (Fig. 3-7). We could also detect Vm signals occurring within layers deeper than the superficial blastomere (Fig. 3-5P-U, Supplementary Video 3-9).

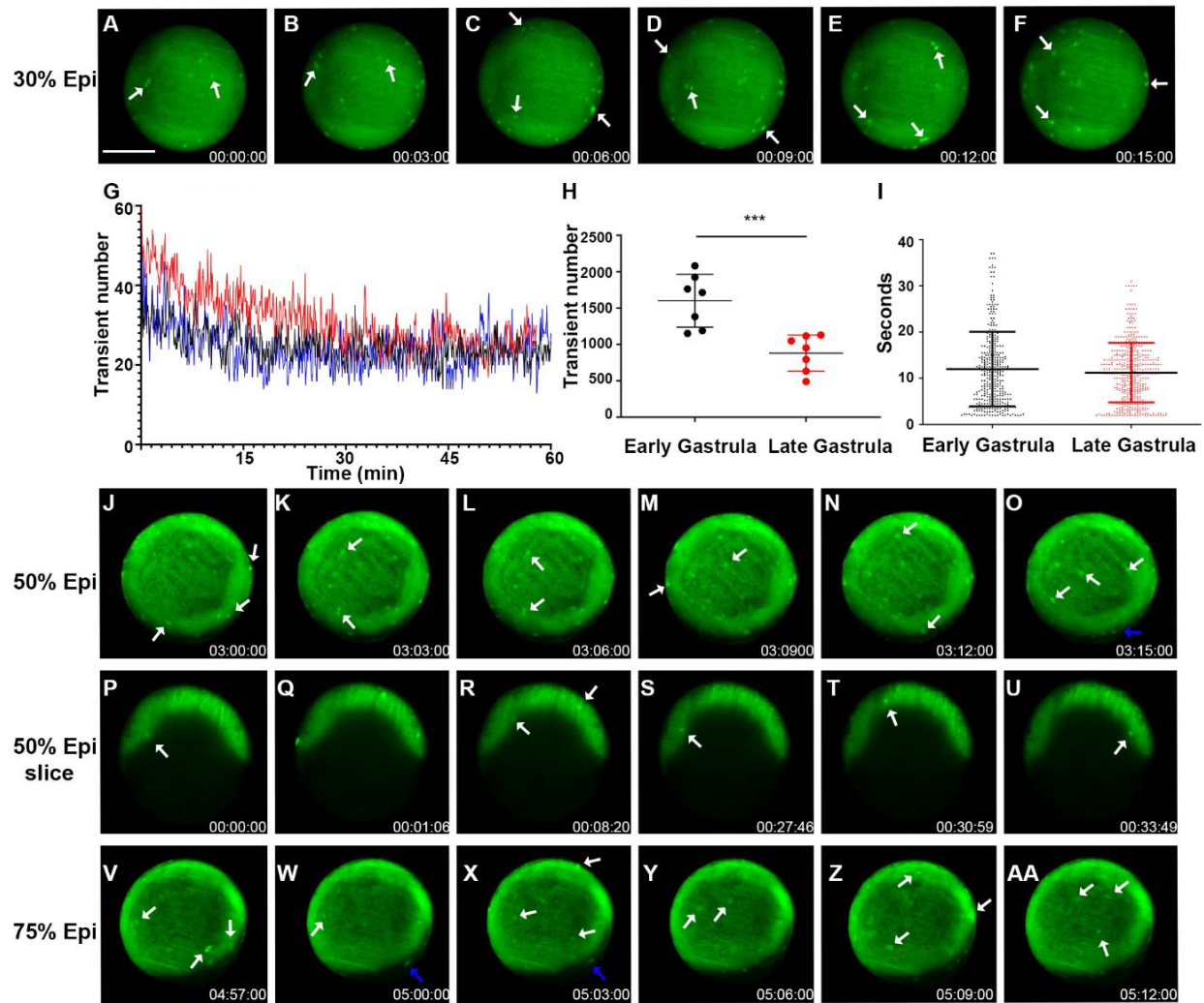


Figure 3-5 Zebrafish gastrulation exhibited whole-cell transient hyperpolarization in both superficial and deep cells.

Early stage gastrula (30%) to 75% epiboly stages of the Tg (*ubi: ASAP1*) zebrafish embryo still-frame representative max-projection images from a time-lapse video (8 h total time, 3 min intervals, Supplementary Video S8). White arrows indicate whole cells that are hyperpolarized. (A–F) Early-stage gastrula embryo (~30% epiboly, animal pole view) showed whole-cell hyperpolarization in the EVL. (G) Average number of transients occurred at a given time point from a 60 min acquisition. The total number of hyperpolarized cells fluctuates over time. Each colored line indicates different fish embryos. (H) The total number of Vm transients occurred within the early (30% epiboly to shield) and late (shield-75% epiboly) gastrula embryo ($n = 7$ embryos for each group). Asterisks indicate a statistical significance of $p < 0.001$. (I) Vm transient duration of the early and late gastrula embryos ($n = 4$ embryos for each group). (J–O) Gastrula period embryos (50% epiboly) images from a time-lapse video (3 min intervals, Supplementary Video S8). Cell signals were seen in both the EVL (white arrows) and YSL (blue arrows). Overall signals were increased along the edge of the embryo where the embryonic shield was forming. (P–U) Time-lapse images of a 50% epiboly gastrula period embryo imaged with a single Z-plane through the center (lateral position). White arrows point to the hyperpolarized cells present within the deep cells (Supplementary Video S9). (V–AA) Gastrula period embryo 75% epiboly images from a time-lapse video (3 min intervals, Supplementary Video S8). Cell signals were seen in both the EVL (white arrows) and YSL (blue arrows). Overall signals were increased along the edge of the embryo where the embryonic shield was forming. Time (lower right corner), hours: minutes: seconds. Scale Bar= 250 μm

3.3.4 During the Segmentation Period, There Are Tissue-Level Dynamic Cellular Bioelectric Signals

When the fish embryos moved into the segmentation period, sporadic transient electric signals continued to occur all over the embryo. However, more tissue-level changes began to occur. Certain regions, such as the somites, became more hyperpolarized than surrounding tissues (Fig. 3-6A-F, Supplementary Video 3-10). The Vm signals in some other tissues, such as the developing heart, also showed more obvious electrical signaling later (Fig. 3-6J-K). At about the 12-somite stage, Middle-aged somites became strongly hyperpolarized (Fig. 3-6G-L, Supplementary Video 3-11). Interestingly, the somite signal was also dynamic, occurring in whole or partial somites. In addition, either unilateral or bilateral somites showed strong hyperpolarization (Fig. 3-6M-R, Supplementary Video 3-12). To quantify these somite signals, we divided the embryo trunk into seven ROIs, starting at the middle of the trunk along the dorsal side down to the tailbud region (Fig. 3-6S). Mean fluorescence intensity changes over time were tracked, and ΔF was calculated. As development progressed, we found that somite region fluorescence intensity gradually

increased as the embryos further developed. Moreover, middle to posterior somite regions, such as ROI-4 and ROI-5, showed a greater amount of signaling events (Fig. 3-6T-U). In contrast, the first few anterior somites did not show many signal fluctuations at this stage (Fig. 3-6T-U). There was a significant difference between the anterior and posterior somites and even significant differences among the other middle regions.

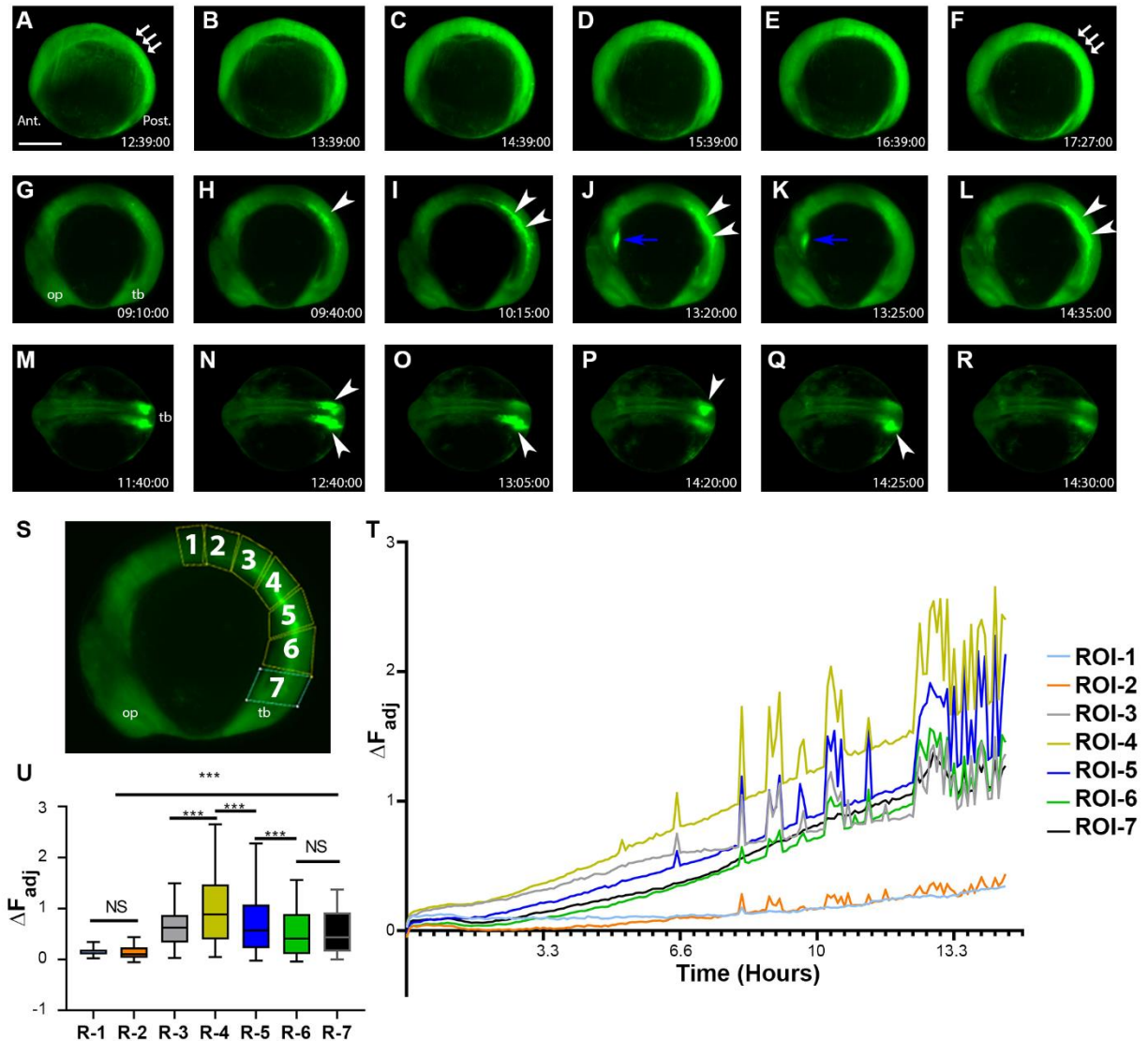


Figure 3-6 During the segment period, more complex and dynamic cellular bioelectric signals occurred at the tissue level.

(A–F) Segmentation period (bud stage-6 somite stage, 1 h intervals, Supplementary Video S10). Somites and the posterior region of the embryo had an increased level of fluorescence. White arrows point to the somites. Note the relatively low fluorescent signals within the head region. (G–L) Left lateral time-lapse images of 10–16 somite zebrafish embryos (Supplementary Video S11). White arrowheads point to the strong hyperpolarization of somites. Blue arrows point to Vm signals in the developing heart. (M–R) Dorsal view time-lapse images of 10–16 somite zebrafish embryos. White arrowheads indicate somite regions with strong hyperpolarization (Supplementary Video S12). (S) Embryo with positions of ROIs (1–7) used to calculate mean fluorescence and corresponding ΔF_{Adj} . (T) ΔF_{Adj} over time of ROIs in panel (S). All colored lines represent the change in fluorescence intensity of the designated ROI at each time point. Signals appeared to increase over time as somites became more developed. The number of fluctuations also increased as more somites were generated. (U) The mean ΔF_{Adj} for each ROI for the entire duration of the time-lapse video. ROIs 1–2 showed the least amount of activity (most anterior somites), ROIs 3–5 showed the most activity (middle age somites), and ROIs 6–7 showed a moderate amount of activity (youngest somites/presomitic mesoderm/tailbud region). Asterisks indicate a statistical significance of $p < 0.001$. NS, not statistically significant. Scale Bar= 250 μm .

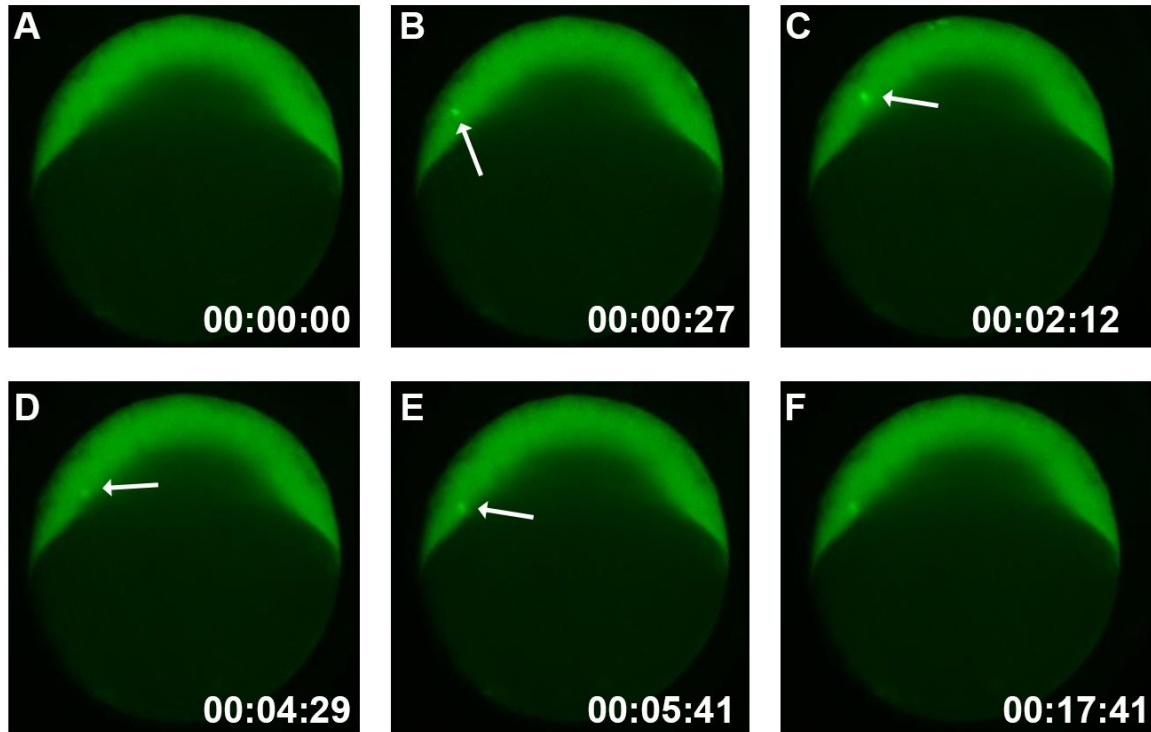


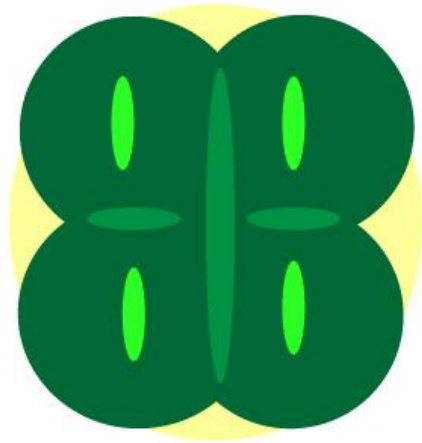
Figure 3-7. Deep cell Vm transient during the 30% epiboly period.

A-F. Time-lapse images of a 30% epiboly gastrula period embryo imaged with a single Z-plane through the center (lateral position). White arrows point to the hyperpolarized cells present within the deep cells. Scale Bar = 250 μm .

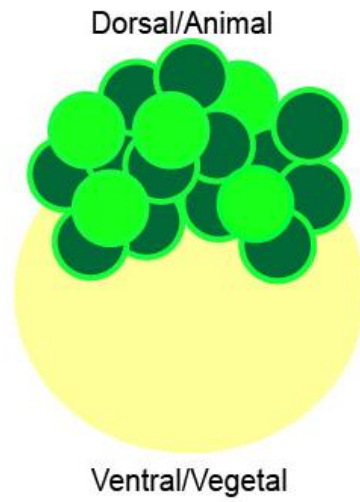
3.4 Discussion

Mounting evidence has suggested that bioelectric signaling plays a significant role in embryonic development. However, direct evidence of embryonic bioelectric signaling has not been available yet. Here, we revealed zebrafish embryos show characteristic bioelectric signals at corresponding embryonic developmental stages (Fig. 3-8) using newly developed technologies such as GEVI and LSM. These results laid the fundamental groundwork for understanding the endogenous electrical signaling patterns accompanying the initial stages of zebrafish embryonic development.

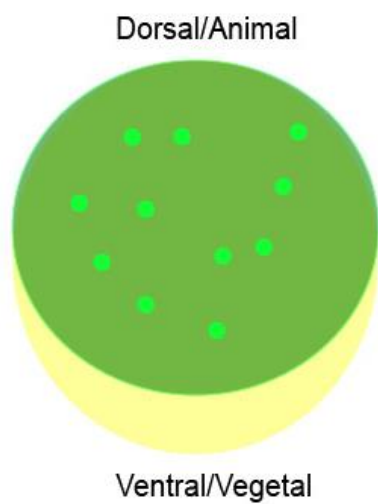
A. Cleavage



B. Blastula



C. Gastrula



D. Somite

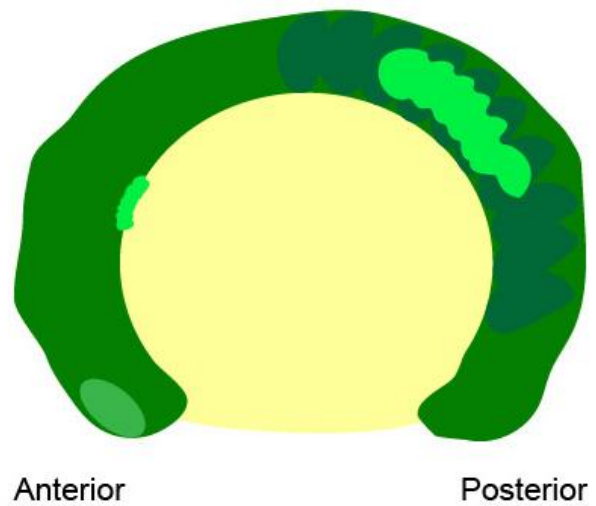


Figure 3-8 Summary of bioelectric signaling during zebrafish embryogenesis.

Each early embryonic zebrafish developmental period has distinct yet overlapping bioelectricity signals and/or patterns. **(A)** The embryonic cleavage period is marked by cleavage furrow-associated Vm fluctuations that precede and persist cytokinesis. These signals become less synchronized and stable, starting around the 16-cell stage. **(B)** Whole-cell transient Vm signals characterize the blastula period. However, these signals are restricted to the superficial blastomere and are not seen within the deeper cells at this stage. In addition, intercellular signaling can be observed between adjacent cells. **(C)** The gastrulation period continues to display whole-cell transient hyperpolarization within the superficial blastomere and begins to occur within the deeper cells during epiboly. **(D)** Strong Vm transient signals mark the somite period. These signals can be whole or partial somites and are either unilateral or bilateral. The signals are more concentrated in the middle and posterior somites (bright green highlights hyperpolarization).

Our study revealed that bioelectric signals are present even within unfertilized embryos and within the initial cleavage plane of the 1-cell stage embryos. Cell membrane hyperpolarization around the cleavage furrow preceded and persisted during the early divisions in a highly dynamic fashion. Moreover, the cleavage furrow signal continued but fluctuated when cytokinesis progressed due to the dynamic process of cytokinesis and the incomplete meroblastic cleavage of zebrafish embryos. Overall, bioelectric signals of this stage remained localized to the furrows and tended to be slightly asynchronous among the newly formed cells. However, we did notice the initial furrow signal could appear within cells on one side of the embryo or cells first appearing diagonally to one another during the 2-to-4 stage transition. However, this scenario was much less frequently observed.

In contrast, the bioelectric signals transitioned to whole-cell Vm transient events once fish embryos reached the blastula period. We found that the Vm transients concentrated in the superficial regions, EVL and YSL, where cell divisions frequently occurred. This suggests that the signal could still be related to cell divisions. Interestingly, we also found intercellular sequential transients, which indicated that electric signaling might also be utilized for tissue-level communication. During the gastrulation period, Vm transients remained dominant in the margin of the embryos. However, they began to show in the deeper cells at about 30% epiboly. Compared to early gastrulation, the Vm transient number decreased in the later stages of gastrulation but not the bioelectric transient duration. This could be due to missed signals because we utilized a lateral position. Only one side of the embryonic cells was captured. Conversely, imaging from the anterior-posterior view would

not detect the signaling of migrating cells down the sides of the yolk. Therefore, imaging half of the embryo might mean the total number of transients at this stage would be roughly doubled.

During the late gastrulation and segment periods, tissue-level hyperpolarization was observed in somites. These tissue-level bioelectric signals may be correlated to tissue differentiation. As the fish embryos marched into the segmental period, strong somite-level bioelectric signals became more dynamic, supporting the idea that they are related to tissue patterning and differentiation. All these characteristic bioelectric signals corresponded to specific embryonic developmental stages, indicating their intrinsic roles. However, the underlying ion channels and connexins that generate these signals are unknown. Our recent gene expression analysis of calcium-gated potassium channels (KCa) and inwardly rectifying potassium channels (Kir) revealed that many (*kcnn1b*, *kcnn3*, *kcnma1a*, *kcnma1b*, *kcnmb2b*, *kcnmb3*, *kcnj4*, *kcnj2a*, *kcnj2b*, *kcnj11*, *kcnj5*, *kcnj21*) have a somite-specific expression at similar developmental stages [87, 88]. Their presence in the developing somites may indicate that these channel activities underlie the tissue-level bioelectricity. Future experiments on disrupting these potassium channels by CRISPR may prove their contribution to somite bioelectrical signaling. Another interesting phenomenon we noticed is that neural tissues did not show more electric activities than other tissues in early zebrafish embryos, especially the newly formed somites. As the embryos are not mobile at this stage, it is unlikely that these strong V_m changes are due to movement. Instead, this may indicate the bioelectric signal could be crucial to somite differentiation, such as epithelial-to-mesenchymal transition and dermomyotome differentiation. Perturbation of such electric signals may have a dramatic impact on adult zebrafish body patterns. For example, the long-fin fish Dhi2059 mutant was caused by an ectopic expression of *kcnj13* in the somites [92]. It is also interesting to note that the location of ectopic *kcnj13* expression in Dhi2059 mutant fish during the somite stage is within the Middle-aged somites. Coincidentally, this is the same tissue where our ASAP1 reporter line showed the most electrical activity.

The functions of these unique developmental stage-specific bioelectric signal patterns during zebrafish embryogenesis remain largely unexplored. They could be related to cell cycle or cytokinesis, as previously suggested by ion channel studies from multiple species [253, 254]. As most V_m transients were found in the peripheral regions during the blastula and gastrula stages,

they likely play instructional roles in cell growth, differentiation, and organ patterning. As electric signals are correlated with calcium signals in neural tissues, it is also possible that the electric transients are just a reflection of calcium signal alterations in certain tissues, although this possibility is not high. Another possibility is the opposite, the electric signals trigger calcium signals.

In the field of neuroscience, calcium signals have been used as a surrogate marker of neuronal firing and electrical activity, and recent comparative studies have confirmed the two have a good correlation [114, 255, 256]. Calcium signaling has been extensively investigated in zebrafish embryos [78, 80, 81, 257, 258]. Our observations of bioelectric signals share many similarities with reported calcium signals. Both are correlated to embryonic developmental stages from cleavage furrow localized patterns to whole-cell transients and intercellular occurrences [78]. These similarities suggest both might be involved in similar biological functions during embryogenesis. It is worth noting that single-cell organisms such as bacteria and protozoans, without a nervous system, still have calcium signaling and electrical activity, evidenced by the presence of ion channels, Vm, and even neurotransmitter activity [259, 260]. Thus, bioelectricity and calcium, as important regulators, may have evolved before the development of neural tissue in these species. In addition to similarities, we did notice differences between the two types of signals. When compared to previously reported calcium signaling by GCaMP6G in zebrafish embryos, we find that transient Vm signals are more numerous and occur more rapidly. This may indicate that the Vm reporter could be more sensitive than the calcium one, due to its nature as a secondary messenger [261, 262]. However, these differences also could be caused by the slower imaging speed in the GCaMP6Gs study [81]. Similarly, it is also difficult to directly compare our data with previously reported studies with calcium dyes [78, 80, 257].

In summary, this report revealed early zebrafish embryos' first real-time endogenous bioelectric signals. Future investigations with improved GEVIs and genetic tools will expand our understanding of bioelectricity, especially its relationships with traditional developmental signaling pathways such as morphogen proteins (*e.g.*, WNT) and transcriptional factors (*e.g.*, HOX) [263, 264]. In the future, the biological roles of embryonic Vm could be further examined with zebrafish ion channel mutants, newly developed optogenetic, or chemogenetic tools such as DREADDs (Designer Receptors Exclusively Activated by Designer Drugs) or uPSAM (ultrapotent Pharmacologically Selective Actuator Modules) [163, 168, 265].

CHAPTER 4. TISSUE-SPECIFIC MODIFICATION OF CELLULAR BIOELECTRICAL ACTIVITIES USING THE CHEMOGENETIC TOOL, DREADD, IN ZEBRAFISH

4.1 Abstract

Cellular electronic activity plays an essential role in neuronal communication. Manipulation and visualization of cellular membrane potential remain essential tasks in order to study electrical signaling in living organisms. Light-controlled optogenetic and designed chemical-controlled chemogenetic tools were developed to manipulate cellular electric activities for neuroscience research. One of the most common chemogenetic tools is DREADD (designer receptors exclusively activated by designer drugs). It has been extensively utilized due to its convenience and long-lasting effects in murine and primate models, but not in zebrafish, a leading model organism in various research fields. Here, we first establish multiple tissue-specific transgenic zebrafish lines that express two different DREADDs with a genetically encoded voltage indicator, ASAP2s. We observed voltage changes in zebrafish melanophores, epidermis, and neurons by hM4DGi or rM3DGs receptors measured by ASAP2s fluorescence intensity. Alteration to melanophore bioelectricity by DREADD generated dynamic electric signals and resulted in morphological alterations to pigment cells. Collectively, our experiments demonstrate that DREADD can be utilized to manipulate cell-specific membrane potential in the zebrafish model. The availability of this tool in zebrafish will offer a new resource for a variety of bioelectricity research fields such as neuroscience, cardiology, and developmental biology.

4.2 Introduction

Cellular bioelectric signaling has been extensively investigated in neuromuscular excitable cells due to the important roles of action potential signals and resting membrane potential [266]. Recently, accumulating evidence reveals that cellular electric signaling is also an important player for regulating hormone release, embryonic development, wound healing, and regeneration [192, 193]. Non-invasive perturbation and visualization of cellular electrical activity in real-time and *in vivo* are the central requirements for studying cellular electric signaling [162].

To meet the rapid growth of neuroscience, genetically encoded tools have been developed for perturbation and visualization of cellular bioelectrical activity [267]. Channelrhodopsin-based optogenetic tools can enhance or repress neuronal firing on a millisecond scale and have been successfully applied to elucidate neuron type, activity, circuits, and behaviors [268, 269]. However, optogenetics generally requires complicated equipment, constrained animals free of movement, and can only modify neuronal activity in the short term (seconds-minutes). The chemogenetic tools were then developed to meet these remaining unmet needs. Chemogenetics use synthesized small molecules to activate engineered proteins (channels or receptors), modifying cellular electricity over a relatively long period [162, 164]. DREADDs (Designer receptors exclusively activated by designer drugs) are one group of the most commonly used chemogenetic tools [163, 270]. The DREADDs are composed of four tools (hM3DGq, rM3DGs, hM4DGi, and KORD) based on different mutated genetically engineered muscarinic receptors. Depending on the downstream G protein-coupled receptor signaling, the DREADD tools can modify cellular bioelectric activity bidirectionally. For example, hM3DGq enhances neuronal excitability, while M4DGi and KORD inhibit cellular excitability. DREADDs have been successfully used to elucidate behavior, circadian disorders, pathways related to cognitive impairments, eating disorders, neuronal plasticity, memory, and more in various animal models [179, 271-273]. Furthermore, improvements have been made to increase the selection of ligands with improved specificity and affinity [271, 274, 275].

Genetically encoded tools for visualizing and measuring cellular electrical activity *in vivo* are equally important for studying cellular electricity. Revolutionary biosensor tools, genetically encoded voltage indicators (GEVIs), for measuring cell membrane voltage have been developed for neuroscience [250, 276, 277]. These GEVIs measure cellular voltage based on either FRET (fluorescence resonance energy transfer) or levels of fluorescence intensity. The advantages over traditional electrical physiology recording include non-invasive, real-time, and nanosecond sensitivity. Among them, the ASAP1-3 (Accelerated Sensor of Action Potentials) have been applied to a variety of model organisms such as fruit fly, mouse, and zebrafish [83, 121, 129, 130, 278].

Zebrafish have extensively been used for studying embryonic development and modeling human diseases, including cancer. This is because of the many advantages such as vertebrate biology, tractable genetics, external development, and early embryo transparency [72, 216]. We and others demonstrated that ASAP1 reported embryonic cellular voltage changes and neural activities in zebrafish [83, 117], and a few optogenetic tools were just successfully adopted to the zebrafish model [108]. However, DREADDs have been tested and reported to be non-functional in zebrafish [166]. Thus, there is still a critical need for a chemogenetic tool that can modify zebrafish cellular electricity in the long term.

Here, we generated DREADD transgenic zebrafish lines and tested their function in zebrafish embryos and larvae using a newly developed agonist. We demonstrated that this chemogenetic tool is functional in melanophore, neuron, and epithelial cells. Thus, the DREADD tools and our transgenic zebrafish lines can be an excellent resource for the zebrafish community for investigating cellular electricity.

4.3 Results

4.3.1 Developing transgenic zebrafish lines to express DREADD

Chemogenetic tools have been demonstrated successfully in neuronal studies with murine and primate models. However, the chemogenetic tools, both DREADD and PSAM (pharmacologically selective effector molecules), were found ineffective in injected zebrafish embryos [166]. Recently, the PSAM tool was reported functional in zebrafish using the Tol2 transposon-based transgenic approach [167]. Thus, we reasoned that the DREADD tool might also work in transgenic zebrafish. We then created melanophore-specific transgenic zebrafish lines to co-express hM4DGi and ASAP2s using the *mitfa2.1* promoter (Fig. 4-1A). This fish will allow us to simultaneously examine bioelectric changes during the process of cell membrane voltage manipulation. Adapting to investigate bioelectricity in multiple tissues, we also take advantage of the Gal4-UAS (Upstream activator sequence) artificial binary gene expression system (Fig. 4-1B)[279]. We made zebrafish lines in which a *UAS* promoter drives either hM4DGi or rM3DGs, together with ASAP2s. Additionally, we made the melanophore (*mitfa2.1* promoter) and basal

epithelial cell (*tp63* promoter) specific Gal4FF fish lines (Fig.4-1C). We chose these two cell types because they are on the surface of the fish embryos, where the agonist chemicals can reach the cells easily, and it is convenient for us to image the cell membrane voltage change. These fish lines allow us to assess the effects of DREADD with different agonists (Fig. 4-1D). All the transgenic fish were outcrossed with wild type to F1 or F2 to clean the genetic background before use for experiments.

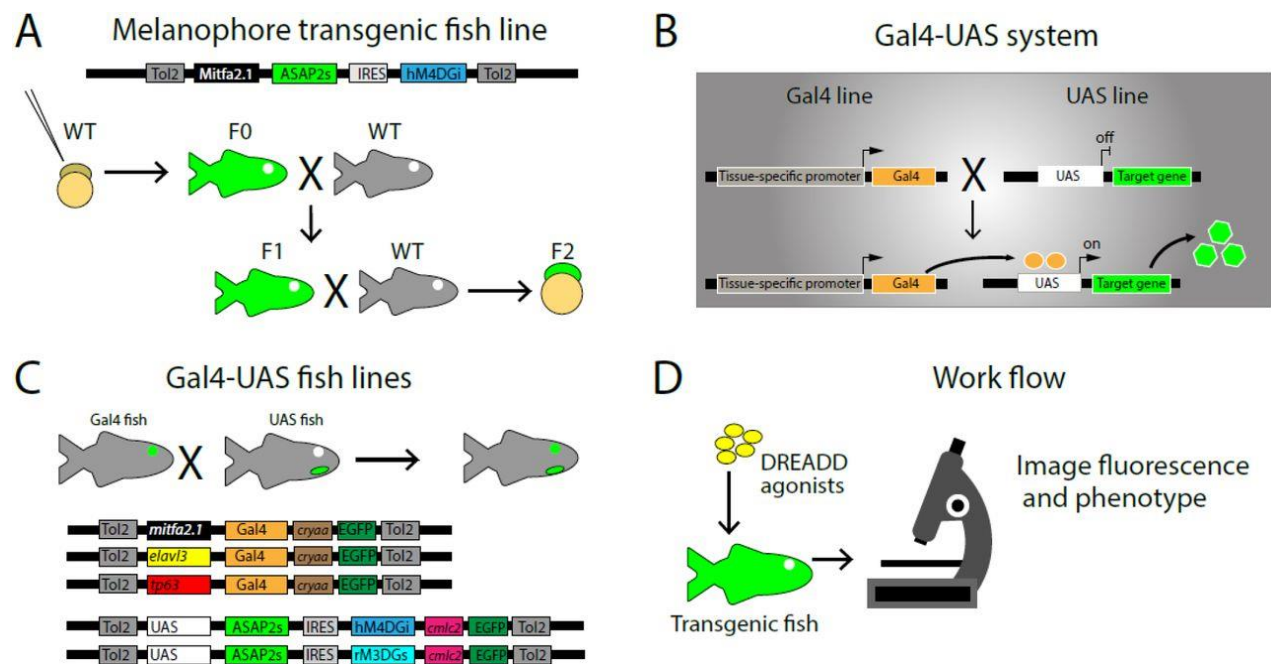


Figure 4-1 Illustration of DREADD transgenic fish lines and experimental workflow.

A. Tol2 constructs and method to produce stable DREADD zebrafish line, Tg (*mitfa2.1*: ASAP2s-IRES-hM4DG). X, fish cross. Black arrow, fish raising or produced. B. Illustration of principles of the Gal4-UAS system. C. Diagrams of the Tol2 transposon plasmid constructs used for the Gal4-UAS transgenic zebrafish lines. The Gal4 fish lines have an eye maker (green), *cryaa*: EGFP. The UAS fish lines have a heart marker (green), *cmlc2*: EGFP. X, fish cross. Black arrow, fish raising or produced. Tol2, Tol2 transposon minimal flanking DNA sequences. IRES, internal ribosome entry site. D. Basic workflow: DREADD agonists were used to treat transgenic DREADD zebrafish embryos to cause cell bioelectric changes, then the fish embryos were subjected to green fluorescence imaging and quantification

4.3.2 DREADDs work in zebrafish embryos, evidenced by ASAP2s fluorescence intensity changes

Since ASAP2s, a sensitive cell membrane voltage reporter, was included in our transgenic zebrafish, we reasoned that the green fluorescence of fish embryos would change if the DREADD tool works. To test this, deschloroclozapine (DCZ), one of the most recently reported highly potent DREADD agonists, was tested with a relatively high dosage by adding 1 μ L of 100mM DCZ to an imaging slide with about 400 μ L of fish system water (\sim 250 μ M). We treated 2dpf (day post-fertilization) Tg(*mitfa2.1:ASAP2s-IRES-hM4DGi*) fish embryos and indeed detected increased fluorescence in the melanophores on the top of the head about 5-10 minutes after treatment (Fig. 4-2A, D). This increased fluorescence is consistent with the hyperpolarizing activity of hM4DGi. Next, we examined epithelial cells using the fish embryos from Tg (*tp63: Gal4VP16; cryaa: EGFP*) and Tg (*4xnrUAS: ASAP2s-IRES-hM4DGi; cmlc2:EGFP*) fish cross. Similarly, the DCZ treatment resulted in fluorescence intensity increases of the epithelial cells in the head region (Fig. 4-2B, E) and caudal fin folds (Fig. 4-2bb, ee). To further test hM4DGi's function in neurons, we first injected the *elavl3* promoter-driven Gal4FF construct into Tg (*4xnrUAS: ASAP2s-IRES-hM4DGi; cmlc2: EGFP*) fish embryos and raised them to 2dpf. Then, we treated the fish embryos with DCZ. As expected, we found the neurons in the neural tube showed enhanced green fluorescence in treated fish embryos (Fig. 4-2C, F). Thus, the inhibitory DREADD, hM4DGi, is indeed able to induce hyperpolarization within zebrafish. To further test the DREADD tools in zebrafish, we examined the excitable DREADD, rM3DGs. Both melanophores (Fig. 4-2G, J) and neurons (Fig. 4-2I, L) showed decreased green fluorescence after DCZ treatment. This decreased green fluorescence is consistent with depolarizing activity of rM3DGs. In contrast, the epithelial cells showed increased green fluorescence (Fig. 4-2H, K). This unexpected opposite result may be caused by the epithelial cell's physiological response to maintaining its resting membrane potential. Overall, our experiments demonstrated that DCZ could activate both hM4DGi and rM3DGs in zebrafish.

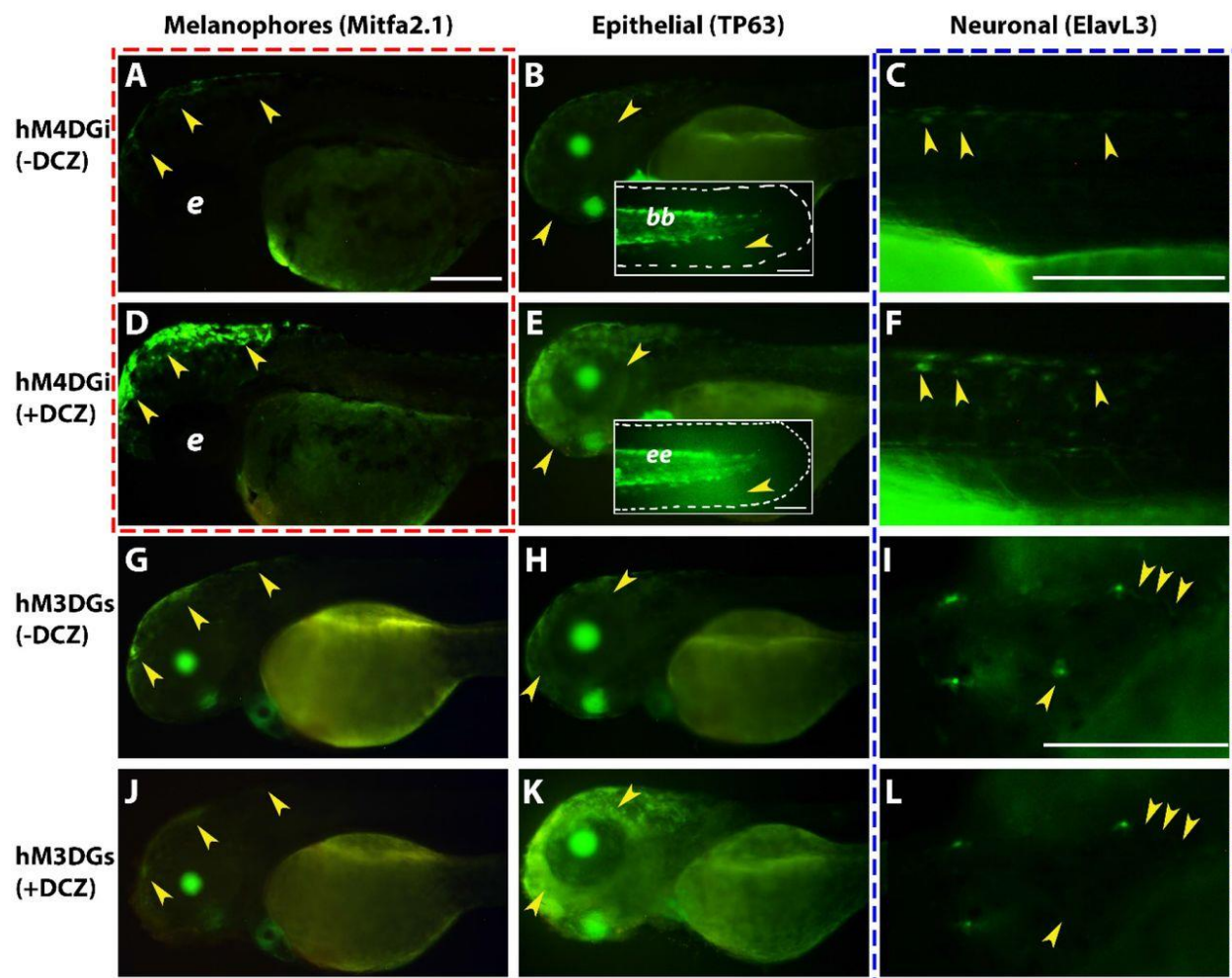


Figure 4-2 Cell membrane voltage manipulation by DREADD in zebrafish embryos.

A-F. Transgenic zebrafish expressing ASAP2s-IRES-hM4DGi in melanophore (*mitfa2.1*), basal epithelial cell (*tp63*), or neuron (*elavl3*) promoter, respectively. A-C. Fish embryos before DCZ treatment. D-F. The same fish corresponding to the A-C panels after treatment with DCZ. Inserts bb & ee: caudal fin images of Tg (*tp63*: ASAP2s-IRES-hM4DGi) fish before and after DCZ treatment, respectively. Yellow arrows indicate specific cells with increased levels of fluorescence. G-L. Transgenic zebrafish expressing ASAP2s-IRES-hM3DGs in melanophore (*mitfa2.1*), basal epithelial cell (*tp63*), or neuron (*elavl3*) promoter, respectively. G-I. Fish embryos before DCZ treatment. J-L. The same fish corresponding to the G-I panels after treatment of DCZ. Panels (A, D) with red dotted lines are from a cross between the Tg (*mitfa2.1*: ASAP2s-IRES-hM4DGi) and wild type. Panels (C, F, I, L) with blue dotted lines were from Tg (UAS: ASAP2s-IRES-hM4DGi) or Tg (UAS: ASAP2s-IRES-hM3DGs) fish injected with *elavl3*: Gal4FF plasmid construct. The remaining panels (B, E, G-H, J-K) were offspring from crosses of Gal4 and UAS transgenic fish lines. All the fish embryos are two days old. Yellow arrows indicate specific cells with altered levels of fluorescence. Only matching (before and after DCZ treated) embryos are directly comparable for fluorescence intensity levels (A & D, B & E, C & F, G & J, H & K, I & L.) Scale bars = 250 μ m except for panel inserts bb and ee where scale bar = 50 μ m.

4.3.3 DREADD activation causes dynamic bioelectric changes in zebrafish melanophores

We have demonstrated that DCZ can activate hM4DGi in the Tg (*mitfa2.1*: ASAP2s-IRES-hM4DGi) fish causing fluorescence to increase after 5-10 minutes. To further examine the exact bioelectric changes that take place after hM4DGi activation leading up to overall fluorescence increase, we decided to record treated larvae with time-lapse imaging immediately. We found that the green fluorescence intensity increase was not linear. Instead, the fluorescence intensity fluctuated, but the overall intensity increased with time extended. In addition, the fluorescence intensity of adjacent melanophores also fluctuated (Fig. 4-3A-G). These results indicate a melanophore membrane potential homeostasis, which may take time to change using DREADD and its agonist. These results also might indicate why all DREADD-expressing cells do not immediately show uniform fluorescence change.

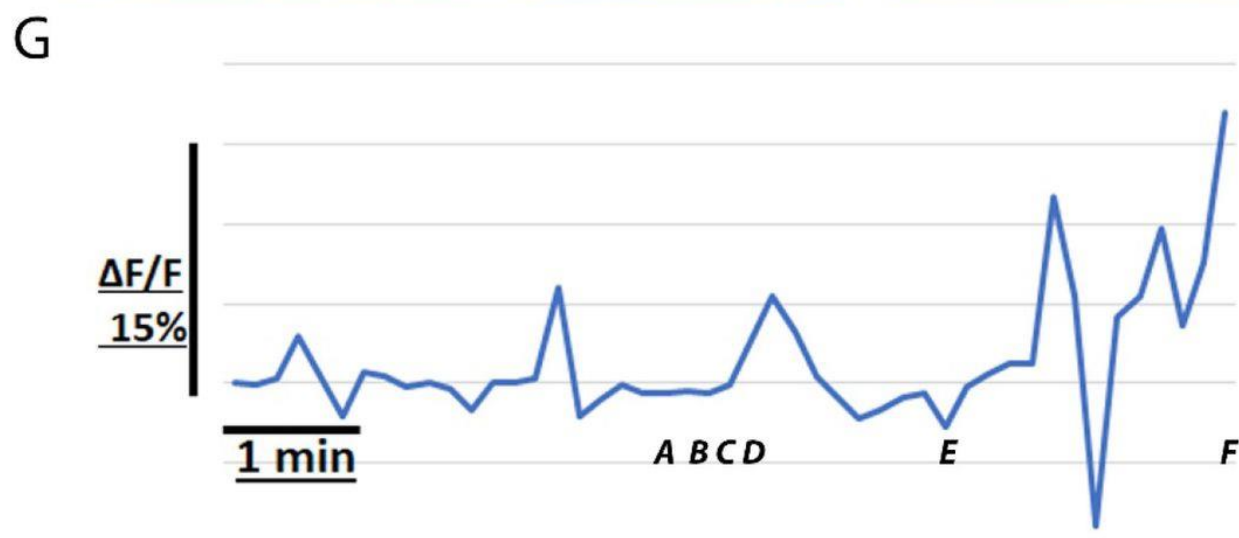
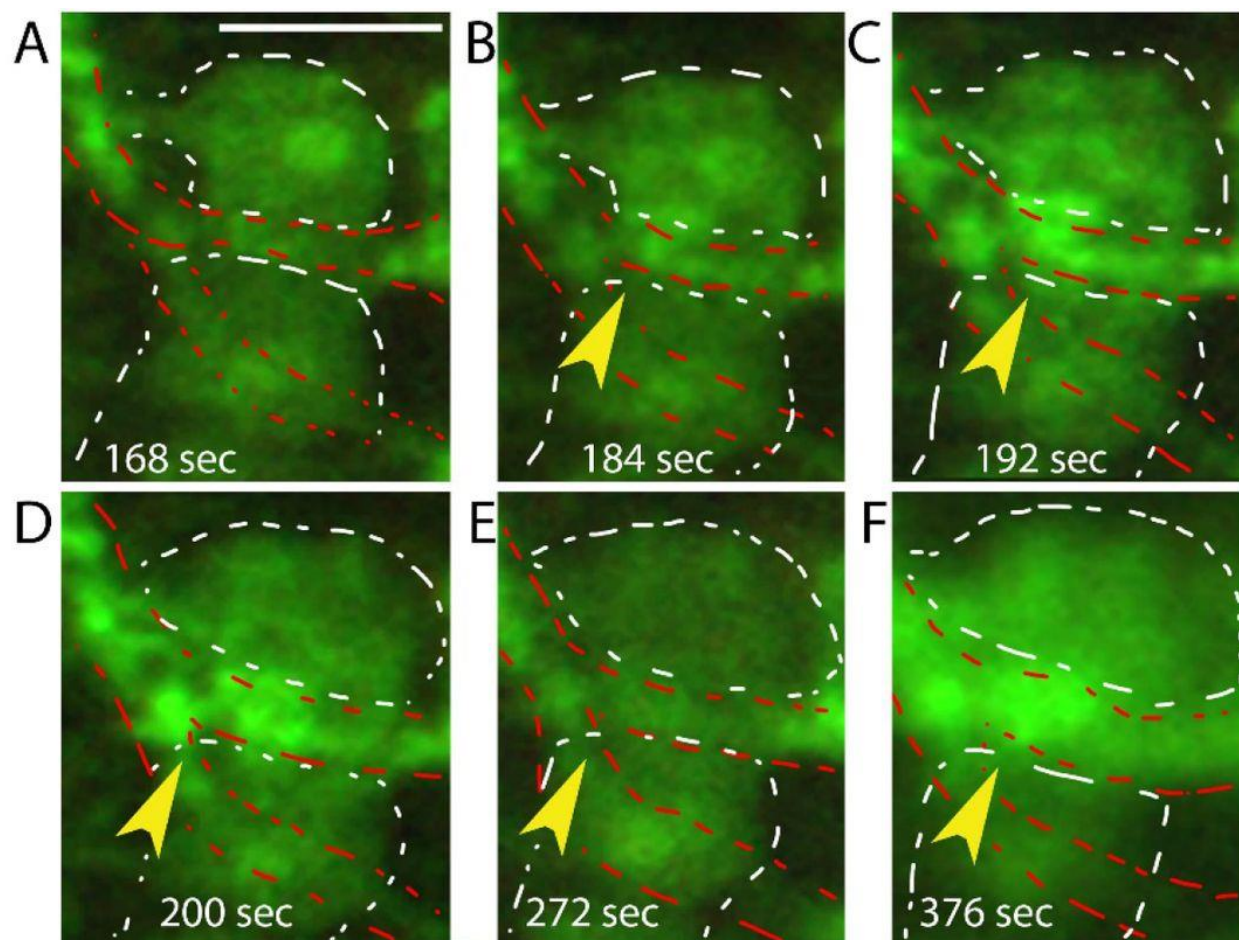


Figure 4-3 Melanophores show dynamic fluorescence changes after DREADD modification.

A-F. Six different time points of melanophore imaging in the head region of a 2dpf Tg (*mitfa2.1: ASAP2s-IRES-hM4DGi*) zebrafish embryo after DREADD activation. The time scale is in seconds. Arrows point to changes in GFP intensity in the same location. The upper white dashed lines outline a melanophore. The lower white dashed lines outline another melanophore. The red dashed lines outline projections from other melanophores. The yellow arrow at the center points to the middle region of the frame used for fluorescence quantification. **G.** $\Delta F/F$ quantification of melanophore fluorescence intensity changes over a 6-minute duration. ASAP2s fluorescence shows fluctuations in intensity. Scale bar = 25 μm . The corresponding time-lapse video can be found in Supplementary Video 4-1.

4.3.4 DREADD functional validation by melanophore morphological changes

We successfully modified cell membrane potential that can be measured via the ASAP2s voltage reporter. Whether this DREADD-induced voltage change is enough to affect the *in vivo* biology remains unknown. To address this question, we treated Tg (*mitfa2.1: ASAP2s-IRES-hM4DGi*) fish larvae and treated them with 20 μM DCZ from 2-3 dpf then raised them until 1 week (4 dpf-7 dpf). We found that the treated fish larvae developed hyperpigmentation compared to the untreated sibling control group (Fig. 4-4A-B). Treated and untreated groups of larvae were assessed for hyperpigmentation phenotype and then individually genotyped to determine if the pigmentation alteration was the result of hM4DGi receptor activation or from off-target agonist effects. Overall, the hyperpigmented phenotype was found in transgene-positive larvae (Fig. 4-4C). There was a statistically greater number that carried the transgene compared to Tg-negative and untreated larvae ($p < 0.001$). To figure out whether this melanophore hyperpigmentation was caused by an increased number of melanophores or melanophore dispersion, we treated these fish larvae with 1mM epinephrine ($\alpha 2$ -adrenoceptor agonist), which is known to cause melanosome aggregation. Epinephrine caused pigment granule contraction in DCZ-treated fish larvae (Fig. 4-4D-E). In summary, our results confirmed that the DREADD tools indeed are functional and can be used for relevant biological studies.

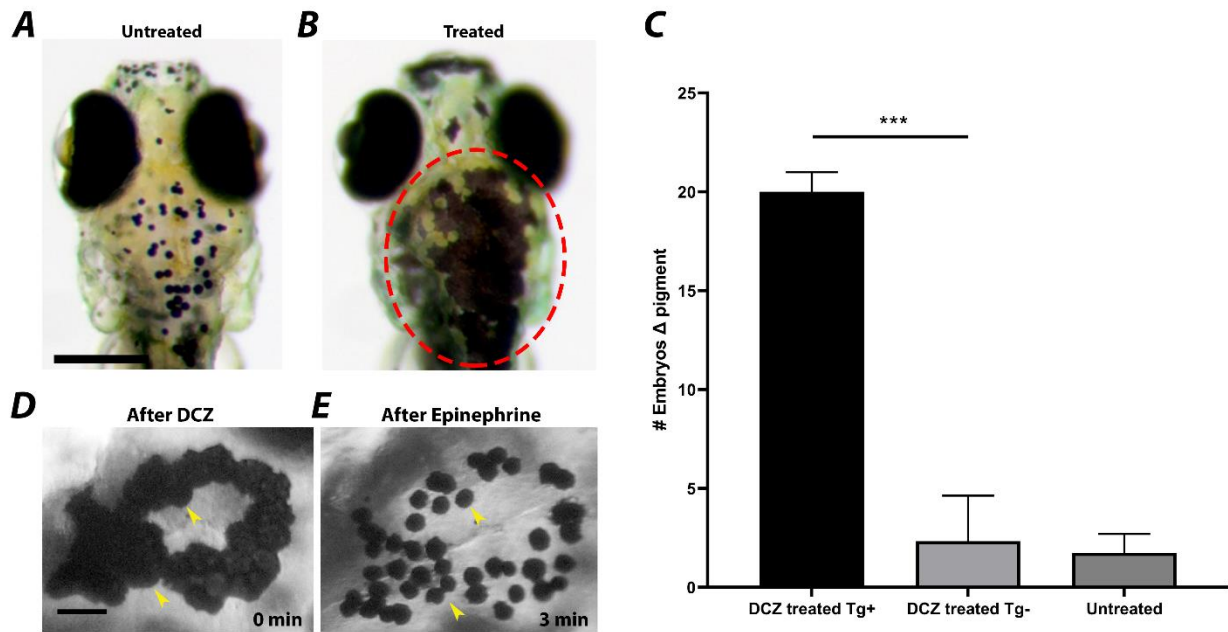


Figure 4-4 Activation of the hM4DGi receptor causes hyperpigmentation in 1-week old fish larvae.

A. A representative untreated 1-week old fish larva. **B.** A representative treated fish larva with hyperpigmentation (circled with a red dotted line). **C.** Quantification of hyperpigmented phenotype from treated embryos. Bars are mean with SD from three independent experiments. The student's T-test was used to determine statistical significance. $p < 0.001$ **D.** Dorsal view of another Tg (*mitfa2.1: ASAP2s-IRES-hM4DGi*) fish larva that was treated with DCZ. The melanophores are dispersed. **E.** The same fish larva was imaged 3 minutes after treatment with 1mM epinephrine. The melanophores are aggregated. Yellow arrows point to melanophores that are dispersed and then contracted, respectively. Scale bar = 250 μ m for **A-B** and 50 μ m for **D-E**.

4.3.5 Discussion

The chemogenetic tools are useful for manipulating bioelectricity and have been demonstrated successfully in neuroscience with murine and primate models. DREADD and PSAM tool adaptation was attempted but not successful in zebrafish [166]. Recently, we showed that the bioelectricity of the somites is involved in fin patterning [92]. To further investigate the roles of bioelectricity during embryonic development, there is a need for chemogenetic tools which allow us to manipulate bioelectricity for days and months. In addition, we have successfully adapted the ASAP1 voltage sensor to zebrafish using the Tol2 transposon-based transgenic approach [83]. Recently, the PSAM tools were demonstrated functional in zebrafish using the same transgenic

approach [167]. This motivated us to re-examine the possibility of adopting DREADDs in zebrafish.

There are a few caveat issues that could make a difference between our work and the previous study. First, the sensitivity of the detection method may be a key factor. We use the newly developed ASAP2s, which were reported to have a high level of sensitivity to cellular membrane voltage changes. In comparison, locomotor activity was used for measuring bioelectric changes previously. It is possible that there is some level of bioelectric change, but not enough to drive the locomotor activity change. Second, we examined the DREADDs using transgenic zebrafish lines, not the direct injection as in the former study. The transgenic fish provide stable and specific DREADD expression in the fish embryos for the targeted tissue. Thus, it reduces many stochastic expressions for measuring electric activities. In contrast, the direct injection of DREADD constructs will yield different levels of expression in many places. When we injected the *elavl3*:Gal4FF plasmid construct into Tg (UAS: DREADD-ASAP2s) transgenic fish embryos, only a few larval neurons were observed with fluorescence changes. One solution is to improve the DREADD expression levels. In the future, zebrafish fish-codon optimization, utilizing the zebrafish Kozak sequence before an ATG start codon, and adding dORF (downstream open reading frame) could be attempted for this purpose [280, 281]. Lastly, the examination time after treatment might also affect the judgment. In our experimental system, a higher concentration of ligand is still needed in order to visualize more impressive fluorescence changes over a shorter period of time (~5 min). This could be caused by tissue penetration, fish metabolism, or chemical potency.

There are numerous zebrafish pigment pattern mutants that affect proteins that regulate charged molecules, such as ion channels and gap junctions [97]. Alteration of these ionic regulators can cause morphological changes to zebrafish pigments and disrupt normal stripe formation. It was previously reported that melanophore cell membrane voltage manipulation with the optogenetic tool ChR2 was able to disrupt stripe formation in metamorphic and adult zebrafish [173]. Here, we chose zebrafish melanophores as a model and tested two DREADDs, hM4DGi and rM3DGs, and four agonists. We demonstrated that both DREADDs are functional to change cell membrane voltage measured by ASAP2s. These voltage alterations were validated in basal epithelial cells and neurons. Moreover, we were able to generate a melanophore hyperpigmentation phenotype

via hM4DGi and DCZ in 1-week larvae, confirming the biological functions of DREADD in zebrafish. hM4DGi activation of metamorphic melanophores also results in hyperpigmentation compared to untreated controls. These results provide additional validation for the biological impact, as well as the potential use of zebrafish DREADDs in older fish over longer periods of time.

In summary, we generated tissue-specific DREADD transgenic zebrafish lines and tested their function in zebrafish embryos and larvae using different agonists. We demonstrated that this chemogenetic tool works in zebrafish melanophores, neurons, and epithelial cells. We expect the DREADD tools and our transgenic fish lines will meet the critical need for neuronal and embryonic bioelectric studies. Moreover, they can be a great resource to the zebrafish community.

CHAPTER 5. OVERALL DISCUSSION

Current zebrafish fish lines for bioelectric research are limited. In this thesis work, we first generated a ubiquitous reporter of zebrafish endogenous Vm (Tg(*ubi*: ASAP1)) [83]. With this transgenic fish, we visualized the bioelectricity of early zebrafish larvae and showed Vm differences between normal and tumor tissue. Next, we carefully tracked and quantified characteristic electric signals from fertilization to the segmentation period during early development [84]. Furthermore, to manipulate Vm/bioelectricity, we adopted the chemogenetic DREADD tools hM4DGi and hM3DGs, which were combined with ASAP2s and generated new transgenic zebrafish lines [169]. Using these fish lines, we were able to examine DREADD function in zebrafish melanophores. Though the ASAP2s reporter is not ideal, we have found zebrafish larva developed a hyperpigmentation phenotype with DREAD agonist treatment. Collectively, the work presented here is a step toward studying how bioelectric signals in zebrafish might contribute to developmental patterning. Future optimization of GEVI and DREADD in zebrafish may yield useful tools for bioelectricity.

A whole-organism Vm reporter like the one here is useful when trying to get an overall picture, or there is not a tissue-specific promoter available, but the cell-specific expression will be needed to answer more in-depth questions on bioelectric regulation. While this work establishes the fundamental groundwork for understanding zebrafish embryonic endogenous bioelectricity, manipulations of these signals are needed to understand their mechanistic significance.

We generated DREADD transgenics with either hM4DGi and hM3DGs that we would be able to make cells more negative or more positive respectively and then directly visualize Vm changes in cells simultaneously expressing the GEVI ASAP2s. We were able to increase ASAP2s fluorescence intensity in cells that also expressed the hyperpolarizing DREADD hM4DGi after treatment with the DREADD agonist DCZ. Next, we decrease ASAP2s fluorescence intensity in cells that also expressed hM3DGs after DCZ treatment. Furthermore, when examined over timelapse imaging, these hM4DGi-induced changes were revealed to be dynamic in zebrafish melanophores. These Vm changes were further functionally validated in melanophores by

inducing a hyperpigmented phenotype in larval fish embryos. The results show optimistic outcomes in future studies; however, more work is needed to improve this tool.

One of the biggest difficulties is the relatively low brightness of the GEVI reporters[282, 283]. The main limitations stemmed from the inherent brightness of reporters and the promoters selected. Even with strong promoters such as ubiquitin, low fluorescence intensity makes imaging the dynamic Vm changes challenging using epifluorescence microscopy, even with LSM. The use of a direct promoter-driven construct for cell-specific expression was not as bright as anticipated. The weak fluorescence could be caused by a few reasons.

First, the *mitfa2.1* promoter could not be strong enough for the expression of GEVI and DREADD in zebrafish melanocytes. Also, the 4XnrUAS promoter could also not be strong enough [284]. While this has been reported to drive high expression levels while reducing silencing via DNA methylation compared to 14XUAS [285], we had difficulties achieving sufficiently high expression levels. Although, the 14XUAS promoter can be silenced after multiple generations due to the repetitive sequence [284] 14XUAS may perform better than 4xnrUAS. Secondly, we used human codon-optimized GEVI and DREADD in our studies. It was reported that zebrafish-specific codon optimization could enhance protein expression levels [281]. Along this line, dORFs were also reported to increase translation efficiency and thus could be added in the future. Thirdly, the ASAP1 reporter may not be bright enough, but studies in other organisms have already demonstrated that it functioned well in the brains of mice, flies, and even zebrafish. The weak ASAP1 in melanocytes could be caused by the intrinsic properties of these cell types. To overcome this, calcium reporters [160, 286] could be an alternative. Since these are intracellular rather than membrane-localized, the amount of fluorescence protein is greatly increased, and these signals are generally brighter than GEVIs in other reports. However, this also has its disadvantages because GECIs are not direct reporters of membrane voltage. Another option would be newly developed GEVIs that reportedly have improved fluorescence signals such as ASAP4 (ref) [130], and Voltron [154].

It was previously reported that DREADD did not function in zebrafish [166], even though it has been successfully adopted in human cells, mice, *drosophila*, and primate studies [106, 271, 287].

The previously mentioned zebrafish study performed experiments within F_0 transiently injected fish and used first-generation agonists. Their assay was also only based on larval movement, which might not be as sensitive to subtle V_m changes. Therefore, we thought to remove these possibilities by generating stable transgenic fish lines, adopting the latest generation agonist, and using real-time GEVI reporters to measure any changes to V_m . In our hand, the DREADD tool seemed to work with high concentrations of agonists but certainly will need to be optimized to draw a clear conclusion that DREADD works well in zebrafish. The pharmacodynamics and the penetration of agonists into fish tissues are less likely the causes, as we selected the zebrafish melanophore for our experiments. The melanophores are close to the surface and relatively visible. Most likely, similar to ASAP1, the DREADD expression may not be ideal for functional studies. Further improvements will be needed to determine if these issues are related to receptor expression levels, pharmacodynamics, GEVI reporter shortcomings, or potentially all three. In addition, voltage validation measurements with patch-clamp will be useful to conclusively determine DREADDs functional activity in zebrafish.

Overall, the future of developmental bioelectricity is an exciting and optimistic avenue for research. The implantation of modern genetically encoded tools provides researchers with a plethora of options to choose from when considering measuring and manipulating endogenous electrical activity. Once the implementation barrier is overcome, new knowledge will be generated for embryonic development, tissue patterning, regeneration, cell migration, and even cancer [1, 192, 193]. Furthermore, elucidating the mechanisms behind this type of regulation outside of the brain will be groundbreaking. For example, future related studies will provide a better biological understanding of channelopathies essential to uncover the contributions to adult final form. This category of channelopathy-type diseases continues to expand and affects a variety of ion channels resulting in nervous system, endocrine, cardiovascular, respiratory, urinary, and immune diseases in addition to physical congenital abnormalities [195, 288]. Furthermore, the possibility of pharmaceutically resolving some of these issues is possible considering the large amount of already approved ion channel drugs [75, 202, 204]. Ergo, such an important regulator that affects such a large and diverse group of diseases, as well as fundamental biological processes, makes the unanswered questions of bioelectricity a priority research field.

CHAPTER 6. MATERIALS AND METHODS

6.1 Visualization of Cellular Electrical Activity in Zebrafish Early Embryos and Tumors

6.1.1 Materials

Table 4 Materials

| Name | Company | Catalog Number | Comments |
|---|------------------------|--|--|
| 14mL cell culture tubes | VWR | 60818-725 | E.Coli culture |
| Agarose electrophoresis tank | Thermo Scientific | Owl B2 | DNA eletrophoresis |
| Agarose RA | Amresco | N605-500G | For making the injection gels |
| Attb1-ASAP1-F primer | IDT DNA | GGGGACAAGTTTGTACAAAAA GCAGGCTTCACCATGGAGACGA CTGTGAGGTATGAACA | ASAP1 coding region amplification for subcloning |
| Attb2-ASAP1-R primer | IDT DNA | GGGGACCACTTTGTACAAGAAA GCTGGGTCTTAGGTTACCACTTC AAGTTGTTTCTTCTGTGAAGCCA | ASAP1 coding region amplification for subcloning |
| Bright field dissection scope | Nikon | SMZ 745 | Dechoriation, microinjection, mounting |
| Color camera | Zeiss | AxioCam MRc | Fish embryo image recording |
| Concave slide | VWR | 48336-001 | For holding fish embryos during imaging process |
| Disposable transfer pipette 3.4 ml | Thermo Scientific | 13-711-9AM | Fish embryos and water transfer |
| Endonuclease enzyme, Not I | NEB | R0189L | For linearizing plasmid DNA |
| Epifluorescent compound scope | Zeiss | Axio Imager.A2 | Fish embryo imaging |
| Epifluorescent stereo dissection scope | Zeiss | Stereo Discovery.V12 | Fish embryo imaging |
| Fluorescent light source | Lumen dynamics | X-cite serie 120 | Light source for fluorescence microscopes |
| Forceps #5 | WPI | 500342 | Dechoriation and needle breaking |
| Gateway BP Clonase II Enzyme mix | Thermo Scientific | 11789020 | Gateway BP recombination cloning |
| Gateway LR Clonase II Plus enzyme | Thermo Scientific | 12538120 | Gateway LR recombination cloning |
| Gel DNA Recovery Kit | Zymo Research | D4002 | DNA gel purification |
| Loading tip | Eppendorf | 930001007 | For loading injection solution into capillary needles |
| Methylcellulose (1600cPs) | Alfa Aesar | 43146 | Fish embryo mounting |
| Methylene blue | Sigma-Aldrich | M9140 | Suppresses fungal outbreaks in Petri dishes |
| Microinjection mold | Adaptive Science Tools | TU-1 | To prepare agarose mold tray for holding fish embryos during injection |
| Microinjector | WPI | Pneumatic Picopump PV820 | Microinjection injector |
| Micro-manipulator | WPI | Microinjector MM3301R | Microinjection operation |

Table 4 Materials- continued

| | | | |
|---|-------------------|-------------------------|---|
| Micropipette puller | Sutter instrument | P-1000 | For preparing capillary needle |
| Mineral oil | Amresco | J217-500ml | For calibrating injection volume |
| mMESSAGE mMACHINE SP6 Transcription Kit | Thermo Scientific | AM1340 | mRNA in vitro transcription |
| Monocolor camera | Zeiss | AxioCam MRm | Fish embryo image recording |
| Plasmid Miniprep Kit | Zymo Research | D4020 | Prepare small amount of plasmid DNA |
| Plastic Petri dishes | VWR | 25384-088 | For holding fish or fish embryos during imaging process |
| RNA Clean & Concentrator-5 | Zymo Research | R1015 | mRNA cleaning after in vitro transcription |
| Spectrophotometer | Thermo Scientific | NanoDrop 2000 | For measuring DNA and RNA concentrations |
| Stage Micrometer | Am Scope | MR100 | Microinjection volume calibration |
| Thermocycler | Bio-Rad | T100 | DNA amplification for gene cloning |
| Thin wall glass capillaries | WPI | TW100F-4 | Raw glass for making capillary needle |
| Tol2-exL1 primer | IDT DNA | GCACAACACCAGAAATGCCCTC | Tol2 excise assay |
| Tol2-exR primer | IDT DNA | ACCCTCACTAAAGGGAACAAAAG | Tol2 excise assay |
| TOP10 Chemically Competent E. coli | Thermo Scientific | C404006 | Used for transformation during gene cloning |
| Tricaine mesylate | Sigma-Aldrich | A5040 | For anesthetizing fish or fish embryos |
| UV trans-illuminator 302nm | UVP | M-20V | DNA visualization |
| Water bath | Thermo Scientific | 2853 | For transformation process of gene cloning |

6.2 Zebrafish embryos display characteristic bioelectric signals during early development

6.2.1 Zebrafish Strains and Transgenic Fish Line Husbandry

Zebrafish were raised and maintained within the Purdue veterinary hospital animal housing facility (West Lafayette, IN. USA), which was approved by the Association for Assessment and Accreditation of Laboratory Animal Care (AAALAC). Purdue Animal Care and Use Committee (PACUC) approved protocols were used to perform experiments. All zebrafish trials were conducted in wild-type TAB fish genetic backgrounds. Zebrafish were maintained according to the zebrafish book, and embryos were staged according to the Kimmel staging guide [232]. The Tg (*ubi*-ASAP1) fish line was generated in our previous report [83].

6.2.2 Imaging Early Zebrafish Embryo Vm Fluorescence and Data Analysis

Multiple Tg (*ubi: ASAP1*) adult fish were in-crossed or out-crossed with TAB fish to acquire green fluorescence-positive offspring. Zebrafish embryos were collected at different desired developmental stages. To better visualize the cellular GEVI-GFP activity, zebrafish embryo chorions were either left in place or carefully removed using a pair of forceps under a dissection scope before mounting in 0.6% low melting agarose (IBI Scientific CAS#9012-36-6) on a sample platform to maintain their positions.

Zebrafish embryos were imaged using a Miltenyi Biotec light sheet microscope, Ultra-Microscope II with a Super Plan Module configuration, a 4x NA 0.35 MI PLAN objective, and InspectorPro software (7.1.4 Lavisision Biotec, Bielefeld, Germany). Image acquisition total times varied from minutes to 16+ hours depending on embryonic stages. Z-stacks between 1 and 20 slices had total intervals between 0.5 s and 3 min. Laser power was set between 50–70% and sheet width at 60% for image acquisition. Water was selected as the imaging medium. Exposure times were between 50 ms and 300 ms, depending on the imaging speed.

Max intensity projections were used to display 3D images by importing TIF files to ImageJ [289]. ROIs were placed over areas of embryos with signals to track mean fluorescence changes over time. Fluorescence intensity data were exported into Excel for further analysis. The ΔF_{Adj} was calculated as $(F_t - F_{0Adj})/F_{0Adj}$, where F_t is the fluorescent value at a given time t , and F_0 is the baseline fluorescence constant value. F_{0Adj} was calculated by averaging at least four frames without any bright GFP signal. Traditional $\Delta F/F$ was also calculated as $(F_t - F_0)/F_0$, where F_0 is equal to $F_{t(n-1)}$. Vm transient signals were analyzed using Imaris software (9.7.2 Bitplane AG). Time-lapse Imaging files were converted to .ims format and imported to the Imaris program. The "spots" function was used to detect electric transient fluorescent signals within an ROI of a given embryo ($n \geq 5$). For the algorithm, default parameters were used. Estimated XY diameter was based on cell diameter measured within the Imaris slice tab and generally fell between 10–20 μm depending on the embryonic stage. Background subtraction was selected. The signal "quality" parameter in Imaris for detection was set at a sufficient "level" using the slide bar, which could detect transient signals without recognizing background noise, generally between 80 and 100+. The "Tracks"

function was used to determine the total number of Vm transients over time so that a signal was counted only one time if appearing in multiple frames to define transient number and duration. Autoregressive motion, an algorithm that allows for tracking back an immediately previous time point, was selected with "Max Distance" set as a value equal to the diameter of the cell and a gap distance of zero. After completing the analysis, data was converted and saved into an Excel file format. "Track Duration" statistics gave the total number of transients and the different transient durations. GraphPad Prism (v9.4.1) was used to generate graphs and perform statistical calculations. The student's t-test was used to determine the statistical significance between groups.

6.3 Tissue-specific modification of cellular bioelectrical activities using the chemogenetic tool, DREADD, in zebrafish

6.3.1 Zebrafish husbandry

Zebrafish were raised and maintained at the Purdue animal housing facility following Association for Assessment and Accreditation of Laboratory Animal Care (AAALAC) approved standards. Experiments were carried out according to Purdue Animal Care and Use Committee (PACUC) approved protocols. All zebrafish experiments were carried out in wild-type TAB fish. Zebrafish were maintained according to the zebrafish book. Zebrafish embryos were staged based on the Kimmel staging guide.

6.3.2 Tol2 constructs, microinjection, and zebrafish transgenic lines

Tol2 transposon plasmids were generated using a three-fragment Gateway cloning-based Tol2 kit (40). The 5' end entry plasmids p5E-*mitfa2.1* (plasmid #81234), p5E-*elavl3* (plasmid #72640) (41), p5E-4xrnUAS (plasmid #61372) (42) were acquired through Addgene. pME-Gal4FF were subcloned from pCR8GW-Gal4-VP16-FRT-kan-FRT (43), a gift from Dr. Koichi Kawakami. p5E-*tp63* was a gift from Dr. Qing Deng (44). The pENTR-D-ASAP2s plasmids were generated by site-directed mutagenesis from pENTR-D-ASAP1 (24) using the primers (ASAP2s-F: ATA TTT CAG CTG GCT TCA CAG AAG AAA CAA CTT GAA GTG G and ASAP2s-R: AGC CAG CTG AAA TAT TCT TAT TAA GAT AAC AAT TCT CAG AAC TCG AAG AAG AG). The p3E-IRES-hM4DGi and p3E-IRES-rM3DGs were generated by subcloning from pAAV-hSyn-

DIO-HA-hM4DGi-IRES-mCitrine (plasmid# 50455) and pAAV-hSyn-DIO-HA-rM3DGs-IRES-mCitrine (plasmid# 50456) into p3E-IRES-EGFP vector (Tol2 kit #389), respectively. All the subcloning and site-directed mutagenesis were performed using the In-Fusion cloning system (Takara Bio). Final entry constructs were verified by Sanger sequencing. The final constructs were built using LR Clonase II Plus enzyme (Thermo Scientific) following the manufacturer's instructions.

pCS-zT2Tp plasmid (a gift from Koichi Kawakami) was used as a template to generate Tol2 transposase messenger RNA (mRNA) using the mMESSAGE mMACHINE SP6 transcription kit (Thermo Scientific). Capped and tailed mRNAs were purified by Monarch RNA Cleanup Kit (NEB) according to the manufactory guide and eluted in DEPC-treated water. Microinjection of Tol2 expression constructs (25 ng/μl) and Tol2 mRNA (50 ng/μl) with 0.025% phenol red (P0290; Sigma) was performed on one-cell-stage zebrafish embryos under a dissection microscope (SMZ445; Nikon, Garden City, NY) using a PV820 pneumatic PicoPump (World Precision Instruments). About ten injected embryos were sampled for gDNA isolation using the HotSHOT method after at least 8 hours (45). Tol2 transposon efficiency was verified with an excise assay (46). Once the excise assays confirmed the Tol2 activity, the remainder of the injected fish embryos were raised to adulthood. TAB wild-type fish were crossed with F0-injected adult fish, and positive fluorescent transgenic zebrafish embryos were selected and raised to adults as stable F1 transgenic fish lines.

6.3.3 DREADD ligand addition and fluorescence imaging

To detect cell membrane potential changes via ASAP2s imaging, embryos were raised to 2 days post fertilization (dpf), then anesthetized in a 0.05% Tricane solution. For fluorescence imaging experiments, embryos were raised in fish system water without methylene blue to reduce autofluorescence and treated with 1X PTU (1-phenyl 2-thiourea, 0.2mM) to reduce pigments. Anesthetized embryos were placed on a glass slide with fish system water and positioned properly for imaging. In order to visualize large changes in fluorescence intensity, 1μL of 100mM DCZ was added to slides containing Tg fish and ~400μL of fish water for a final concentration of 250 μM. Untreated images were taken before agonist addition. After treatment, embryos were either

monitored for 5-15 minutes for fluorescence changes and then imaged, or immediately recorded with time-lapse imaging. Exposure was set at the start of imaging (between 4000 and 8000 ms) and kept consistent for the entire length of time the same individual larva was imaged in order to compare levels of fluorescence intensity between images directly. All the DREADD agonists were purchased from HelloBio and diluted in water as 100mM stock solutions that were stored in a -20C freezer before use. Described concentrations of DREADD agonist were then added to the fish system water on the slide. Embryos were monitored for positional shifts and adjusted if they drifted from their original location. Next, time-lapse imaging was continued for 5-15 minutes. Cellular $\Delta F/F = ((F_t - F_0)/F_0)$ was quantified using ImageJ to define a region of interest for mean fluorescence intensity at each time point. F_t is the fluorescent value at a given time t , and F_0 is the starting fluorescence value. All images were acquired using a Zeiss AxioCam MRc camera on Stereo Discovery.V12 or Axio Imager 2 compound microscope. For *elavl3*: Gal4FF, Tol2 plasmid was injected into 1-cell stage Tg (UAS: DREADD-ASAP2s) transgenic fish embryos. UAS fish lines were prepared for one-cell-stage microinjection as described above. Injected embryos were monitored and raised to 2dpf. Embryos with positive fluorescence, via GFP eye and heart markers, were sorted and used for agonist addition and fluorescence imaging, as previously mentioned. Unless specified otherwise, this type of signal is expressed as a fractional change in fluorescence intensity $\Delta F/F_0$.

6.3.4 Tracking 1-week larvae for DREADD induced phenotype

To track pigmentation changes caused by DREADD treatments, we crossed Tg (*mitfa2.1*: *ASAP2s-IRES-hM4DGi*) with TAB fish. Dechorionated 2dpf embryos were separated into groups of about 40 and placed into 6-well plates containing fish water with 0.05% methylene blue. This mixed group of siblings contained wildtype and transgenic larvae. Next, the water was replaced with fresh water containing a designated concentration of DREADD agonists. Embryos were treated once at 2dpf and raised until 7dpf. At 7dpf, larvae in each well were counted to obtain the number with increased head pigmentation. This was repeated, and both trials later added to the total number of fish tracked for each DREADD agonist (n=128).

For genotyping a representative portion of DREADD-treated embryos, 96-well plates were used to separate single embryos from Tg (*mitfa2.1: ASAP2s-IRES-hM4DGi*) crossed with wild-type fish. Dechorionated 2dpf embryos were separated and placed into individual wells containing fish water with methylene blue. This mixed group of siblings contained wildtype and transgenic larvae. Next, water was replaced with 200uL of fresh fish water containing designated amounts of DREADD ligand. These two-day-old fish embryos were treated with either DCZ, JHU37160, C21, or CNO (n=48 for each agonist), respectively. Each well was raised for seven days to observe pigmentation changes. On the seventh day, the number of embryos with increased head pigmentation was counted. All embryos were then harvested for genotype using 100 mM NaOH (hotshot method). PCR primers (ASAP1-genoF: ATA TGA CCT ACT CCT TCT CTG ACC and ASAP1-genoR: AGG TTA AGG TGG TCA CCA GG) were used to amplify the ASAP2s transgene to validate transgenic mutant correlation with phenotypic changes. These percentages were calculated as a representative of a total of 128 tracked embryos for each agonist.

For examining the variation of melanophore morphology, 7dpf larvae were treated with epinephrine (1mM) to determine any changes to total pigment cell count and assess the dispersion of pigment granules. The larvae were placed on a glass slide with fish system water and imaged under regular epifluorescence light. For evaluating the impact of bioelectric changes on metamorphic fish melanophores, transgenic larvae that were about two weeks of development (~6.5mm) were treated with DCZ (20 μ M) for one week every two days. Once fish reached about 30 days old (9-10mm), they were imaged under a microscope for pigmentation changes. Comparable-sized untreated transgenic fish were also imaged as a control.

REFERENCES

1. Chang, F. and N. Minc, *Electrochemical Control of Cell and Tissue Polarity*. Annual Review of Cell and Developmental Biology, 2014. **30**(1): p. 317-336.
2. Levin, M., *Molecular bioelectricity: how endogenous voltage potentials control cell behavior and instruct pattern regulation in vivo*. Molecular Biology of the Cell, 2014. **25**(24): p. 3835-3850.
3. Levin, M., G. Pezzulo, and J.M. Finkelstein, *Endogenous Bioelectric Signaling Networks: Exploiting Voltage Gradients for Control of Growth and Form*. Annual Review of Biomedical Engineering, 2017. **19**(1): p. 353-387.
4. Mathews, J. and M. Levin, *The body electric 2.0: recent advances in developmental bioelectricity for regenerative and synthetic bioengineering*. Current Opinion in Biotechnology, 2018. **52**: p. 134-144.
5. Chrysafides, S.M. and S. Sharma, *Physiology, Resting Potential*, in *StatPearls*. 2019, StatPearls Publishing: Treasure Island (FL).
6. Levin, M. and C.J. Martyniuk, *The bioelectric code: An ancient computational medium for dynamic control of growth and form*. Biosystems, 2018. **164**: p. 76-93.
7. Catterall, W.A., G. Wisedchaisri, and N. Zheng, *The Chemical Basis for Electrical Signaling*. Nature chemical biology, 2017. **13**(5): p. 455-463.
8. Stratford, J.P., et al., *Electrically induced bacterial membrane-potential dynamics correspond to cellular proliferation capacity*. Proceedings of the National Academy of Sciences of the United States of America, 2019. **116**(19): p. 9552-9557.
9. Chimere, C., et al., *Indole prevents Escherichia coli cell division by modulating membrane potential*. Biochimica et Biophysica Acta, 2012. **1818**(7): p. 1590-1594.
10. Wayne, R., *The excitability of plant cells: with a special emphasis on characean internodal cells*. The Botanical Review; Interpreting Botanical Progress, 1994. **60**(3): p. 265-367.
11. Martinac, B., Y. Saimi, and C. Kung, *Ion channels in microbes*. Physiological reviews, 2008. **88**(4): p. 1449-1490.
12. Adamatzky, A., *Language of fungi derived from their electrical spiking activity*. Royal Society Open Science, 2022. **9**(4).
13. Dehshibi, M.M. and A. Adamatzky, *Electrical activity of fungi: Spikes detection and complexity analysis*. Biosystems, 2021. **203**: p. 104373.
14. Babikova, Z., et al., *Underground signals carried through common mycelial networks warn neighbouring plants of aphid attack*. Ecol Lett, 2013. **16**(7): p. 835-43.
15. Volkov, A.G. and Y.B. Shtessel, *Underground electrotonic signal transmission between plants*. Communicative & Integrative Biology, 2020. **13**(1): p. 54-58.
16. Niebur, E., *Electrical properties of cell membranes*. Scholarpedia, 2008. **3**(6): p. 7166.

17. Binggeli, R. and R.C. Weinstein, *Membrane potentials and sodium channels: Hypotheses for growth regulation and cancer formation based on changes in sodium channels and gap junctions*. Journal of Theoretical Biology, 1986. **123**(4): p. 377-401.
18. Bernd Nilius, G.S., and Guy Droogmans, *Control of intracellular calcium by membrane potential in human melanoma cells*. The American Physiological Society, 1993. **265**(6): p. C1501-C1510.
19. Stanisz, H., et al., *ORAI1 Ca²⁺ Channels Control Endothelin-1-Induced Mitogenesis and Melanogenesis in Primary Human Melanocytes*. Journal of Investigative Dermatology, 2012. **132**(5): p. 1443-1451.
20. Bellono, N.W. and E. Oancea, *UV light phototransduction depolarizes human melanocytes*. Channels, 2013. **7**(4): p. 243-248.
21. Rorsman, P. and F.M. Ashcroft, *Pancreatic beta-Cell Electrical Activity and Insulin Secretion: Of Mice and Men*. Physiol Rev, 2018. **98**(1): p. 117-214.
22. DECOURSEY, T.E., *Hypothesis: do voltage-gated H1 channels in alveolarepithelial cells contribute to CO₂elimination by the lung?* American Journal of Physiology - Cell Physiology, 2000. **278**(1): p. C1-C10.
23. Sridhar, S., N. Vandersickel, and A.V. Panfilov, *Effect of myocyte-fibroblast coupling on the onset of pathological dynamics in a model of ventricular tissue*. Scientific Reports, 2017. **7**(1): p. 40985.
24. Yao, X., *Expression of KCNA10, a Voltage-Gated K Channel, in Glomerular Endothelium and at the Apical Membrane of the Renal Proximal Tubule*. Journal of the American Society of Nephrology, 2002. **13**(12): p. 2831-2839.
25. Forsberg, A.M., et al., *Resting Membrane Potential of Skeletal Muscle Calculated from Plasma and Muscle Electrolyte and Water Contents*. Clinical Science, 1997. **92**(4): p. 391-396.
26. Kumar, V., et al., *The Importance of Incorporating OCT2 Plasma Membrane Expression and Membrane Potential in IVIVE of Metformin Renal Secretory Clearance*. Drug Metabolism and Disposition, 2018. **46**(10): p. 1441-1445.
27. Pangalos, M., et al., *Action potentials in primary osteoblasts and in the MG-63 osteoblast-like cell line*. Journal of Bioenergetics and Biomembranes, 2011. **43**(3): p. 311-322.
28. Stone, M.S., L. Martyn, and C.M. Weaver, *Potassium Intake, Bioavailability, Hypertension, and Glucose Control*. Nutrients, 2016. **8**(7).
29. Wright, S.H., *Generation of resting membrane potential*. Advances in Physiology Education, 2004. **28**(4): p. 139-142.
30. Hodgkin, A.L. and A.F. Huxley, *A quantitative description of membrane current and its application to conduction and excitation in nerve*. The Journal of Physiology, 1952. **117**(4): p. 500-544.
31. *Office of Dietary Supplements - Potassium*.

32. Renigunta, V., G. Schlichthörl, and J. Daut, *Much more than a leak: structure and function of K2P-channels*. Pflügers Archiv - European Journal of Physiology, 2015. **467**(5): p. 867-894.
33. *Ion Channels*. British Journal of Pharmacology, 2011. **164**(Suppl 1): p. S137-S174.
34. Janata, J., *Historical review. Twenty years of ion-selective field-effect transistors*. Analyst, 1994. **119**(11): p. 2275-2278.
35. Hutchings, C.J., P. Colussi, and T.G. Clark, *Ion channels as therapeutic antibody targets*. mAbs, 2019. **11**(2): p. 265-296.
36. *Ion channels / HUGO Gene Nomenclature Committee*.
37. *Ion channel families / IUPHAR/BPS Guide to PHARMACOLOGY*.
38. Hille, B., *Ion Channels of Excitable Membranes*. 3 edition ed. 2001, Sunderland, Mass: Sinauer Associates is an imprint of Oxford University Press. 814.
39. Eskova, A., et al., *Gain-of-function mutations in Aqp3a influence zebrafish pigment pattern formation through the tissue environment*. Development, 2017. **144**(11): p. 2059-2069.
40. Latorre, R., et al., *Voltage and Temperature Gating of ThermoTRP Channels*, in *TRP Ion Channel Function in Sensory Transduction and Cellular Signaling Cascades*, W.B. Liedtke and S. Heller, Editors. 2007, CRC Press/Taylor & Francis: Boca Raton (FL).
41. Parpaite, T. and B. Coste, *Piezo channels*. Curr Biol, 2017. **27**(7): p. R250-R252.
42. Josselyn, S.A., *The past, present and future of light-gated ion channels and optogenetics*. eLife, 2018. **7**.
43. Hibino, H., et al., *Inwardly Rectifying Potassium Channels: Their Structure, Function, and Physiological Roles*. Physiological Reviews, 2010. **90**(1): p. 291-366.
44. Dong, A., S. Liu, and Y. Li, *Gap Junctions in the Nervous System: Probing Functional Connections Using New Imaging Approaches*. Frontiers in Cellular Neuroscience, 2018. **12**.
45. Scemes, E., D.C. Spray, and P. Meda, *Connexins, pannexins, innexins: novel roles of "hemi-channels"*. Pflugers Archiv : European journal of physiology, 2009. **457**(6): p. 1207-1226.
46. Cottrell, G.T. and J.M. Burt, *Functional consequences of heterogeneous gap junction channel formation and its influence in health and disease*. Biochimica et Biophysica Acta (BBA) - Biomembranes, 2005. **1711**(2): p. 126-141.
47. Koval, M., S.A. Molina, and J.M. Burt, *Mix and match: Investigating heteromeric and heterotypic gap junction channels in model systems and native tissues*. FEBS Letters, 2014. **588**(8): p. 1193-1204.
48. Adams, D.S. and M. Levin, *Endogenous voltage gradients as mediators of cell-cell communication: strategies for investigating bioelectrical signals during pattern formation*. Cell and Tissue Research, 2013. **352**(1): p. 95-122.
49. Sherer, N.M. and W. Mothes, *Cytonemes and tunneling nanotubules in cell-cell communication and viral pathogenesis*. Trends in cell biology, 2008. **18**(9): p. 414-420.

50. Eom, D.S., et al., *Long-distance communication by specialized cellular projections during pigment pattern development and evolution*. eLife, 2015. **4**: p. e12401.
51. Ribeiro-Rodrigues, T.M., et al., *Role of connexin 43 in different forms of intercellular communication – gap junctions, extracellular vesicles and tunnelling nanotubes*. Journal of Cell Science, 2017. **130**(21): p. 3619-3630.
52. Lecanda, F., et al., *Connexin43 Deficiency Causes Delayed Ossification, Craniofacial Abnormalities, and Osteoblast Dysfunction*. Journal of Cell Biology, 2000. **151**(4): p. 931-944.
53. Srinivas, M., V.K. Verselis, and T.W. White, *Human diseases associated with connexin mutations*. Biochim Biophys Acta Biomembr, 2018. **1860**(1): p. 192-201.
54. Pizzagalli, M.D., A. Bensimon, and G. Superti-Furga, *A guide to plasma membrane solute carrier proteins*. The FEBS Journal, 2021. **288**(9): p. 2784-2835.
55. Lin, L., et al., *SLC transporters as therapeutic targets: emerging opportunities*. Nature Reviews Drug Discovery, 2015. **14**(8): p. 543-560.
56. Antinucci, P. and R. Hindges, *A crystal-clear zebrafish for in vivo imaging*. Scientific Reports, 2016. **6**(1): p. 29490.
57. Lanni, J.S., et al., *Integrated K⁺ channel and K⁺Cl⁻ cotransporter functions are required for the coordination of size and proportion during development*. Developmental Biology, 2019. **456**(2): p. 164-178.
58. Nyquist, M.D., B. Prasad, and E.A. Mostaghel, *Harnessing Solute Carrier Transporters for Precision Oncology*. Molecules, 2017. **22**(4): p. 539.
59. Schuetze, S.M., *The discovery of the action potential*. Trends in Neurosciences, 1983. **6**: p. 164-168.
60. *Some observations on potential differences across the ectoplasm membrane of Paramecium*. Protoplasma, 1935. **22**(1): p. 631-631.
61. Hodgkin, A.L. and B. Katz, *The effect of sodium ions on the electrical activity of the giant axon of the squid*. The Journal of Physiology, 1949. **108**(1): p. 37-77.
62. Schwiening, C.J., *A brief historical perspective: Hodgkin and Huxley*. The Journal of Physiology, 2012. **590**(11): p. 2571-2575.
63. Raz, A. and M. Perouansky, *8 - Central Nervous System Physiology: Neurophysiology*, in *Pharmacology and Physiology for Anesthesia (Second Edition)*, H.C. Hemmings and T.D. Egan, Editors. 2019, Elsevier: Philadelphia. p. 145-173.
64. Endo, M., *Calcium Ion as a Second Messenger With Special Reference to Excitation-Contraction Coupling*. Journal of Pharmacological Sciences, 2006. **100**(5): p. 519-524.
65. Maqoud, F., et al., *Cell Cycle Regulation by Ca²⁺-Activated K⁺ (BK) Channels Modulators in SH-SY5Y Neuroblastoma Cells*. International Journal of Molecular Sciences, 2018. **19**(8).

66. Tolstykh, G.P., et al., *Receptor- and store-operated mechanisms of calcium entry during the nanosecond electric pulse-induced cellular response*. Biochimica et Biophysica Acta (BBA) - Biomembranes, 2019. **1861**(3): p. 685-696.
67. Rorsman, P. and F.M. Ashcroft, *Pancreatic β -Cell Electrical Activity and Insulin Secretion: Of Mice and Men*. Physiological Reviews, 2017. **98**(1): p. 117-214.
68. Zhou, Y., et al., *Membrane potential modulates plasma membrane phospholipid dynamics and K-Ras signaling*. Science (New York, N.Y.), 2015. **349**(6250): p. 873-876.
69. Houart, C., *Zebrafish as an Experimental Organism*. Encyclopedia of Life Sciences, 2001.
70. Howe, K., et al., *The zebrafish reference genome sequence and its relationship to the human genome*. Nature, 2013. **496**(7446): p. 498-503.
71. Veldman, M.B. and S. Lin, *Zebrafish as a Developmental Model Organism for Pediatric Research*. Pediatric Research, 2008. **64**(5): p. 470-476.
72. Santoriello, C. and L.I. Zon, *Hooked! Modeling human disease in zebrafish*. The Journal of Clinical Investigation, 2012. **122**(7): p. 2337-2343.
73. Cassar, S., et al., *Use of Zebrafish in Drug Discovery Toxicology*. Chemical Research in Toxicology, 2020. **33**(1): p. 95-118.
74. Nikam, V.S., et al., *Zebrafish: An emerging whole-organism screening tool in safety pharmacology*. Indian Journal of Pharmacology, 2020. **52**(6): p. 505-513.
75. Murugan, N.J., et al., *Acute multidrug delivery via a wearable bioreactor facilitates long-term limb regeneration and functional recovery in adult *Xenopus laevis**. Science Advances, 2022. **8**(4): p. eabj2164.
76. Rodriguez-Sastre, N., C.F. Thomas, and C.A. Bradham, *Chapter 20 - Measuring voltage and ion concentrations in live embryos*, in *Methods in Cell Biology*, A. Hamdoun and K.R. Foltz, Editors. 2019, Academic Press. p. 459-472.
77. KLINE, D., *Ion currents and membrane domains in the cleaving *Xenopus* egg*. The Journal of Cell Biology, 1983. **97**(6): p. 1753-1761.
78. Webb, S.E. and A.L. Miller, *Ca²⁺ signaling and early embryonic patterning during zebrafish development*. Clinical and Experimental Pharmacology and Physiology, 2007. **34**(9): p. 897-904.
79. Nanos, V. and M. Levin, *Rewiring Endogenous Bioelectric Circuits in the *Xenopus laevis* Embryo Model*, in *Programmed Morphogenesis: Methods and Protocols*, M.R. Ebrahimkhani and J. Hislop, Editors. 2021, Springer US: New York, NY. p. 93-103.
80. Webb, S.E. and A.L. Miller, *Ca²⁺ signaling and early embryonic patterning during the blastula and gastrula periods of zebrafish and *Xenopus* development*. Biochim Biophys Acta, 2006. **1763**(11): p. 1192-208.
81. Chen, J., et al., *Imaging early embryonic calcium activity with GCaMP6s transgenic zebrafish*. Developmental biology, 2017. **430**(2): p. 385-396.
82. Wong, R., et al., *PIP2 Hydrolysis and Calcium Release Are Required for Cytokinesis in *Drosophila* Spermatocytes*. Current Biology, 2005. **15**(15): p. 1401-1406.

83. Silic, M.R. and G. Zhang, *Visualization of Cellular Electrical Activity in Zebrafish Early Embryos and Tumors*. JoVE (Journal of Visualized Experiments), 2018(134): p. e57330.
84. Silic, M.R., et al., *Zebrafish Embryos Display Characteristic Bioelectric Signals during Early Development*. Cells, 2022. **11**(22): p. 3586.
85. Liu, J., et al., *Cleavage Furrow Organization Requires PIP2-Mediated Recruitment of Anillin*. Current Biology, 2012. **22**(1): p. 64-69.
86. Field, S.J., et al., *PtdIns(4,5)P₂ Functions at the Cleavage Furrow during Cytokinesis*. Current Biology, 2005. **15**(15): p. 1407-1412.
87. Silic, M.R., M.M. Black, and G. Zhang, *Phylogenetic and developmental analyses indicate complex functions of calcium-activated potassium channels in zebrafish embryonic development*. Developmental Dynamics, 2021. **250**(10): p. 1477-1493.
88. Silic, M.R., et al., *Evolution of inwardly rectifying potassium channels and their gene expression in zebrafish embryos*. Developmental Dynamics, 2022. **251**(4): p. 687-713.
89. Harris, M.P., J.M. Daane, and J. Lanni, *Through veiled mirrors: Fish fins giving insight into size regulation*. Wiley Interdiscip Rev Dev Biol, 2021. **10**(4): p. e381.
90. Stewart, S., et al., *longfin causes cis-ectopic expression of the *kcnh2a* ether-a-go-go K⁺ channel to autonomously prolong fin outgrowth*. Development, 2021. **148**(11).
91. Perathoner, S., et al., *Bioelectric Signaling Regulates Size in Zebrafish Fins*. PLOS Genetics, 2014. **10**(1): p. e1004080.
92. Silic, M.R., et al., *Potassium Channel-Associated Bioelectricity of the Dermomyotome Determines Fin Patterning in Zebrafish*. Genetics, 2020. **215**(4): p. 1067-1084.
93. Iovine, M.K., et al., *Mutations in connexin43 (*GJA1*) perturb bone growth in zebrafish fins*. Dev Biol, 2005. **278**(1): p. 208-19.
94. Green, J., et al., *A gain of function mutation causing skeletal overgrowth in the rapunzel mutant*. Developmental Biology, 2009. **334**(1): p. 224-234.
95. McGowan, K.A. and G.S. Barsh, *How the zebrafish got its stripes*. eLife, 2016. **5**: p. e14239.
96. Patterson, L.B. and D.M. Parichy, *Zebrafish Pigment Pattern Formation: Insights into the Development and Evolution of Adult Form*. Annual Review of Genetics, 2019. **53**(1): p. 505-530.
97. Singh, Ajeet P. and C. Nüsslein-Volhard, *Zebrafish Stripes as a Model for Vertebrate Colour Pattern Formation*. Current Biology, 2015. **25**(2): p. R81-R92.
98. Inaba, M., H. Yamanaka, and S. Kondo, *Pigment Pattern Formation by Contact-Dependent Depolarization*. Science, 2012. **335**(6069): p. 677-677.
99. Iwashita, M., et al., *Pigment Pattern in jaguar/obelix Zebrafish Is Caused by a Kir7.1 Mutation: Implications for the Regulation of Melanosome Movement*. PLOS Genetics, 2006. **2**(11): p. e197.
100. Irion, U., et al., *Gap junctions composed of connexins 41.8 and 39.4 are essential for colour pattern formation in zebrafish*. eLife. **3**.

101. Morokuma, J., et al., *Modulation of potassium channel function confers a hyperproliferative invasive phenotype on embryonic stem cells*. Proceedings of the National Academy of Sciences, 2008. **105**(43): p. 16608-16613.
102. Mollinedo-Gajate, I., C. Song, and T. Knöpfel, *Genetically Encoded Voltage Indicators*. 2021, Springer Singapore. p. 209-224.
103. Choe, M. and D.V. Titov, *Genetically encoded tools for measuring and manipulating metabolism*. Nature Chemical Biology, 2022. **18**(5): p. 451-460.
104. Poth, K.M., P. Texakalidis, and N.M. Boulis, *Chemogenetics: Beyond Lesions and Electrodes*. Neurosurgery, 2021. **89**(2): p. 185-195.
105. Ozawa, A. and H. Arakawa, *Chemogenetics drives paradigm change in the investigation of behavioral circuits and neural mechanisms underlying drug action*. Behav Brain Res, 2021. **406**: p. 113234.
106. Keifer, O., et al., *Chemogenetics a robust approach to pharmacology and gene therapy*. Biochem Pharmacol, 2020. **175**: p. 113889.
107. Chen, W., et al., *The Roles of Optogenetics and Technology in Neurobiology: A Review*. Front Aging Neurosci, 2022. **14**: p. 867863.
108. Antinucci, P., et al., *A calibrated optogenetic toolbox of stable zebrafish opsin lines*. eLife, 2020. **9**: p. e54937.
109. Deisseroth, K., *Optogenetics: 10 years of microbial opsins in neuroscience*. Nature Neuroscience, 2015. **18**(9): p. 1213-1225.
110. Zhang, G. and J. Cui, *Patch-Clamp and Perfusion Techniques to Study Ion Channels Expressed in Xenopus Oocytes*. Cold Spring Harbor Protocols, 2018. **2018**(4): p. pdb.prot099051.
111. Gest, A.M.M., et al., *VoltageFluor dyes and fluorescence lifetime imaging for optical measurement of membrane potential*, in *Methods in Enzymology*, D.L. Minor and H.M. Colecraft, Editors. 2021, Academic Press. p. 267-293.
112. Muto, A. and K. Kawakami, *Imaging functional neural circuits in zebrafish with a new GCaMP and the Gal4FF-UAS system*. Communicative & Integrative Biology, 2011. **4**(5): p. 566-568.
113. Kim, C.K., et al., *Prolonged, brain-wide expression of nuclear-localized GCaMP3 for functional circuit mapping*. Front Neural Circuits, 2014. **8**: p. 138.
114. DeMarco, E., et al., *Neuron types in the zebrafish optic tectum labeled by an id2b transgene*. The Journal of Comparative Neurology, 2020. **528**(7): p. 1173-1188.
115. Muto, A. and K. Kawakami, *Calcium Imaging of Neuronal Activity in Free-Swimming Larval Zebrafish*. 2016, Springer New York. p. 333-341.
116. Hou, J.H., et al., *Simultaneous mapping of membrane voltage and calcium in zebrafish heart in vivo reveals chamber-specific developmental transitions in ionic currents*. Front Physiol, 2014. **5**: p. 344.

117. Miyazawa, H., et al., *Optical interrogation of neuronal circuitry in zebrafish using genetically encoded voltage indicators*. Scientific Reports, 2018. **8**(1): p. 6048.
118. Hiyoshi, K., et al., *In vivo wide-field voltage imaging in zebrafish with voltage-sensitive dye and genetically encoded voltage indicator*. Development, Growth & Differentiation, 2021. **63**(8): p. 417-428.
119. Raccuglia, D., et al., *Presynaptic GABA Receptors Mediate Temporal Contrast Enhancement in Drosophila Olfactory Sensory Neurons and Modulate Odor-Driven Behavioral Kinetics*. eNeuro, 2016. **3**(4): p. ENEURO.0080-16.
120. Raccuglia, D., et al., *Network-Specific Synchronization of Electrical Slow-Wave Oscillations Regulates Sleep Drive in Drosophila*. Current Biology, 2019. **29**(21): p. 3611-3621.e3.
121. Chamberland, S., et al., *Fast two-photon imaging of subcellular voltage dynamics in neuronal tissue with genetically encoded indicators*. eLife, 2017. **6**: p. e25690.
122. Helen, et al., *Subcellular Imaging of Voltage and Calcium Signals Reveals Neural Processing In Vivo*. Cell, 2016. **166**(1): p. 245-257.
123. Cao, G., et al., *Genetically Targeted Optical Electrophysiology in Intact Neural Circuits*. Cell, 2013. **154**(4): p. 904-913.
124. Shimaoka, D., et al., *The impact of bilateral ongoing activity on evoked responses in mouse cortex*. eLife, 2019. **8**.
125. Song, C., et al., *Cortical signatures of wakeful somatosensory processing*. Scientific Reports, 2018. **8**(1).
126. Platasa, J., et al., *Voltage imaging in the olfactory bulb using transgenic mouse lines expressing the genetically encoded voltage indicator ArcLight*. Scientific Reports, 2022. **12**(1).
127. Treger, J.S., M.F. Priest, and F. Bezanilla, *Single-molecule fluorimetry and gating currents inspire an improved optical voltage indicator*. eLife, 2015. **4**: p. e10482.
128. Limapichat, W., et al., *Real-time detection of changes in yeast plasma membrane potential using genetically encoded voltage indicator proteins*. FEMS Yeast Research, 2020. **20**(5): p. foaa041.
129. St-Pierre, F., et al., *High-fidelity optical reporting of neuronal electrical activity with an ultrafast fluorescent voltage sensor*. Nature neuroscience, 2014. **17**(6): p. 884-889.
130. Villette, V., et al., *Ultrafast Two-Photon Imaging of a High-Gain Voltage Indicator in Awake Behaving Mice*. Cell, 2019. **179**(7): p. 1590-1608.e23.
131. Zhang, Y., et al., *Imaging sensory transmission and neuronal plasticity in primary sensory neurons with genetically-encoded voltage indicator, ASAP4.4-Kv*. 2021, Cold Spring Harbor Laboratory.
132. Platasa, J., et al., *Directed Evolution of Key Residues in Fluorescent Protein Inverses the Polarity of Voltage Sensitivity in the Genetically Encoded Indicator ArcLight*. ACS Chemical Neuroscience, 2017. **8**(3): p. 513-523.

133. Abdelfattah, A.S., et al., *A Bright and Fast Red Fluorescent Protein Voltage Indicator That Reports Neuronal Activity in Organotypic Brain Slices*. The Journal of Neuroscience, 2016. **36**(8): p. 2458-2472.
134. Jin, L., et al., *Single Action Potentials and Subthreshold Electrical Events Imaged in Neurons with a Fluorescent Protein Voltage Probe*. Neuron, 2012. **75**(5): p. 779-785.
135. Lee, S., et al., *Improving a genetically encoded voltage indicator by modifying the cytoplasmic charge composition*. Scientific Reports, 2017. **7**(1).
136. Sepehri Rad, M., et al., *Monitoring voltage fluctuations of intracellular membranes*. Scientific Reports, 2018. **8**(1).
137. Akemann, W., et al., *Imaging brain electric signals with genetically targeted voltage-sensitive fluorescent proteins*. Nature Methods, 2010. **7**(8): p. 643-649.
138. Lam, A.J., et al., *Improving FRET dynamic range with bright green and red fluorescent proteins*. Nature Methods, 2012. **9**(10): p. 1005-1012.
139. Akemann, W., et al., *Imaging neural circuit dynamics with a voltage-sensitive fluorescent protein*. J Neurophysiol, 2012. **108**(8): p. 2323-37.
140. Mishina, Y., et al., *Exploration of genetically encoded voltage indicators based on a chimeric voltage sensing domain*. Front Mol Neurosci, 2014. **7**: p. 78.
141. Gautam, S.G., et al., *Exploration of fluorescent protein voltage probes based on circularly permuted fluorescent proteins*. Front Neuroeng, 2009. **2**: p. 14.
142. Perron, A., et al., *Red-shifted voltage-sensitive fluorescent proteins*. Chem Biol, 2009. **16**(12): p. 1268-77.
143. Tsutsui, H., et al., *Improving membrane voltage measurements using FRET with new fluorescent proteins*. Nature Methods, 2008. **5**(8): p. 683-685.
144. Sung, U., et al., *Developing Fast Fluorescent Protein Voltage Sensors by Optimizing FRET Interactions*. PLOS ONE, 2015. **10**(11): p. e0141585.
145. Liu, Z., et al., *Sustained deep-tissue voltage recording using a fast indicator evolved for two-photon microscopy*. Cell, 2022. **185**(18): p. 3408-3425.e29.
146. Kralj, J.M., et al., *Optical recording of action potentials in mammalian neurons using a microbial rhodopsin*. Nature Methods, 2012. **9**(1): p. 90-95.
147. Hochbaum, D.R., et al., *All-optical electrophysiology in mammalian neurons using engineered microbial rhodopsins*. Nature Methods, 2014. **11**(8): p. 825-833.
148. Adam, Y., et al., *Voltage imaging and optogenetics reveal behaviour-dependent changes in hippocampal dynamics*. Nature, 2019. **569**(7756): p. 413-417.
149. Zou, P., et al., *Bright and fast multicoloured voltage reporters via electrochromic FRET*. Nature Communications, 2014. **5**(1).
150. Piatkevich, K.D., et al., *A robotic multidimensional directed evolution approach applied to fluorescent voltage reporters*. Nature Chemical Biology, 2018. **14**(4): p. 352-360.

151. Gong, Y., et al., *High-speed recording of neural spikes in awake mice and flies with a fluorescent voltage sensor*. Science, 2015. **350**(6266): p. 1361-1366.
152. Beck, C. and Y. Gong, *A high-speed, bright, red fluorescent voltage sensor to detect neural activity*. Scientific Reports, 2019. **9**(1).
153. Kannan, M., et al., *Fast, in vivo voltage imaging using a red fluorescent indicator*. Nature Methods, 2018. **15**(12): p. 1108-1116.
154. Abdelfattah, A.S., et al., *Bright and photostable chemigenetic indicators for extended in vivo voltage imaging*. bioRxiv, 2018: p. 436840.
155. Abdelfattah, A.S., et al., *A general approach to engineer positive-going eFRET voltage indicators*. Nature Communications, 2020. **11**(1).
156. Chanda, B., et al., *A hybrid approach to measuring electrical activity in genetically specified neurons*. Nature Neuroscience, 2005. **8**(11): p. 1619-1626.
157. Grenier, V., et al., *Spying on Neuronal Membrane Potential with Genetically Targetable Voltage Indicators*. Journal of the American Chemical Society, 2019. **141**(3): p. 1349-1358.
158. Inagaki, S., et al., *Genetically encoded bioluminescent voltage indicator for multi-purpose use in wide range of bioimaging*. Scientific Reports, 2017. **7**(1): p. 42398.
159. Srinivasan, P., et al., *An Autonomous Molecular Bioluminescent Reporter (AMBER) for Voltage Imaging in Freely Moving Animals*. Adv Biol (Weinh), 2021. **5**(12): p. e2100842.
160. Dana, H., et al., *High-performance calcium sensors for imaging activity in neuronal populations and microcompartments*. Nature Methods, 2019. **16**(7): p. 649-657.
161. Dana, H., et al., *Sensitive red protein calcium indicators for imaging neural activity*. eLife, 2016. **5**: p. e12727.
162. Sternson, S.M. and B.L. Roth, *Chemogenetic Tools to Interrogate Brain Functions*. Annual Review of Neuroscience, 2014. **37**(1): p. 387-407.
163. Roth, B.L., *DREADDs for Neuroscientists*. Neuron, 2016. **89**(4): p. 683-694.
164. Atasoy, D. and S.M. Sternson, *Chemogenetic Tools for Causal Cellular and Neuronal Biology*. Physiological Reviews, 2018. **98**(1): p. 391-418.
165. Peeters, L.M., et al., *Combining designer receptors exclusively activated by designer drugs and neuroimaging in experimental models: A powerful approach towards neurotheranostic applications*. British Journal of Pharmacology, 2020. **177**(5): p. 992-1002.
166. Chen, S., et al., *TRP channel mediated neuronal activation and ablation in freely behaving zebrafish*. Nature methods, 2016. **13**(2): p. 147-150.
167. Beckwith-Cohen, B., et al., *Controlling Horizontal Cell-Mediated Lateral Inhibition in Transgenic Zebrafish Retina with Chemogenetic Tools*. eNeuro, 2020. **7**(5).
168. Magnus, C.J., et al., *Ultrapotent chemogenetics for research and potential clinical applications*. Science, 2019. **364**(6436): p. eaav5282.

169. Silic, M.R. and G. Zhang, *Tissue-specific modification of cellular bioelectrical activities using the chemogenetic tool, DREADD, in zebrafish*. 2021, Cold Spring Harbor Laboratory.
170. Arrenberg, A.B., F. Del Bene, and H. Baier, *Optical control of zebrafish behavior with halorhodopsin*. Proceedings of the National Academy of Sciences, 2009. **106**(42): p. 17968-17973.
171. Monesson-Olson, B.D., et al., *Optical Stimulation of Zebrafish Hair Cells Expressing Channelrhodopsin-2*. PLoS ONE, 2014. **9**(5): p. e96641.
172. Jeong, Y.-M., et al., *Optogenetic Manipulation of Olfactory Responses in Transgenic Zebrafish: A Neurobiological and Behavioral Study*. International Journal of Molecular Sciences, 2021. **22**(13): p. 7191.
173. Aramaki, T. and S. Kondo, *Method for disarranging the pigment pattern of zebrafish by optogenetics*. Developmental Biology, 2020. **460**(1): p. 12-19.
174. Daane, J.M., et al., *Bioelectric-calcineurin signaling module regulates allometric growth and size of the zebrafish fin*. Scientific Reports, 2018. **8**.
175. Cao, Z., et al., *Calcineurin controls proximodistal blastema polarity in zebrafish fin regeneration*. Proceedings of the National Academy of Sciences, 2021. **118**(2): p. e2009539118.
176. Cairns, D.M., et al., *Ivermectin Promotes Peripheral Nerve Regeneration during Wound Healing*. ACS Omega, 2018. **3**(10): p. 12392-12402.
177. Pai, V.P., et al., *HCN4 ion channel function is required for early events that regulate anatomical left-right patterning in a Nodal- and Lefty asymmetric gene expression-independent manner*. Biology Open, 2017. **6**(10): p. 1445-1457.
178. Adams, D.S., A.-S. Tseng, and M. Levin, *Light-activation of the Archaelhodopsin H⁺-pump reverses age-dependent loss of vertebrate regeneration: sparking system-level controls *in vivo**. Biology Open, 2013. **2**(3): p. 306-313.
179. Vardy, E., et al., *A New DREADD Facilitates the Multiplexed Chemogenetic Interrogation of Behavior*. Neuron, 2015. **86**(4): p. 936-946.
180. Boyden, E.S., et al., *Millisecond-timescale, genetically targeted optical control of neural activity*. Nature Neuroscience, 2005. **8**(9): p. 1263-1268.
181. Zhang, C., et al., *Optimized photo-stimulation of halorhodopsin for long-term neuronal inhibition*. BMC Biology, 2019. **17**(1).
182. Ganjawala, T.H., et al., *Improved CoChR Variants Restore Visual Acuity and Contrast Sensitivity in a Mouse Model of Blindness under Ambient Light Conditions*. Molecular Therapy, 2019. **27**(6): p. 1195-1205.
183. Ochs, A.R., et al., *Optogenetic Stimulation Using Anion Channelrhodopsin (GtACR1) Facilitates Termination of Reentrant Arrhythmias With Low Light Energy Requirements: A Computational Study*. Front Physiol, 2021. **12**: p. 718622.
184. Magnus, C.J., et al., *Chemical and Genetic Engineering of Selective Ion Channel–Ligand Interactions*. Science, 2011. **333**(6047): p. 1292-1296.

185. Mahn, M., et al., *High-efficiency optogenetic silencing with soma-targeted anion-conducting channelrhodopsins*. Nature Communications, 2018. **9**(1).
186. Alberio, L., et al., *A light-gated potassium channel for sustained neuronal inhibition*. Nature Methods, 2018. **15**(11): p. 969-976.
187. Hight, A.E., et al., *Superior temporal resolution of Chronos versus channelrhodopsin-2 in an optogenetic model of the auditory brainstem implant*. Hearing Research, 2015. **322**: p. 235-241.
188. Krol, A., et al., *Two eARCT3.0 Lines for Optogenetic Silencing of Dopaminergic and Serotonergic Neurons*. Front Neural Circuits, 2019. **13**: p. 4.
189. Klapoetke, N.C., et al., *Independent optical excitation of distinct neural populations*. Nature Methods, 2014. **11**(3): p. 338-346.
190. Weir, G.A., et al., *Using an engineered glutamate-gated chloride channel to silence sensory neurons and treat neuropathic pain at the source*. Brain, 2017. **140**(10): p. 2570-2585.
191. Stanley, S.A., et al., *Bidirectional electromagnetic control of the hypothalamus regulates feeding and metabolism*. Nature, 2016. **531**(7596): p. 647-650.
192. Levin, M., *Bioelectric signaling: Reprogrammable circuits underlying embryogenesis, regeneration, and cancer*. Cell, 2021. **184**(8): p. 1971-1989.
193. Harris, M.P., *Bioelectric signaling as a unique regulator of development and regeneration*. Development, 2021. **148**(10).
194. Yang, M. and W.J. Brackenbury, *Membrane potential and cancer progression*. Frontiers in Physiology, 2013. **4**.
195. Srivastava, P., et al., *A Meta-Analysis of Bioelectric Data in Cancer, Embryogenesis, and Regeneration*. Bioelectricity, 2021. **3**(1): p. 42-67.
196. Manville, R.W., M. Papanikolaou, and G.W. Abbott, *Direct neurotransmitter activation of voltage-gated potassium channels*. Nature Communications, 2018. **9**(1): p. 1847.
197. Tanguay, J., K.M. Callahan, and N. D'Avanzo, *Characterization of drug binding within the HCN1 channel pore*. Scientific Reports, 2019. **9**(1): p. 465.
198. De Silva, A.M., R.W. Manville, and G.W. Abbott, *Deconstruction of an African folk medicine uncovers a novel molecular strategy for therapeutic potassium channel activation*. Science Advances, 2018. **4**(11): p. eaav0824.
199. Manville, R.W. and G.W. Abbott, *Ancient and modern anticonvulsants act synergistically in a KCNQ potassium channel binding pocket*. Nature Communications, 2018. **9**(1): p. 3845.
200. Okada, M., et al., *Pore-forming spider venom peptides show cytotoxicity to hyperpolarized cancer cells expressing K⁺ channels: A lentiviral vector approach*. PloS One, 2019. **14**(4): p. e0215391.

201. Capatina, A.L., D. Lagos, and W.J. Brackenbury, *Targeting Ion Channels for Cancer Treatment: Current Progress and Future Challenges*. 2020, Springer International Publishing. p. 1-43.
202. Leanza, L., et al., *Pharmacological targeting of ion channels for cancer therapy: In vivo evidences*. Biochimica et Biophysica Acta (BBA) - Molecular Cell Research, 2016. **1863**(6, Part B): p. 1385-1397.
203. Gao, X., et al., *Membrane potential drives direct translocation of cell-penetrating peptides*. Nanoscale, 2019. **11**(4): p. 1949-1958.
204. Herrera-Rincon, C., et al., *Brief Local Application of Progesterone via a Wearable Bioreactor Induces Long-Term Regenerative Response in Adult Xenopus Hindlimb*. Cell Reports, 2018. **25**(6): p. 1593-1609.e7.
205. Huang, X. and L.Y. Jan, *Targeting potassium channels in cancer*. The Journal of Cell Biology, 2014. **206**(2): p. 151-162.
206. Ramasubramanian, S. and Y. Rudy, *The Structural Basis of IKs Ion-Channel Activation: Mechanistic Insights from Molecular Simulations*. Biophysical Journal, 2018. **114**(11): p. 2584-2594.
207. Dmitriev, A.V., A.A. Dmitriev, and R.A. Linsenmeier, *The logic of ionic homeostasis: Cations are for voltage, but not for volume*. PLoS computational biology, 2019. **15**(3): p. e1006894.
208. Cervera, J., et al., *Bioelectrical coupling in multicellular domains regulated by gap junctions: A conceptual approach*. Bioelectrochemistry (Amsterdam, Netherlands), 2018. **123**: p. 45-61.
209. Churchill, C.D.M., et al., *EDEn-Electroceutical Design Environment: Ion Channel Tissue Expression Database with Small Molecule Modulators*. iScience, 2019. **11**: p. 42-56.
210. Ait Ouares, K., et al., *Two Distinct Sets of Ca²⁺ and K⁺ Channels Are Activated at Different Membrane Potentials by the Climbing Fiber Synaptic Potential in Purkinje Neuron Dendrites*. The Journal of Neuroscience: The Official Journal of the Society for Neuroscience, 2019. **39**(11): p. 1969-1981.
211. Manville, R.W. and G.W. Abbott, *Teamwork: Ion channels and transporters join forces in the brain*. Neuropharmacology, 2019.
212. Schultheis, C., et al., *Optogenetic Long-Term Manipulation of Behavior and Animal Development*. PLOS ONE, 2011. **6**(4): p. e18766.
213. Shen, Y., et al., *Genetically encoded fluorescent indicators for imaging intracellular potassium ion concentration*. Communications Biology, 2019. **2**(1): p. 18.
214. Storace, D., et al., *Toward better genetically encoded sensors of membrane potential*. Trends in neurosciences, 2016. **39**(5): p. 277-289.
215. Inagaki, S. and T. Nagai, *Current progress in genetically encoded voltage indicators for neural activity recording*. Curr Opin Chem Biol, 2016. **33**: p. 95-100.
216. Lieschke, G.J. and P.D. Currie, *Animal models of human disease: zebrafish swim into view*. Nat Rev Genet, 2007. **8**(5): p. 353-67.

217. Kawakami, K., A. Shima, and N. Kawakami, *Identification of a functional transposase of the <i>Tol2</i> element, an <i>Ac</i>-like element from the Japanese medaka fish, and its transposition in the zebrafish germ lineage*. Proceedings of the National Academy of Sciences, 2000. **97**(21): p. 11403-11408.
218. Urasaki, A., K. Asakawa, and K. Kawakami, *Efficient transposition of the Tol2 transposable element from a single-copy donor in zebrafish*. Proceedings of the National Academy of Sciences, 2008. **105**(50): p. 19827-19832.
219. Kwan, K.M., et al., *The Tol2kit: A multisite gateway-based construction kit for Tol2 transposon transgenesis constructs*. Developmental Dynamics, 2007. **236**(11): p. 3088-3099.
220. Mosimann, C., et al., *Ubiquitous transgene expression and Cre-based recombination driven by the ubiquitin promoter in zebrafish*. Development, 2011. **138**(1): p. 169-177.
221. Lorenz, T.C., *Polymerase Chain Reaction: Basic Protocol Plus Troubleshooting and Optimization Strategies*. Journal of Visualized Experiments, 2012(63).
222. Ordovas, J.M., *Separation of Small-Size DNA Fragments Using Agarose Gel Electrophoresis*. Humana Press. p. 35-42.
223. Downey, N., *Extraction of DNA from Agarose Gels*. Humana Press. p. 137-140.
224. Desjardins, P. and D. Conklin, *NanoDrop Microvolume Quantitation of Nucleic Acids*. Journal of Visualized Experiments, 2010(-1).
225. Green, M.R., Sambrook, J., *Molecular cloning : a laboratory manual*. . 2012: Cold Spring Harbor Laboratory Press
226. Zhang, S. and M.D. Cahalan, *Purifying Plasmid DNA from Bacterial Colonies Using the Qiagen Miniprep Kit*. Journal of Visualized Experiments, 2007(6).
227. Meeker, N.D., et al., *Method for isolation of PCR-ready genomic DNA from zebrafish tissues*. BioTechniques, 2007. **43**(5): p. 610-614.
228. Kawakami, K., et al., *Excision of the tol2 transposable element of the medaka fish, Oryzias latipes, in zebrafish, Danio rerio*. Gene, 1998. **225**(1-2): p. 17-22.
229. Westerfield, M., *The zebrafish book. A guide for the laboratory use of zebrafish (Danio rerio)*. 4th edn ed. 2000: Univ. of Oregon Press
230. Amsterdam, A., et al., *Many Ribosomal Protein Genes Are Cancer Genes in Zebrafish*. PLoS Biology, 2004. **2**(5): p. e139.
231. Lai, K., et al., *Many ribosomal protein mutations are associated with growth impairment and tumor predisposition in zebrafish*. Developmental Dynamics, 2009. **238**(1): p. 76-85.
232. Kimmel, C.B., et al., *Stages of embryonic development of the zebrafish*. Developmental Dynamics, 1995. **203**(3): p. 253-310.
233. Zhang, G., et al., *Comparative Oncogenomic Analysis of Copy Number Alterations in Human and Zebrafish Tumors Enables Cancer Driver Discovery*. PLoS Genetics, 2013. **9**(8): p. e1003734.

234. Zhang, G., et al., *Highly aneuploid zebrafish malignant peripheral nerve sheath tumors have genetic alterations similar to human cancers*. Proceedings of the National Academy of Sciences, 2010. **107**(39): p. 16940-16945.
235. Urrego, D., et al., *Potassium channels in cell cycle and cell proliferation*. Philosophical Transactions of the Royal Society B: Biological Sciences, 2014. **369**(1638).
236. Sugiyama, M., et al., *Illuminating cell-cycle progression in the developing zebrafish embryo*. Proceedings of the National Academy of Sciences, 2009. **106**(49): p. 20812-20817.
237. Nakajima, K.-i., et al., *KCNJ15/Kir4.2 couples with polyamines to sense weak extracellular electric fields in galvanotaxis*. Nature Communications, 2015. **6**(1): p. 8532.
238. Dahal, G.R., et al., *An inwardly rectifying K⁺ channel is required for patterning*. Development, 2012. **139**(19): p. 3653-3664.
239. Dahal, G.R., S.J. Pradhan, and E.A. Bates, *Inwardly rectifying potassium channels influence Drosophila wing morphogenesis by regulating Dpp release*. Development, 2017. **144**(15): p. 2771-2783.
240. Villanueva, S., et al., *Cleft Palate, Moderate Lung Developmental Retardation and Early Postnatal Lethality in Mice Deficient in the Kir7.1 Inwardly Rectifying K⁺ Channel*. PLoS One, 2015. **10**(9): p. e0139284.
241. Yin, W., et al., *The potassium channel KCNJ13 is essential for smooth muscle cytoskeletal organization during mouse tracheal tubulogenesis*. Nat Commun, 2018. **9**(1): p. 2815.
242. Pai, V.P., et al., *Transmembrane voltage potential controls embryonic eye patterning in Xenopus laevis*. Development, 2012. **139**(2): p. 313-23.
243. Sims, K., D.M. Eble, and M.K. Iovine, *Connexin43 regulates joint location in zebrafish fins*. Developmental Biology, 2009. **327**(2): p. 410-418.
244. Daane, J.M., et al., *Modulation of bioelectric cues in the evolution of flying fishes*. Current Biology, 2021. **31**(22): p. 5052-5061.e8.
245. Sakai, C., S. Ijaz, and E.J. Hoffman, *Zebrafish Models of Neurodevelopmental Disorders: Past, Present, and Future*. Front Mol Neurosci, 2018. **11**: p. 294.
246. Vaz, R., W. Hofmeister, and A. Lindstrand, *Zebrafish Models of Neurodevelopmental Disorders: Limitations and Benefits of Current Tools and Techniques*. Int J Mol Sci, 2019. **20**(6).
247. Gonzalez-Rosa, J.M., *Zebrafish Models of Cardiac Disease: From Fortuitous Mutants to Precision Medicine*. Circ Res, 2022. **130**(12): p. 1803-1826.
248. Crouzier, L., et al., *Use of Zebrafish Models to Boost Research in Rare Genetic Diseases*. International Journal of Molecular Sciences, 2021. **22**(24): p. 13356.
249. McConnell, A.M., H.R. Noonan, and L.I. Zon, *Reeling in the Zebrafish Cancer Models*. Annual Review of Cancer Biology, 2021. **5**(1): p. 331-350.
250. Bando, Y., et al., *Genetic voltage indicators*. BMC Biology, 2019. **17**(1): p. 71.
251. Stelzer, E.H., *Light-sheet fluorescence microscopy for quantitative biology*. Nat Methods, 2015. **12**(1): p. 23-6.

252. Stelzer, E.H.K., et al., *Light sheet fluorescence microscopy*. Nature Reviews Methods Primers, 2021. **1**(1): p. 73.
253. Tosti, E., R. Boni, and A. Gallo, *Ion currents in embryo development*. Birth Defects Research Part C: Embryo Today: Reviews, 2016. **108**(1): p. 6-18.
254. Moody, W.J., et al., *Development of ion channels in early embryos*. Journal of Neurobiology, 1991. **22**(7): p. 674-684.
255. Turrini, L., et al., *Optical mapping of neuronal activity during seizures in zebrafish*. Sci Rep, 2017. **7**(1): p. 3025.
256. Migault, G., et al., *Whole-Brain Calcium Imaging during Physiological Vestibular Stimulation in Larval Zebrafish*. Curr Biol, 2018. **28**(23): p. 3723-3735 e6.
257. Webb, S.E., R.A. Fluck, and A.L. Miller, *Calcium signaling during the early development of medaka and zebrafish*. Biochimie, 2011. **93**(12): p. 2112-25.
258. Creton, R., J.E. Speksnijder, and L.F. Jaffe, *Patterns of free calcium in zebrafish embryos*. J Cell Sci, 1998. **111** (Pt 12): p. 1613-22.
259. Djamgoz, M.B.A. and M. Levin, *Bioelectricity: A Quick Reminder of a Fast-Advancing Discipline!* Bioelectricity, 2020. **2**(3): p. 208-209.
260. Schofield, Z., et al., *Bioelectrical understanding and engineering of cell biology*. J R Soc Interface, 2020. **17**(166): p. 20200013.
261. Clapham, D.E., *Calcium signaling*. Cell, 2007. **131**(6): p. 1047-58.
262. Bootman, M.D., M.J. Berridge, and H.L. Roderick, *Calcium signalling: more messengers, more channels, more complexity*. Curr Biol, 2002. **12**(16): p. R563-5.
263. Rogers, K.W. and A.F. Schier, *Morphogen gradients: from generation to interpretation*. Annu Rev Cell Dev Biol, 2011. **27**: p. 377-407.
264. Pearson, J.C., D. Lemons, and W. McGinnis, *Modulating Hox gene functions during animal body patterning*. Nat Rev Genet, 2005. **6**(12): p. 893-904.
265. Tan, P., et al., *Optophysiology: Illuminating cell physiology with optogenetics*. Physiological Reviews, 2022. **102**(3): p. 1263-1325.
266. Purves, D., Augustine, G. J., Fitzpatrick, D., Hall, W. C., LaMantia, A. S., McNamara, J. O., and Williams, S. M. , *Neuroscience*. 3rd ed ed. 2004, Sunderland, Mass: Sinauer Associates, Publishers. 1.
267. Luo, L., E.M. Callaway, and K. Svoboda, *Genetic Dissection of Neural Circuits: A Decade of Progress*. Neuron, 2018. **98**(2): p. 256-281.
268. Grosenick, L., J.H. Marshel, and K. Deisseroth, *Closed-loop and activity-guided optogenetic control*. Neuron, 2015. **86**(1): p. 106-139.
269. Fenno, L., O. Yizhar, and K. Deisseroth, *The Development and Application of Optogenetics*. Annual Review of Neuroscience, 2011. **34**(1): p. 389-412.

270. Urban, D.J. and B.L. Roth, *DREADDs (Designer Receptors Exclusively Activated by Designer Drugs): Chemogenetic Tools with Therapeutic Utility*. Annual Review of Pharmacology and Toxicology, 2015. **55**(1): p. 399-417.
271. Bonaventura, J., et al., *High-potency ligands for DREADD imaging and activation in rodents and monkeys*. Nature Communications, 2019. **10**(1): p. 4627.
272. Carter, M.E., et al., *Genetic identification of a neural circuit that suppresses appetite*. Nature, 2013. **503**(7474): p. 111-114.
273. Ferguson, S.M., et al., *Direct-pathway striatal neurons regulate the retention of decision-making strategies*. The Journal of Neuroscience: The Official Journal of the Society for Neuroscience, 2013. **33**(28): p. 11668-11676.
274. Nagai, Y., et al., *Deschloroclozapine, a potent and selective chemogenetic actuator enables rapid neuronal and behavioral modulations in mice and monkeys*. Nature Neuroscience, 2020. **23**(9): p. 1157-1167.
275. Chen, X., et al., *The First Structure–Activity Relationship Studies for Designer Receptors Exclusively Activated by Designer Drugs*. ACS Chemical Neuroscience, 2015. **6**(3): p. 476-484.
276. Yang, H.H. and F. St-Pierre, *Genetically Encoded Voltage Indicators: Opportunities and Challenges*. Journal of Neuroscience, 2016. **36**(39): p. 9977-9989.
277. Lee, S., Y.K. Song, and B.J. Baker, *Engineering Photoactivatability in Genetically Encoded Voltage and pH Indicators*. Front Cell Neurosci, 2019. **13**: p. 482.
278. Bando, Y., et al., *Comparative Evaluation of Genetically Encoded Voltage Indicators*. Cell Reports, 2019. **26**(3): p. 802-813.e4.
279. Scheer, N. and J.A. Campos-Ortega, *Use of the Gal4-UAS technique for targeted gene expression in the zebrafish*. Mechanisms of Development, 1999. **80**(2): p. 153-158.
280. Wu, Q., et al., *Translation of small downstream ORFs enhances translation of canonical main open reading frames*. The EMBO Journal, 2020. **39**(17).
281. Horstick, E.J., et al., *Increased functional protein expression using nucleotide sequence features enriched in highly expressed genes in zebrafish*. Nucleic Acids Res, 2015. **43**(7): p. e48.
282. Rhee, J.K., et al., *Biophysical Parameters of GEVIs: Considerations for Imaging Voltage*. Biophysical Journal, 2020. **119**(1): p. 1-8.
283. Platasa, J. and V.A. Pieribone, *Genetically encoded fluorescent voltage indicators: are we there yet?* Current Opinion in Neurobiology, 2018. **50**: p. 146-153.
284. Akitake, C.M., et al., *Transgenerational analysis of transcriptional silencing in zebrafish*. Dev Biol, 2011. **352**(2): p. 191-201.
285. Rorth, P., *A modular misexpression screen in Drosophila detecting tissue-specific phenotypes*. Proceedings of the National Academy of Sciences, 1996. **93**: p. 12418-12422.
286. Grienberger, C. and A. Konnerth, *Imaging Calcium in Neurons*. Neuron, 2012. **73**(5): p. 862-885.

- 287. Becnel, J., et al., *DREADDs in Drosophila: a pharmacogenetic approach for controlling behavior, neuronal signaling, and physiology in the fly*. Cell Rep, 2013. **4**(5): p. 1049-59.
- 288. Kim, J.-B., *Channelopathies*. Korean Journal of Pediatrics, 2014. **57**(1): p. 1-18.
- 289. Schneider, C.A., W.S. Rasband, and K.W. Eliceiri, *NIH Image to ImageJ: 25 years of image analysis*. Nat Methods, 2012. **9**(7): p. 671-5.

PUBLICATIONS

1. **Silic, M. R.**, Dong Z, Chen Y, Kimbrough A, Zhang G. (2022). Zebrafish Embryos Display Characteristic Bioelectric Signals during Early Development. *Cells*, 11(22):3586. <https://doi.org/10.3390/cells11223586>
2. **Silic, M. R.**, & Zhang, G. (2021). Tissue-specific modification of cellular bioelectrical activities using the chemogenetic tool, DREADD, in zebrafish. *bioRxiv* 449481. <https://doi.org/10.1101/2021.06.22.449481> **In Revision**
3. **Silic, M. R.**, Murata, S. H., Park, S. J., & Zhang, G. (2021). Evolution of inwardly rectifying potassium channels and their gene expression in zebrafish embryos. *Developmental dynamics*, 251(4): 687- 713. <https://doi.org/10.1002/dvdy.425>
4. Han, H., Jiang, G., Kumari, R., **Silic, M. R.**, Owens, J. L., Hu, C. D., Mittal, S. K., & Zhang, G. (2021). Loss of smarcad1a accelerates tumorigenesis of malignant peripheral nerve sheath tumors in zebrafish. *Genes, chromosomes & cancer*, 60(11), 743–761. <https://doi.org/10.1002/gcc.22983>
5. **Silic, M. R.**, Black, M. M., & Zhang, G. (2021). Phylogenetic and developmental analyses indicate complex functions of calcium-activated potassium channels in zebrafish embryonic development. *Developmental dynamics*, 250: 1477-1493. <http://10.1002/dvdy.329>
6. **Silic, M. R.**, Wu, Q., Kim, B. H., Golling, G., Chen, K. H., Freitas, R., Chubykin, A. A., Mittal, S. K., & Zhang, G. (2020). Potassium Channel-Associated Bioelectricity of the Dermomyotome Determines Fin Patterning in Zebrafish. *Genetics*, 215(4), 1067–1084. <https://doi.org/10.1534/genetics.120.303390>
7. Zhang, R., **Silic, M. R.**, Schaber, A., Wasel, O., Freeman, J. L., & Sepúlveda, M. S. (2020). Exposure route affects the distribution and toxicity of polystyrene nanoplastics in zebrafish. *The Science of the total environment*, 724, 138065. <https://doi.org/10.1016/j.scitotenv.2020.138065>

8. Kumari, R., **Silic, M. R.**, Jones-Hall, Y. L., Nin-Velez, A., Yang, J. Y., Mittal, S. K., & Zhang, G. (2018). Identification of RECK as an evolutionarily conserved tumor suppressor gene for zebrafish malignant peripheral nerve sheath tumors. *Oncotarget*, 9(34), 23494–23504. <https://doi:10.18632/oncotarget.25236>
9. **Silic, M. R.**, & Zhang, G. (2018). Visualization of Cellular Electrical Activity in Zebrafish Early Embryos and Tumors. *Journal of visualized experiments: JoVE*, (134), 57330. <https://doi:10.3791/57330>